Progress in Retinal and Eye Research 86 (2022) 100976

Contents lists available at ScienceDirect

Progress in Retinal and Eye Research

journal homepage: www.elsevier.com/locate/preteyeres

Detecting retinal cell stress and apoptosis with DARC: Progression from lab to clinic

Maria Francesca Cordeiro [a,b,c,d,*], Daniel Hill, MSc [a,1], Radhika Patel, MBBS [b,c,1], Paolo Corazza, MD [b,c], John Maddison, PhD [d], Saad Younis, MD [b,c]

[a] UCL Institute of Ophthalmology, London, UK
[b] Western Eye Hospital Imperial College Healthcare NHS Trust, London, UK
[c] ICORG, Imperial College, London, UK
[d] Novai Ltd, Reading, UK

ARTICLE INFO

Keywords:
DARC
Annexin
Retina
RGC
In vivo
Apoptosis
Biomarker
Wet AMD
Geographic atrophy
Glaucoma
Cell stress

ABSTRACT

DARC (Detection of Apoptosing Retinal Cells) is a retinal imaging technology that has been developed within the last 2 decades from basic laboratory science to Phase 2 clinical trials. It uses ANX776 (fluorescently labelled Annexin A5) to identify stressed and apoptotic cells in the living eye. During its development, DARC has undergone biochemistry optimisation, scale-up and GMP manufacture and extensive preclinical evaluation. Initially tested in preclinical glaucoma and optic neuropathy models, it has also been investigated in AMD, Alzheimer's, Parkinson's and Diabetic models, and used to assess efficacy of therapies. Progression to clinical trials has not been speedy. Intravenous ANX776 has to date been found to be safe and well-tolerated in 129 patients, including 16 from Phase 1 and 113 from Phase 2. Results on glaucoma and AMD patients have been recently published, and suggest DARC with an AI-aided algorithm can be used to predict disease activity. New analyses of DARC in GA (Geographic Atrophy) prediction are reported here. Although further studies are needed to validate these findings, it appears there is potential for the technology to be used as a biomarker. Much larger clinical studies will be needed before it can be considered as a diagnostic, although the relatively non-invasive nature of the nasal as opposed to intravenous administration would widen its acceptability in the future as a screening tool.

This review describes DARC development and its progression into Phase 2 clinical trials from lab-based research. It discusses hypotheses, potential challenges, and regulatory hurdles in translating technology.

1. Introduction

DARC (Detection of Apoptosing Retinal Cells) is an original technique that capitalises on the unique transparent optical properties of the eye to enable stressed and apoptotic cells to be visualised in the retina using a fluorescently-labelled annexin A5. Annexin A5 has been utilised for many years in cell biology labs in the cytological detection of cells undergoing apoptosis using fluorescein isothiocyanate-labelled annexin A5 (FITC-annexin A5 or 488-annexin A5). Radiolabelled annexin A5 has been applied clinically in diseases such as cancer (García-Santos et al., 2006) and cardiovascular disease (Blankenberg et al., 1998) and in these applications annexin was put forward as a measure of disease activity. This led us to consider utilising fluorescence retinal imaging instead of radiolabelled annexin as this technique is routinely used in ophthalmology including autofluorescence, fluorescein sodium and indocyanine green for angiography (Keane and Sadda, 2010). Thus the DARC project was born with the first publication in 2004 (Cordeiro et al., 2004). The rationale for DARC is that rather than providing an estimate of healthy cells, it highlights unhealthy and sick cells, to give an indication of disease activity.

Here we review the development of DARC from this very first paper, and comment on the findings and translatability.

2. Basic principles

2.1. Annexin A5, apoptosis and stressed cells

Annexin A5 has been linked to the detection of apoptosis for many years. Apoptosis is a type of programmed cell death where individual

* Corresponding author. UCL Institute of Ophthalmology, 11-43 Bath Street, London, EC1V 9EL, UK.
E-mail address: m.cordeiro@ucl.ac.uk (M.F. Cordeiro).
[1] Daniel Hill and Radhika Patel contributed equally to this paper.

https://doi.org/10.1016/j.preteyeres.2021.100976
Received 24 December 2020; Received in revised form 21 May 2021; Accepted 26 May 2021
Available online 5 June 2021

Abbreviations

^{18}F	fluorine-18
^{124}I	iodine-124
^{99m}Tc	Technetium-99 m
AD	Alzheimer's disease
AI	Artificial intelligence
AMD	Age-related macular degeneration
Anti-VEGF	Anti-vascular endothelial growth factor
ANX776	Annexin – fluorescent at 776 nm
AO	Adaptive optics
AUC	Area under the curve
BMI	Body mass index
CNN	Convoluted neural network
CNV	Choroidal neovascularisation
CSF	Cerebrospinal fluid
CSF-P	Cerebrospinal fluid pressure
cSLO	Confocal scanning laser ophthalmoscope
CTA	Clinical Trial authorisation
cTIMP	Clinical Trial of an Investigational Medicinal Product
DARC	Detection of apoptosing retinal cells
DAPI	4,6-diamidino-2-phenylindole
Dy-776-mal	Dy-776 maleimide fluorescent dye
EAE	Experimental autoimmune encephalomyelitis
FDA	Food and Drug Adminstration (USA)
GMP	Good manufacturing practice
MHRA	Medicines & Healthcare products Regulatory Agency (UK)
IB	Investigator's Brochure
IMP	Investigational Medicinal Product
IOP	Intraocular pressure
mGluR	Metabotropic glutamate receptor
MRI	Magnetic resonance imaging
MS	Multiple sclerosis
NMDA	N-methyl-D aspartic acid
NOAEL	No Observed Adverse Effect Level
NTG	Normal tension glaucoma
OCT	Optical coherence tomography
OHT	Ocular hypertension
PACG	Primary angle closure glaucoma
PD	Parkinson's disease
PET	Position emission tomography
POAG	Primary open angle glaucoma
PPV	Positive predicted value
pRNFL	peripapillary RNFL
PS	Phosphatidylserine
RGC	Retinal ganglion cell
RNFL	Retinal nerve fibre layer
RoP	Rate of Progression
RPE	Retinal pigment epithelium
SPECT	single photon emission computed tomography
TUNEL	terminal deoxynucleotidyl transferase dUTP nick end-labeling
VEGF	Vascular endothelial growth factor

cells and their nuclear contents shrink and fragment into apoptotic blebs in a controlled manner. These blebs are then phagocytosed by macrophages and do not cause an inflammatory response unlike necrosis (Ahmad, 2017). Thus, compared to necrosis, apoptosis is a regulated process of cell death, associated with chromatin condensation, DNA fragmentation, oxidative damage and autophagic degeneration and commonly proceeding via either extrinsic or intrinsic caspase dependent pathways (Hofstra et al., 2000). The apoptosis cascade is initiated by key enzymes called caspases that cleave target proteins when activated leading to controlled cell death.

One of the earliest stages in this cascade process is thought to be translocation of phosphatidylserine (PS) molecules onto the outer layer of the bilayer plasma cell membrane. These molecules are normally present on the inner layer of the plasma membrane of cells and are maintained by phospholipid enzymes called scrambalase, floppase and flippase (Daleke, 2007; Hankins et al., 2015). PS is moved to the outer plasma membrane in the early stages of apoptosis and acts as an 'eat-me' signal to phagocytic cells to clear up the debris produced from the apoptotic process (Fadok et al., 1992).

Recently, there has been recognition of the changes in cellular membranes when under stress which include externalisation of PS. This can be initiated through changes in the intracellular or extracellular environment, and identified through annexin binding (Monastyrskaya et al., 2009). However, the process of PS externalisation has been shown to be inducible, reversible, and independent of cytochrome *c* release, caspase activation, and DNA fragmentation (Balasubramanian et al., 2007). The externalisation of PS can be a marker of cell stress and does not have to be associated with ultimate apoptotic cell death (Calianese and Birge, 2020; Nagata et al., 2016). In addition, there is increasing literature suggesting that apoptosis is reversible and "not a one-way street" (Gong et al., 2019).

DARC technology uses the presence of phosphatidylserine molecules on the outer leaflet of the membrane to fluorescently label apoptosing and stressed cells through the binding of annexin A5.

Annexin A5 is an endogenous 36 kDa calcium-dependent phospholipid binding protein that has a high affinity for the phosphatidylserine molecules that are expressed on the cell surface in apoptosis, as shown in Fig. 1 below (Meers and Mealy, 1993). It is therefore widely used as a sensitive probe to detect apoptosis in its early stages. The word annexin is derived from the Greek word *annex*, which means to hold or bind together (Gerke and Moss, 2002). The biological role of annexin A5 is not fully understood, however, like all other annexins, it is thought to have a role in binding molecules together, in particular in the membranes. It is believed to act as a membrane-membrane or membrane-cytoskeleton linker and may have a role in endocytosis and the stabilization of both the cell plasma membrane and individual organelle membranes (Rescher and Gerke, 2004). Annexin A5 has also been reported to have a role in the promotion of autophagy by induction of autophagosome-lysosome fusion and may act as a ligand for the complement protein C1q during apoptosis induction (Creutz et al., 2012; Ghislat et al., 2012; Martin et al., 2012; Park et al., 2016). It is important to note that PS is not externalised and annexin will therefore not bind, in sarmoptosis and parthanatos.

While no member of the annexin family has shown evidence of being a disease-causing gene through loss, mutation or translocation, changes in their expression levels can contribute indirectly to conditions such as cardiovascular disease or cancer (Hayes and Moss, 2004). Annexin 1 has been shown to have an anti-inflammatory role while Annexin 2 has an anti-fibrinolytic role (Gerke and Moss, 2002). The therapeutic potential of Annexin 1 in ischaemic reperfusion injury from strokes and myocardial infarctions is promising due to its anti-inflammatory potential and has been an area of focus for novel drug development programs (Ansari et al., 2018). However it is the role of annexin A5 in apoptosis and stress, and its properties that allow it to bind to the phosphatidylserine molecules on the cell membrane that has been harnessed as the basis of DARC technology (Hayes and Moss, 2004).

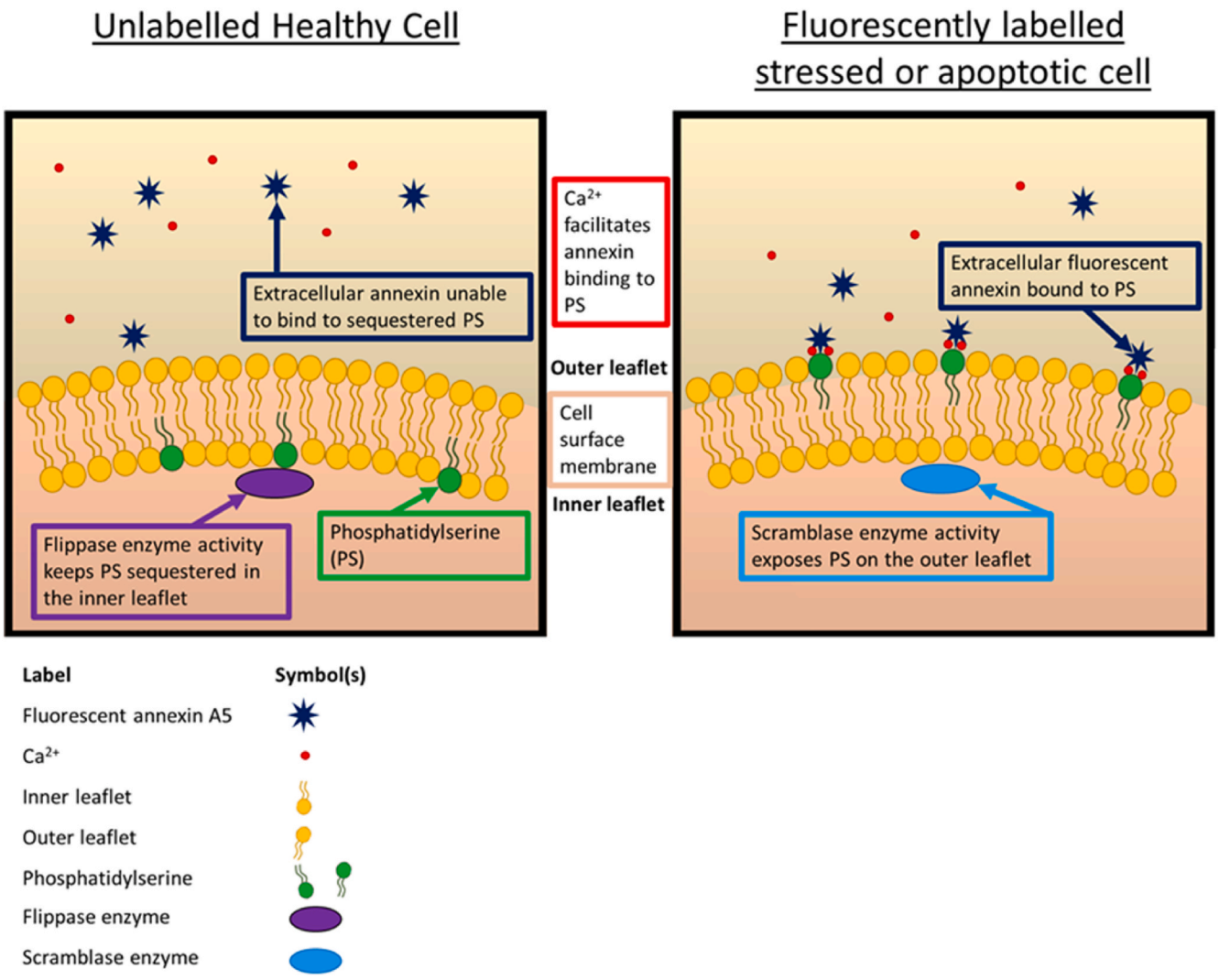

Fig. 1. Diagram of annexin labelling a stressed or apoptotic cell via PS (phosphatidylserine) binding. Fluorescently labelled annexin A5 is only able to bind to PS that is externalised on stressed and apoptosing cell membranes in a calcium-dependent manner, through the downregulation of flippase and activation of scramblases.

2.1.1. Principles of use

In 1995, Vermes et al. first took advantage of the phosphatidylserine-binding property of annexin A5 and proposed its use as an early stage marker of *in vitro* apoptosis using flow cytometry (Vermes et al., 1995). Since this discovery, annexin A5 has been used in several applications either labelled fluorescently or biotinylated as an *in vitro* assay to identify apoptotic cells from necrotic and healthy cells. It has uses both in flow cytometry and imaging. Several cell biology kits that involve annexin A5 are currently in use in flow cytometry for the detection of apoptotic cells. Annexin was first used *in vivo* with radiolabels fluorine-18 (^{18}F), iodine-124 (^{124}I) and Technetium-99 m (^{99m}Tc). Murakami et al. examined the use of ^{18}F labelled annexin A5 and compared it to ^{99m}Tc labelled annexin A5 in the myocardium of the left ventricle of rats after induction of myocardial ischaemia and showed accumulation of both tracers in infarcted areas on positron emission tomography (PET) (Murakami et al., 2004). Similarly Ohtsuki et al. used ^{99m}Tc labelled annexin A5 as a non-invasive method to visualise apoptosis in the thymus of rodents (Ohtsuki et al., 1999). There have been several advances *in vivo* using single-photon emission computed tomography (SPECT) imaging in rodent models with dual radio and fluorescently-labelled annexin A5 investigating the infiltration of macrophages in atherosclerotic plaques, visualisation of apoptosis in tumours, development of infections in prosthetic joints and even models of stroke despite some controversy surrounding this (Belhocine et al., 2015a; Blankenberg et al, 1998, 2006; Ohtsuki et al., 1999; Rescher and Gerke, 2004). While studies have shown the use of annexin A5 in detecting cerebral ischaemia, Zille et al. were unable to utilise annexin A5 to image brain cell death in their model and postulated this could be due to its short half-life or an inability to cross the blood brain barrier (Zille et al., 2014).

More recent research involves various conjugations of annexin A5 into functionalised nanoparticles, core-cross-linked polymeric micelles and cross-linked iron oxide (CLIO) magnetic nanoparticles (Chen et al., 2011; Li et al., 2016). These have allowed for multimodal *in vivo* non-invasive imaging in rodents in various tissues (blood, heart, liver, spleen, kidney, lung, stomach, intestine, muscle, bone, brain and tumour) (Belhocine et al., 2015b).

^{99m}Tc labelled annexin A5 has been used safely in humans in over 30 clinical trials including assessing the response of tumour apoptosis in lymphoma, lung, breast cancer, head and neck cancer to chemotherapy and radiotherapy, severity of stroke and infections in prosthetic joints, summarised in Table 1 below.

2.1.2. Imaging annexin in the retina

Imaging the retina directly is possible in the eye as the cornea and lens are generally transparent allowing the use of techniques such as confocal scanning laser ophthalmoscopy (cSLO) (Webb and Hughes, 1981) and optical coherence tomography (OCT) (Huang et al., 1991).

Table 1
Radiolabelled Annexin A5 Clinical trials.

	INDICATION	PATIENTS	REFERENCE
1	Acute myocardial infarction	7	Hofstra et al. (2000)
2	Cardiac allograft rejection	18	Narula et al. (2001)
3	Lung cancer	10	Belhocine et al. (2002)
	Lymphoma	3	
	Breast cancer	2	
4	Myocardial infarct	12	Boersma et al. (2003)
	Heart failure	4	
	Other heart dis.	3	
	Healthy	1	
5	Healthy	6	Kemerink et al. (2003)
6	Head & neck cancer	20	Van de Wiele et al. (2003)
7	Healthy	6	Lahorte et al. (2003)
8	Myocardial infarction	9	Thimister et al. (2003)
9	Head & neck cancers	33	Kartachova et al. (2004)
10	Atherosclerosis	4	Kietselaer et al. (2004)
11	Head & neck cancers	13	Vermeersch et al. (2004c)
12	Head & neck cancers	18	Vermeersch et al. (2004a)
13	Head & neck cancers	28	Vermeersch et al. (2004b)
14	Follicular lymphoma	11	Haas et al. (2004)
15	Ischaemic muscle pre-conditioning	44	Rongen et al. (2005)
16	Dementia	12	Lampl et al. (2006)
17	Acute stroke	12	Lorberboym et al. (2006)
18	Treatment-induced normal tissue (cancer)	18	Kartachova et al. (2006)
19	Lung cancer	16	Kartachova et al. (2007)
20	Heart failure	9	Kietselaer et al. (2007)
21	Crohn's Disease	14	Van Den Brande et al. (2007)
22	Outcome prediction cancer treatment	38	Kartachova et al. (2008)
23	Breast cancer	10	Kurihara et al. (2008)
24	Head & neck cancers	24	Hoebers et al. (2008)
25	Statin Therapy in I/R injury	60	Meijer et al. (2009)
26	I/R Injury, Angiotensin II Receptor blocker	20	Meijer P. et al. (2011)
27	Cardiac I/R Injury, Rosuvastatin	65	Meijer et al. (2009)
28	Diabetes I/R	36	Engbersen et al. (2012)
29	Carotid atherosclerosis	17	Massalha et al. (2018)
30	Breast cancer	9	Massalha et al. (2018)

Most of the clinical trials performed in the 2000s used GMP 99 mTc-HYNIC–annexin V manufactured by Theseus Imaging Corporation Cambridge, Massachusetts, although this source was closed down by North American Scientific in 2005(Blankenberg, 2009). However, in 2014, Advanced Accelerator Applications began producing GMP 99 mTc-rhAnnexin V-128 kits which have since been in clinical trials (NCT02182609, NCT02677714, NCT02667457, NCT03232580, NCT02978885).

However, it is more difficult to visualise individual retinal cells using these techniques although advances in adaptive optics (AO) have greatly improved photoreceptor imaging, although not widely available. While it is technically possible to obtain an image of single RGCs, the field of view is small and there is a prolonged image analysis and acquisition time (Liu et al., 2017; Rossi et al., 2017).

DARC technology uses fluorescently labelled annexin which acts as a contrasting agent and allows better visualisation of individual retinal cells. DARC studies have trialled several different fluorescent labels of annexin A5. For example, Alexa Fluor 488-labelled annexin A5 was initially used in animal models where DARC was identified in RGCs in real time with non-invasive imaging (Cordeiro et al., 2004). This label has an excitation wavelength on 495 nm and an emission wavelength of 519 nm which enables it to be excited with an Argon laser at 488 nm. The clinical DARC annexin is labelled with the fluorophore DY-776 (Cordeiro et al., 2017) to give ANX776. ANX776 has a near infrared excitation wavelength, peaking at 771 nm, and an emission wavelength peaking at 793 nm. DY-776 was specifically chosen because of its fluorescence excitation and emission spectra being similar to indocyanine green – which is commonly used in retinal angiography (Hassenstein and Meyer, 2009). Compared to 488 nm excitation, NIR wavelengths cause the patient minimal discomfort with less interference from media opacities and luteal pigment, and reduced intrinsic autofluorescent signals (Holz et al., 2017). The binding affinity and biological activity of ANX776 have been extensively tested using *in vivo* and *in vitro* assays and are discussed in detail further below (Cordeiro et al., 2017; Tait et al., 2004).

The process of apoptosis and the presence of externalised PS in apoptosing cells has been shown to last 24 h in various *in vitro* models (Gelles and Edward Chipuk, 2016; Meloni et al., 2011; Wallberg et al., 2016). The application of ANX776 *in vivo* should therefore detect all cells exposing PS in different stages of apoptosis within the preceding 24 h period, in addition to those under stress, and not dying or entering apoptosis. This is important in using DARC to assess retinal disease activity.

2.1.2.1. Confocal scanning laser ophthalmoscopy (cSLO). cSLO has to date been the main instrument used to image the retina with DARC technology. By applying the confocal principle based on a pinhole aperture, image resolution can be enhanced using a point source laser of specific wavelength. Scanning over the whole retina is performed rapidly to minimise both exposure and light scattering, improving patient comfort and compliance.

cSLO allows imaging of sections through biological tissues with better control over depth of field when compared to conventional optical microscopy (A. Maass et al., 2007). As the laser wavelength approaches the excitation wavelength of the fluorescently labelled annexin molecules they are excited and the reflected light from the emission wavelength from the molecules is filtered and acquired as an image. These fluorescently labelled areas highlight the binding of annexin molecules to PS, and therefore cells undergoing stressful conditions and apoptosis (Yap et al., 2018). The images are optimised to remove large non-enhancing structures such as the blood vessels and the optic nerve and are analysed to produce a DARC count to detect the number of annexin A5 labelled spots. Fig. 2 shows an example of the hyperfluorescent DARC spots seen on imaging.

For optimisation of image capture, use of averages of 100 frames combined with eye-tracking has been found to attain a higher signal-to-noise ratio. These spots are seen as hyperfluorescent spots measuring between 12 and 16 μm in diameter in the human eye.

In the first demonstration of DARC, it was possible to visualise the dual-labelling annexin A5 and caspase-3 positive RGCs, and to demonstrate histologically that these DARC spots corresponded to apoptosing RGCs. The RGCs were labelled retrogradely by injecting DiAsp (4-(4-(didecylamino)styryl)-*N*-methylpyridinium iodide) into the superior colliculi of rats (Cordeiro et al., 2004). Sections were then taken and stained with 4,6-diamidino-2-phenylindole (DAPI) to assess the nuclei and Cy5-labelled anti-caspase-3 to confirm apoptosis which correlated to the fluorescent-labelled annexin A5 DARC spots seen *in vivo* (Cordeiro et al., 2004; Yap et al., 2018).

3. Diseases with DARC potential

A number of diseases have had apoptosis identified as being an important aspect of their pathology. Importantly, there is increasing recognition that the retina is involved in CNS disease, with similar mechanisms being involved in the eye and the brain. In addition to being associated with glaucoma and AMD, retinal apoptotic changes have been demonstrated in Alzheimer's & Parkinson's diseases and multiple sclerosis (Cordeiro, 2016).

Table 2 below summarises some of the conditions where apoptosis has been identified in the retina. These are discussed in turn below.

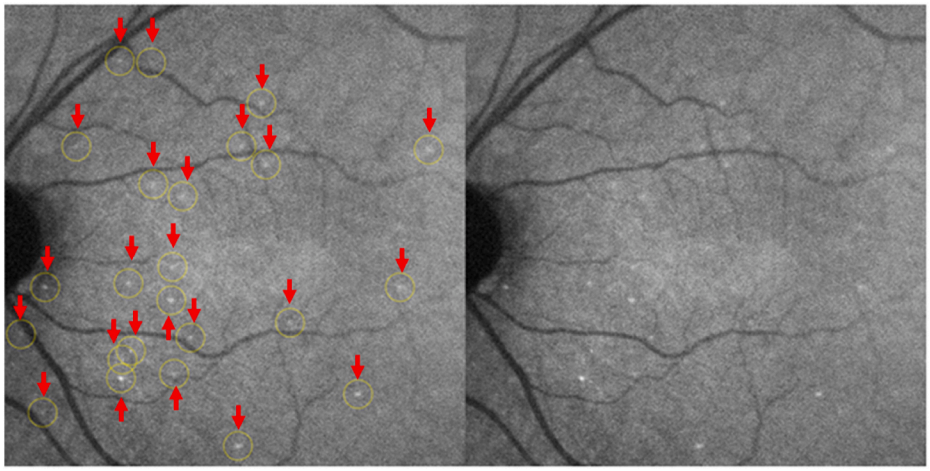

Fig. 2. DARC image of human eye identifying apoptosing RCGs as hyperfluorescent spots (yellow circles with arrows on the left, unannotated image on the right) after injection of ANX776.

Table 2
Conditions in which retinal cell apoptosis has been demonstrated.

Diseases	Retinal Apoptotic Cell	Reference
Glaucoma	Retinal ganglion cells	(Garcia-Valenzuela et al., 1995; Kerrigan et al., 1997; Weinreb et al., 2004)
Age-related macular degeneration	Retinal pigment epithelium, photoreceptors, and inner nuclear layer cells	(Dunaief et al., 2002; Telegina et al., 2017)
Optic Neuritis	Retinal ganglion cells	Shindler et al. (2008)
Alzheimer's disease	Retinal ganglion and photoreceptor cells	(Cao et al., 2013; Ding et al., 2011)
Parkinson's disease	Retinal ganglion and amacrine cells	(Guo et al., 2018; Wilding et al., 2014)

3.1. Glaucoma

Damage to RGCs, and by extension, the vital connection they form between retina and brain is characteristic of glaucoma, an optic neuropathy and leading cause of bilateral blindness worldwide (Weinreb et al., 2016). Whilst IOP-lowering drugs are available to effectively manage and slow glaucoma progression (Brubaker, 2003), early diagnosis and treatment are essential to minimise loss of visual function resulting from irreversible neurodegeneration. Despite the importance of timely treatment, diagnostic rates of glaucoma are poor (Gupta and Chen, 2016; Tielsch et al., 1991; Weinreb et al., 2014), with estimates of as few as 10–50% of all glaucoma cases having been diagnosed (Jonas et al., 2017; Weinreb et al., 2014). Poor diagnostic rates stem from two facets of glaucoma; firstly, the pathology is insidious and variable between patients, secondly, diagnostic tools are often either not sensitive enough, or not applicable to all cases of glaucoma.

3.1.1. Pathologies

The underlying pathology of glaucoma can be categorised based on the angle formed between the iris and the cornea. The two most common types of glaucoma are primary open angle glaucoma (POAG) and primary angle closure glaucoma (PACG) (Shen et al., 2008), with some prevalence as shown below in Table 3.

3.1.1.1. Normal tension glaucoma. Despite IOP being a major risk factor for glaucoma (Parviz et al., 2017), at diagnosis, up to 50% of patients with primary glaucoma have IOP within the normal range (Gupta and Chen, 2016; Jonas et al., 2017). The prevalence of normal tension glaucoma (NTG) has led to IOP no longer being included as a diagnostic criterion for glaucoma (Chang and Goldberg, 2012).

Table 3
Prevalence of glaucoma.

Glaucoma pathology	Prevalence among glaucoma cases	Notes
Primary open angle glaucoma (POAG)	>70% (Jonas et al., 2017) 74% (Quigley and Broman, 2006)	Global prevalence 3.1% (Jonas et al., 2017). Varies with ethnicity and age: highest in Blacks 5.2% at 60 years and 12.2% at 80 years and lowest in East Asians 1.8% at 60 years and 3.8% at 80 years (Kapetanakis et al., 2016)
Primary angle closure glaucoma (PACG)	3.5% (Shen et al., 2008)	Global prevalence 0.6% (Zhang et al., 2021)More common in Asian countries, which account for approximately 77% of worldwide PACG cases (Sun et al., 2017) Corresponds to a disproportionately high number of bilateral blindness cases (3.9 million) compared to POAG (4.5 million) (Sun et al., 2017)

While glaucoma can (and often does) occur in absence of OHT, this does not discount the existing understanding that pressure-gradient related mechanical disturbance of the lamina cribrosa is the primary mechanism of glaucomatous RGC death. It is worth noting that in cases of NTG, reduction of IOP can often successfully slow and manage glaucomatous pathology (Anderson, 2003) despite the lack of OHT. This implies that the eyes of some patients may be more susceptible to glaucoma at lower IOPs.

It has been suggested that predisposition to glaucoma at normal IOP may be affected by CSF pressure (CSF–P). Using magnetic resonance imaging (MRI) to measure the volume of the optic nerve subarachnoid space as a surrogate for CSF-P, NTG patients were observed to exhibit lower CSF-P than POAG patients and healthy controls (Wang et al., 2012). This supports the notion that a pressure gradient across the back of the eye is instrumental in glaucoma pathology, as lowering CSF-P is equivalent to raising IOP. Additionally, it has been observed that the thickness of the lamina cribrosa, as measured by OCT, is significantly lower in NTG patients compared to POAG patients (Park et al., 2012), implicating that resilience (or lack thereof) to structural deformation may indicate predisposition to NTG.

3.1.2. Apoptosis and stress

Apoptosis has been identified as one of the earliest processes occurring in retinal ganglion cells in glaucoma (Garcia-Valenzuela et al., 1995; Kerrigan et al., 1997), with increasing evidence of RGC axonal and dendritic changes occurring beforehand (Calkins, 2012). Annexin 5

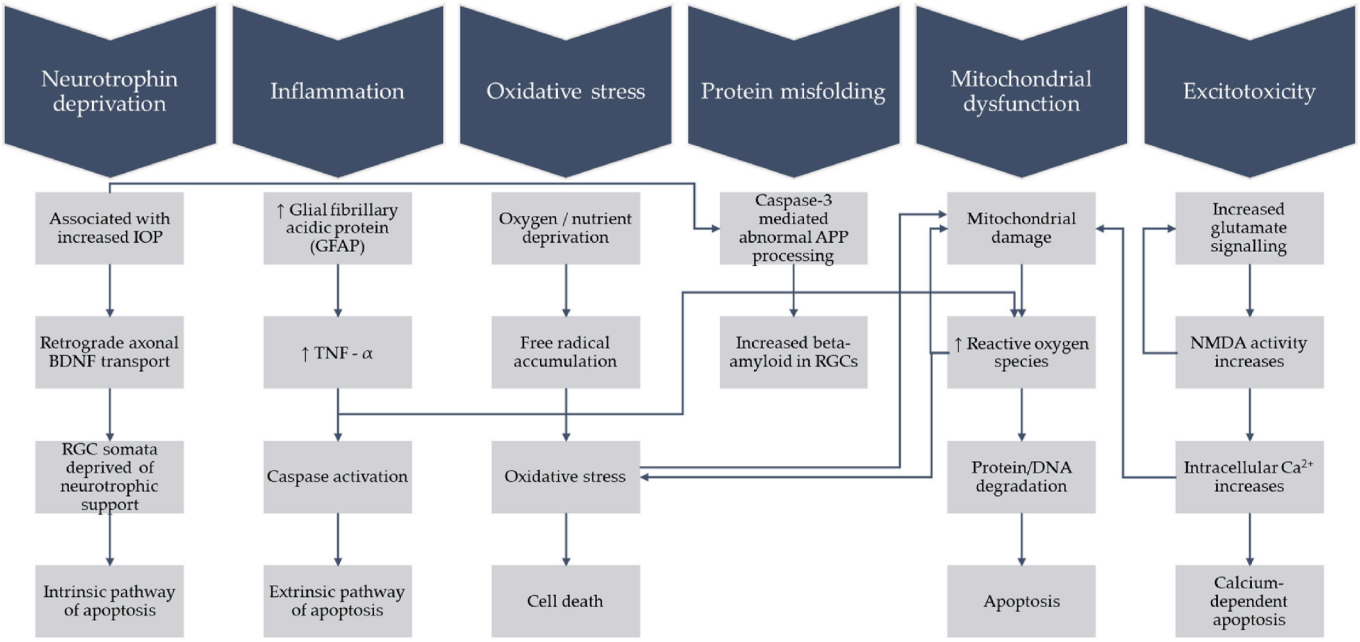

Fig. 3. Processes leading to retinal ganglion cell apoptosis and cell death.

DARC labelling has been colocalised to RGC undergoing apoptosis, as discussed in section 5.1.2. RGC apoptosis has been attributed to a number of different insults, summarised in Fig. 3 below.

3.1.3. *Existing diagnostic tools*

Currently there is no method of diagnosing glaucoma that is applicable to all pathologies and allows for timely detection. For example, tonometry, which measures IOP, while useful in detecting OHT and monitoring response to treatment (as the only approved treatment for

Table 4
Strengths and weaknesses of existing glaucoma diagnostic methods.

	Monitoring method	Measured parameters	Strengths of method	Limitations of method
Slit-lamp examination	Applanation Tonometry	IOP is measured and compared to a 'normal' range (12–21 mmHg).	OHT is a major risk factor for glaucoma (Parviz et al., 2017) and instrumental in pathological disruption of the lamina cribrosa The only clinically-approved disease modifying treatment of glaucoma is IOP reduction A patient's post-medication IOP can correlate with pathology outcome (Leske et al., 2003)	IOP can fluctuate (Malerbi et al., 2005; Sit, 2014), by up to several mmHg over the course of 24 h (Tojo et al., 2016) There is non-trivial measurement variability between different tonometers. At diagnosis, approximately 50% of glaucoma patients have an IOP that would be considered normal (Gupta and Chen, 2016; Jonas et al., 2017)
	Gonioscopy	Drainage angle	Vital in determining potential risk of developing PACG, which may attack suddenly, quickly resulting in irreversible damage (Sun et al., 2017)	Cannot indicate susceptibility to open angle glaucoma
Structural assessment	Fundus photography	Cup to disc ratio, Disc asymmetry	The loss of RCGs and thinning of the neuroretinal rim in glaucoma causing excavation of the optic nerve head is well established. The use of deep learning and artificial intelligence algorithms is being tested in order to automate this assessment, with a view to develop a faster, higher quality system.(De Fauw et al., 2018)	Multiple examinations assessing the change in the optic nerve structure is needed to diagnose glaucoma as a single examination is usually not sufficient due to the variability seen in optic nerve structure. (Khaw and Elkington, 2004; Weinreb et al., 2014) Early diagnosis is not possible as the changes seen in the optic nerve head are as a result of RCG loss and so only apparent after the damage has occurred.
	OCT	RNFL Macular Optic Nerve Head	OCT has been proven to be an objective method to measure RNFL loss, macular thickness and Bruch's membrane opening. Deep learning algorithms also applied to these images. (Tatham and Medeiros, 2017; Wu et al., 2011)	Early diagnosis is not possible as the changes seen in the optic nerve head are as a result of RCG loss and so only apparent after the damage has occurred. Additionally, there is a floor effect with OCT such that RNFL changes are not detectable beyond a certain level of RNFL loss
Functional assessment	Visual field test	Patient's detection of visual stimuli.	Visual field tests are used routinely in clinics throughout the world. Standardised modules have been developed to allow for ageing changes.	Similar to the optic nerve head, visual field defects in glaucoma are only visible until the loss of at least 30–50% of RCGs. Early diagnosis is therefore not possible. There is also the subjectivity and variability of these tests, with reliability and variability between tests major issues (Alasil et al., 2015; Gupta and Chen, 2016; Weinreb et al., 2014)

glaucoma is to reduce IOP), is not effective in cases of normal tension glaucoma. Gonioscopy can reveal the risk of developing PACG, but this is not relevant to the majority of glaucoma cases. Structural changes to the optic nerve are present in all forms of glaucoma (Y. X. Wang et al., 2020), however such assessment often requires historical patient data and precludes early detection. OCT is frequently used for patient assessment in glaucoma. The most commonly used OCT parameter is RNFL thickness, which reflects the damage of RGC axons in the retinal nerve fibre layer. The rate of RNFL loss has been shown to be predictive of visual field loss (Tatham and Medeiros, 2017; Yu et al., 2016) and the rate of progression has been incorporated into most OCT instrument modules, though this does not enable diagnosis prior to loss of retinal cells. A psychophysical visual field test can reveal blind spots in the patient's vision resulting from any kind of glaucoma, but the development of visual blind spots occurs only after substantial and irreversible vision loss has occurred. Table 4 summarises the strengths and limitations of techniques used to clinically diagnose and monitor glaucoma.

3.1.4. Potential glaucoma assessment tools

A gold standard of glaucoma diagnosis needs to paint a detailed and nuanced picture of retinal health, providing measurements that are sensitive enough to detect pathological conditions before substantial damage occurs (Beykin et al., 2021).

One interesting line of research which continues to be developed concerns the assessment of CSF-P. While it is known that IOP is a poor indication of the presence of glaucoma, current understanding of the disease suggests that when IOP is measured to be within the 'normal' range, a lower CSF-P can generate a pathological pressure gradient across the lamina cribrosa, resulting in glaucoma (Wang et al., 2012). By using MRI to measure the orbital subarachnoid space width and using this as an estimate for CSF-P, the difference between IOP and CSF-P can be calculated. This has recently demonstrated promising efficacy in discriminating between ocular hypertensive subjects and controls (Xie et al., 2018). While the applicability of such a technique may be hindered by its reliance upon MRI, it critically could identify pathological pressure gradients across the lamina cribrosa before noticeable vision loss takes place. It is unclear however, if the combination of IOP, CSF-P and MRI would have a high enough specificity or sensitivity to be useful in clinical practice.

A more direct approach to investigating retinal health would be to image retinal cells at a high enough resolution to identify pathology. Unfortunately, resolving the intricate cellular structure of retinal cells *in vivo* is confounded by the very property of the eye that makes it suitable to visual investigation; the optical properties of the eye impart major aberrations onto imaging equipment, limiting resolution and preventing detailed analysis of individual cells. Adaptive optics (AO) overcomes this limitation by measuring aberrations in the eye, and adjusting a deformable mirror to compensate accordingly (Liang et al., 1997; Wynne et al., 2021). In recent years, the enhanced resolution afforded by AO has been paired with OCT and scanning laser ophthalmoscopy (Choi et al., 2011; Dong et al., 2017; Takayama et al., 2013) and has provided extremely high resolution images of retinal cells in glaucoma *in vivo*. Despite presenting a vast enhancement to established retinal imaging techniques, adaptive optics do not yet provide a novel diagnostic tool for glaucoma; imaging structural changes in the eye (such as with OCT) necessitates that substantial cell loss has already occurred. While the improved resolution offered by the introduction of AO may allow more subtle structural changes to be detected, such an approach still precludes early detection. There have been some advances in obtaining images of single RGCs, but currently the small field of view, prolonged acquisition time and complex image analysis make this difficult technology to roll out to clinic (Liu et al., 2017; Rossi et al., 2017).

An evolving area of research is the *in vivo* imaging of labelled retinal cells in experimental models. Rather than simply observing the structure of cells, exogenous fluorescent labels are applied to identify specific populations of cells (Beykin et al., 2021). Retrograde labelling of RGCs using cholera toxin subunit B and fluorogold have both been explored (Yao et al., 2018), based on the principle of only healthy cells supporting retrograde transport to the retina. Additionally, use of an adeno-viral vector has been assessed in mice (Smith and Chauhan, 2018). The resulting retinal fluorescence image can provide data describing the density and distribution of healthy RGCs in the retina, which may highlight a pathological reduction in cells, but application to clinical testing is still unknown.

A more prospective approach to identifying unhealthy RGCs is to directly label these unhealthy cells, thereby avoiding the reliance upon the loss of cells and allowing earlier detection of pathological conditions. This is the basis of using DARC. The caspase-binding probe TcapQ, and its successor KcapQ have been used to fluorescently identify apoptosing RGCs *in vivo* in a rat model of NMDA-induced glaucoma (Davis et al., 2016; P. Wang et al., 2020). This approach enables the identification of retinal pathology prior to structural changes in animal models, however KcapQ his still confined to preclinical testing.

3.1.5. Glaucoma modelling

The loss of RGCs in glaucoma can occur as early as 10 years before it manifests symptomatically in patients as visual field defects (Ahmad, 2017). By detecting these dying cells early, it may be possible to recognise the disease process and intervene before irreversible damage and loss of vision occurs. While the pathophysiology of glaucoma is not fully understood, the main mechanism proposed for degeneration of RGCs is through apoptosis (Almasieh et al., 2012; Baudouin et al., 2020). Early detection may reduce the lag between the start of apoptosis of RGCs and the diagnosis of glaucoma and commencement of treatment. DARC has enabled research into this crucial area using advanced optical techniques to image and track individual RGCs *in vivo* over time. This has also enabled examination of cellular mechanisms that lead to their degeneration (Cordeiro, 2007).

The figure below (Fig. 4), attempts to model the hypothetical trajectory of the visual function of a patient with glaucoma (pathological DARC count) to sight impairment, and is adapted from a visual field model by Dr Moraes et al. (De Moraes et al., 2017). A patient with disease detected early with DARC would be able to undergo early intervention and preserve their visual function (green line). A patient identified later would receive late intervention (orange line) and also benefit by treatment delaying their progression to sight impairment when compared to no intervention. A patient receiving no intervention would progress to sight impairment much faster and at a much younger age. As there is a significant difference in visual function in the early intervention group, there is evidence to suggest early detection and

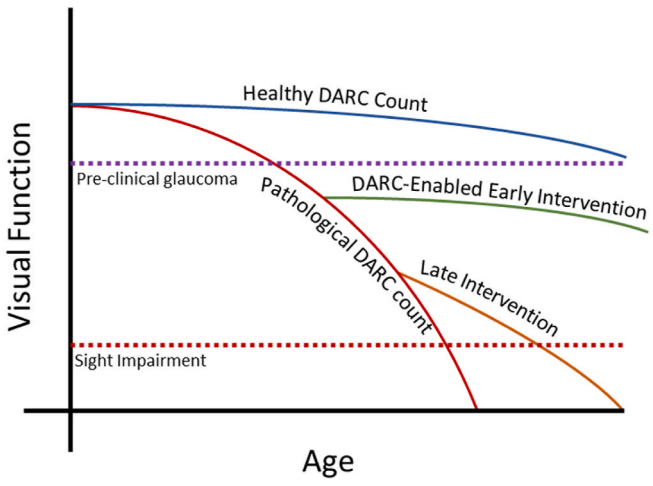

Fig. 4. Modelling the hypothetical deterioration in visual function and DARC counts in a patient with glaucoma to highlight how early detection and intervention could delay progression to sight impairment.

intervention in these patients dramatically improves survival of the RCG population and preserves visual function (see Fig. 4).

3.2. Age related macular degeneration

Age related macular degeneration (AMD) is the leading cause of blindness in the developed world (Boyer et al., 2017; Lambert et al., 2016; Seddon, 2017). As the life expectancy in developed countries continues to increase, the incidence of AMD has grown substantially creating a significant global burden of disease. It is characterised by progressive loss of central vision due to degenerative changes at the macula, the area of the retina that is responsible for detailed central vision (Chopdar et al., 2003).

3.2.1. Pathologies

The Age-Related Eye Disease Study (AREDS) divided AMD into 5 different categories to assess its severity based on the amount, size and nature of drusen present, the area and location of retinal pigment epithelium atrophy and the presence of neovascularisation (Kassoff et al., 2001). Based on this, it can be classified into early, intermediate or advanced disease (Lambert et al., 2016). Early AMD is categorised by irregularities in the retinal pigment epithelium (RPE) and deposition of small drusen (<63 mm) (Datta et al., 2017). Intermediate AMD had larger size drusen which are arranged more confluently and advanced disease manifests as geographic atrophy or neovascularisation (Lambert et al., 2016).

It can also broadly be characterised into two forms – 'wet' AMD where intraretinal and subretinal fluid are prevalent as result of choroidal neovascularisation (CNV) and 'dry' AMD where vision loss is irreversible due to geographic atrophy.

In early "dry" AMD, as RPE transport function deteriorates, drusen deposition occurs and overlying photoreceptor damage (Kanagasingam et al., 2014). A recent finding with OCT has suggested that in early AMD, the RPE/Bruch's membrane complex thickens whilst photoreceptor layer thins (Brandl et al., 2019). With increasing damage, there ensues photoreceptor, RPE and choriocapillaris atrophy, with sharply defined areas of depigmentation (L. S. Lim et al., 2012). Photoreceptor dysfunction has been reported in intermediate AMD along with significant RPE thickening (Parisi et al., 2020). More recently, the occurrence of photoreceptor atrophy without RPE atrophy has been recognised. Histological correlation with OCT findings are incorporated in the Classification of Atrophy Meetings (CAM) grading of Macular Atrophy including: cRORA (complete retinal pigment epithelium (RPE) and outer retinal atrophy), iRORA (incomplete RPE and outer retinal atrophy), cORA (complete outer retinal atrophy) and iORA (incomplete outer retinal atrophy) (Sadda et al., 2018). Moreover, cRORA is defined by specific OCT criteria: (1) a region of hypertransmission of at least 250 μm in diameter, (2) a zone of attenuation or disruption of the RPE of at least 250 μm in diameter, (3) evidence of overlying photoreceptor degeneration, and (4) absence of scrolled RPE or other signs of an RPE tear. Table 5

Table 5
Risk Factors associated with AMD.

Risk Factor	
Age	Increasing age is the strongest risk factor for developing AMD (Heesterbeek et al., 2020; Lambert et al., 2016)
Sex	No clear evidence. Some studies suggest female sex have a higher progression to AMD but this remains to be established (Heesterbeek et al., 2020; Lambert et al., 2016)
Smoking	2-4 times more likely to develop AMD if smoker (Heesterbeek et al., 2020)
Obesity	High BMI associated with increased risk of developing AMD (Heesterbeek et al., 2020; Lambert et al., 2016)
Diet	Diets high in antioxidants, vegetables and fruits may have a role in preventing progression of AMD (Heesterbeek et al., 2020) As per AREDS2 study, there may be a role in vitamin supplements containing vitamin C and E, beta carotene and zinc in early AMD (Chew et al., 2012)
Ethnicity	Caucasians may have higher rate of developing AMD, especially neovascular AMD (Lambert et al., 2016)
Genetic	Over 40 genes identified including complement factor H, ARMS2/ HTRA1 gene and lipid metabolism genes (Cascella et al., 2018; Heesterbeek et al., 2020; Lambert et al., 2016)

3.2.2. Retinal apoptosis and stress

The occurrence of apoptosis in RPE, photoreceptors and inner nuclear cells has been linked to the development of AMD (Dunaief et al., 2002; Kaarniranta et al., 2020; Telegina et al., 2017). Annexin 5 DARC labelling has been colocalised to photoreceptors and inner nuclear cells undergoing apoptosis, as discussed in section 5.1.2.3. In neovascular AMD, the externalisation of phosphatidylserine in stressed endothelial cells has been highlighted as the very earliest sign of angiogenesis (Corazza et al., 2020; Li et al., 2015).

3.2.3. Existing diagnostic tools

OCT (optical coherence tomography) is the gold standard imaging technique used in detecting changes at the macula and diagnosing AMD (Gualino et al., 2019). Unlike its predecessors, fluorescein angiography and indocyanine green angiography, it is a non-invasive method of imaging the retina (Rosenfeld, 2016). It allows clear visualisation of the layers of the retina, presence of drusen and intraretinal and subretinal fluid, allowing easy comparison when assessing response to treatment. The RPE cells, photoreceptors and inner retinal cells are damaged in AMD.

The treatments for AMD are centred around neovascular AMD at present (as no treatment has been approved for geographic atrophy or the dry form of AMD). This is in the form of anti-angiogenic intravitreal injections (anti-vascular endothelial growth factor or anti-VEGF) that inhibit the formation of new blood vessels and prevent leakage from these that creates further damage to the macula and manifests as visual loss (Mettu et al., 2020). Patients may require several injections over a long period of time, with the risk of infection and loss of the eye associated with every injection. The cost of these invasive therapies is significant with each injection costing up to £1000 in the UK and some patients requiring monthly injections (Raftery et al., 2007).

With the healthcare costs of managing patients with neovascular AMD increasing significantly, early diagnosis AMD is crucial in addition to developing robust methods to identify its progression early (Keenan et al., 2020; J. H. Lim et al., 2012).

3.2.4. AMD modelling

3.2.4.1. Neovascular AMD. Neovascular AMD is characterised by the presence of intraretinal fluid, subretinal fluid and choroidal neovascularisation. These changes occur due to angiogenic activity, development of new immature blood vessels that cause leakage of fluid under the retina that can quickly progress to blindness if not treated promptly (Ambati and Fowler, 2012). Treatments aimed at neovascular AMD are therefore anti-angiogenic in the form of anti-VEGF injections.

An *in vivo* pilot study conducted in rabbits demonstrated this angiogenic activity of VEGF. Fig. 5 describes the findings from the study. Human VEGF (1 μg in 50 μl) was injected into the left eye only of three rabbits after gaining appropriate ethical approval. The rabbits received an intravenous ANX776 injection 48 h after the anti-VEGF injection and underwent DARC imaging. When compared to the control eye, all eyes treated with human VEGF had higher DARC counts. The rabbits also underwent fluorescein angiography 4 days after administration of VEGF, which showed increased fluorescein leakage in the treated eyes compared to the control suggesting DARC was identifying the early changes of angiogenesis in the retina (Corazza et al., 2020).

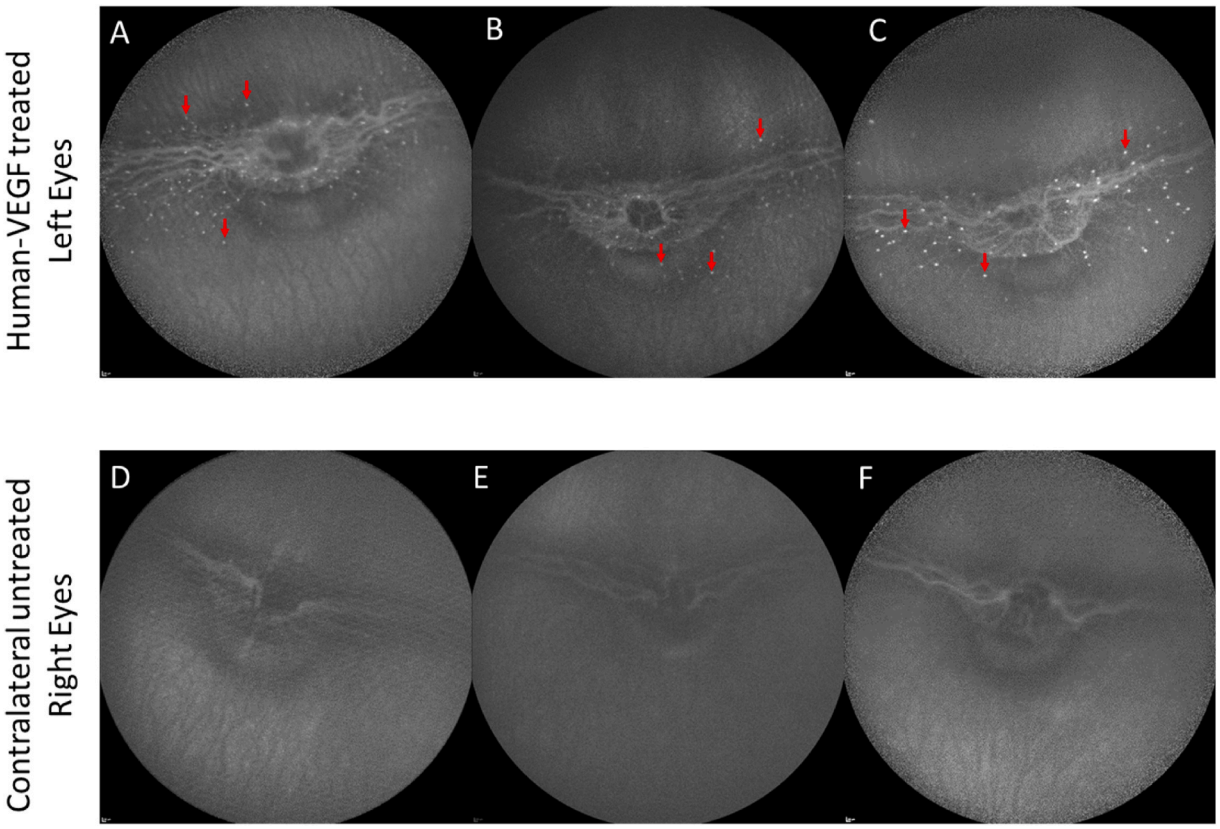

Fig. 5. Comparison of rabbit eyes treated with human VEGF (A–C) to their corresponding control untreated eye (D-F; respectively) showing DARC spots in VEGF-treated eyes only. Three examples of hyperfluorescent spots are highlighted with red arrows in each eye that contains DARC spots.

It is thought that phosphatidylserine translocation in endothelial cells occurs as part of the early stages of angiogenesis in CNV(Li et al., 2015). In their paper, Li et al. clearly showed in a laser model of CNV that PS was exposed in CNV endothelium, and that its targeting with PS-antibodies led to a significant reduction of CNV formation (Li et al., 2015).

By labelling exposed PS in endothelium, DARC identifies areas of endothelial cell stress which can predict new vessel formation, leakage and development of subretinal fluid before it causes permanent visual loss, as described in Corazza et al. (2020). However, the detection of stress by DARC may result in an effect that is relatively rapid and short-lasting.

3.2.4.2. Dry AMD. The pathophysiology of dry AMD is not fully understood and as described previously there are no current treatments available to halt its development or progression.

There is some evidence that the geographic atrophy seen in dry AMD is caused by increased apoptosis of the retinal cells at the macula. Analysis of post-mortem human retinas with AMD with terminal deoxynucleotidyl transferase dUTP nick end-labelling (TUNEL) used to detect fragmented chromatin in the cells showed a statistically significant increase in apoptosis in the inner choroid, retinal pigment epithelial (RPE) cells, the photoreceptor cells and the inner nuclear layer of the retina when compared to normal retinas (Dunaief et al., 2002). These areas of increased apoptotic activity were more significant at the edges of RPE atrophy which correlated clinically with expanding areas of visual field loss in patients and support the role of apoptosis in the pathogenesis of dry AMD. Using DARC technology we may be able to predict this expanding macular atrophy by detecting these apoptosing cells early, as discussed later.

3.3. Alzheimer's disease

Alzheimer's disease (AD) is currently the leading cause of dementia worldwide. As the ageing population grows, its prevalence increases and it currently accounts for 80% of all diagnoses of dementia (Weller and Budson, 2018). The increasing aging population projects the number of AD cases in the United States to triple by 2050, accompanied by soaring economic and social burden (Brookmeyer et al., 2018). This has highlighted the need for non-invasive, inexpensive, and highly accessible biomarkers to enable early detection of AD with the hope that population-based screening will aid the progress in managing this devastating condition (Alber et al., 2020).

3.3.1. Pathologies

AD is characterised histologically by the deposition of beta amyloid plaques in the brain and neurofibrillary tangles formed by aggregation of tau (Weller and Budson, 2018). Amyloid-β and tau have been shown to cause apoptosis by deregulating the oxidative phosphorylation system in mitochondria, causing damage and triggering apoptosis via the caspase pathway (Wong et al., 2020). Amyloid-β and tau have been shown to have a role in upregulating pro-apoptotic molecules such as BAX and downregulating anti-apoptotic BCL-2 causing further neuronal cell death through apoptosis (Paradis et al., 1996).

It is now thought there is a pre-clinical stage of AD where evidence of amyloid plaques in the brain may be present years prior to the onset of any cognitive changes. However there are currently no clinical criteria to diagnose this stage (Budson and Solomon, 2012). The second stage, mild cognitive impairment in AD, is detected once mild changes to memory and other cognitive abilities is apparent and the third stage is dementia due to AD where patients exhibit loss of two or more cognitive functions leading to loss of the ability to carry out activities of daily function (Budson and Solomon, 2012). Visual defects in AD may occur

early in the disease process as manifest as reduced visual acuity, colour perception, contrast sensitivity and visual field defects (Yap et al., 2019).

3.3.2. Retinal cell apoptosis

In vitro studies have demonstrated Amyloid β-induced RGC and RPE apoptosis, with animal models providing further evidence(Cao et al., 2013; Ding et al., 2011; Gupta et al., 2020). Recently, both RGC (Grimaldi et al., 2018) and amacrine (L. Gao et al., 2015) apoptosis have been described in transgenic models. In fact Grimaldi et al. suggested RGC apoptosis in young asymptomatic 3xTg-AD mice, occurred early with parallel changes of protein aggregates and neurodegeneration in the brain (Grimaldi et al., 2018). We recently reported DARC could be used as an early indicator of neuroprotective treatment in this same model (Shamsher et al., 2019).

3.3.3. Existing diagnostic tools

As a definitive diagnosis of AD requires a post-mortem examination of brain tissue, current diagnostic tools involve assessing the cerebrospinal fluid for elevated tau levels and presence of beta amyloid, demonstrating temporal and medial parietal cortex atrophy on MRI scans or PET scans showing reduced metabolism in the temporal and parietal cortex (Budson and Solomon, 2012). Using fluorodeoxyglucose PET and imaging it is possible to detect this neuronal injury but there is no current tool available to image individual cells (Marcus et al., 2014).

Pathological studies looking at the eye in AD post-mortem have shown evidence of axonal neurodegeneration in RCG cells and loss of RNFL. While several transgenic models of AD have shown the presence of amyloid deposition and tau aggregates in the retina, there is no clear consensus regarding the extent to which this occurs in the retina of human patients with AD (Ho et al., 2014). OCT imaging of the optic disc categorising RNFL thinning as well as OCT imaging of the macula may be useful in detecting early cognitive impairment (Chan et al., 2019; Ferrari et al., 2017). Studies have shown changes in the macular volume and ganglion cell and inner plexiform layers may correlate with lower mini-mental state examination scores, which are used in the diagnosis of dementia (Iseri et al., 2006).

3.3.4. Alzheimer's disease modelling

The characteristic amyloid beta aggregates seen in the brain of patients with AD are also present in the retina in humans (Koronyo et al, 2012, 2017). Additionally, some hyperphosphorylated tau protein has been detected in the retina of some patients with AD (Ho et al., 2014). The significance of these changes are therefore unclear and may suggest there is secondary neurodegeneration in AD (Yap et al., 2019). In mouse models of AD (APPSWE/PS1ΔE9) retinal amyloid-β plaques were detected in increased quantities correlating with disease progression (Koronyo-Hamaoui et al., 2011). Supporting studies have demonstrated retinal plaques in mice developed prior to any changes seen in the brain highlighting the importance of retinal imaging for early diagnosis (More and Vince, 2015).

RNFL thinning around the disc in AD, on the other hand, has been proven to be a significant finding in examination of these patients with OCT. The rate of this thinning appears to be faster when compared to thinning due to the normal ageing process and thinning in the inferior sector of the pRNFL is thought to be the most sensitive marker to detect progression of cognitive decline in AD (Kesler et al., 2011; Shen et al., 2013). As described previously there is also growing evidence of thinning of the RNFL, ganglion cell layer and the inner plexiform layer on examination of the posterior pole with OCT imaging that has been correlated with worse cognitive function (Choi et al., 2016; L. Y. Gao et al., 2015). As these changes are thought to occur due to apoptosis of cells, DARC technology can be used to detect these cells at risk early. With the significant disease burden of AD increasing there is an unmet need for early diagnosis and treatment of patients.

Changes seen in the brain in Down's syndrome are similar to those described in autosomal dominant Alzheimer's disease and are seen more than two decades before the onset of Alzheimer's disease (Fortea et al., 2020). Therefore, patients with Down's syndrome are thought to be a suitable population for clinical trials for Alzheimer's disease and have been used as a model in DARC clinical trials.

3.4. Parkinson's disease

Parkinson's disease (PD) is a neurodegenerative condition characterised by a triad of bradykinesia, rigidity and a resting tremor (Duyckaerts et al., 1993). It can also affect the autonomic nervous system, cause cognitive decline, mood disorders and affect visual functioning (Chaudhuri et al., 2006). It is currently the second most common neurodegenerative condition worldwide after AD (Kouli et al., 2018).

3.4.1. Pathologies

Deposition of alpha synuclein in the substantia nigra leading to loss of dopaminergic neurons is the pathological hallmark of PD (Duyckaerts et al., 1993). Neuronal loss is not limited to the substantia nigra and post-mortem examination of the retinas of patients with PD have shown similar deposition of alpha synuclein in the inner nuclear layer, inner plexiform and the ganglion cell layers as well as reduced dopamine (Bodis-Wollner et al., 2014; Harnois and Di Paolo, 1990). While the exact pathogenesis of neuronal loss in PD is still not apparent, there is significant evidence of the role of apoptosis with increased caspase activity seen when compared to healthy controls (Mogi et al., 2000).

Similar to AD, it is thought that there is a pre-clinical, asymptomatic stage in PD that may occur as early as 14 years prior to the manifestation of motor symptoms and loss of function. These early signs may include autonomic dysfunction, psychiatric disturbances and rapid eye movement sleep disorders (Kouli et al., 2018). The classic motor symptoms may not present until there is significant loss of dopaminergic neurons of at least 50–80% (DeMaagd and Philip, 2015).

3.4.2. Apoptosis of RGC and amacrine cells

The process of apoptosis has been identified in the nigrostriatal pathway as a mechanism of dopaminergic loss, and demonstrated in the retina (Guo et al., 2018; Mogi et al., 2000; Wilding et al., 2014). RGC, photoreceptor and amacrine degeneration have all been identified in a rotenone model of Parkinson's disease (Biehlmaier et al., 2007; Esteve-Rudd et al., 2011), with DARC showing early changes, and being predictive of treatment efficacy in this same model (E.M. Normando et al., 2016).

3.4.3. Existing diagnostic tools

PD is currently diagnosed clinically by the presence of two of the motor symptoms described. Definitive diagnosis is histological with the presence of Lewy bodies in neurons that represent the deposition of alpha synuclein (Kouli et al., 2018). No specific brain imaging technique has been recommended for routine diagnosis of PD in clinical practice however, SPECT, PET and MRI scans can be used to differentiate between other causes of symptoms such as normal pressure hydrocephalus that may present similarly or between other forms of parkinsonism (Pagano et al., 2016).

RNFL thinning particularly around the optic nerve (called peripapillary RNFL or pRNFL) in PD has been reported by several studies as a sign in PD that is different from that seen in AD. A 5 year prospective longitudinal study looking at the association between pRNFL thinning on OCT and symptoms in PD showed some correlation between the symptom severity and progression with increased pRNFL thinning (Satue et al., 2017). In addition to this, studies assessing the RNFL thinning seen on OCT, retinal function and dopaminergic activity in the substantia nigra using PET and MRI scans have some correlation supporting the hypothesis that there may be some benefit in attempting to identify retinal biomarkers for PD (Ahn et al., 2018; Garcia-Martin et al., 2014; Mailankody et al., 2015).

3.5. Multiple sclerosis

Multiple sclerosis is an autoimmune demyelinating disorder of the central nervous system (Compston and Coles, 2008).

3.5.1. Pathologies

Demyelination of the axons causes loss of function and progressive neurological disability affecting the motor, sensory, autonomic and visual pathways (Krieger et al., 2016). Optic neuritis is the ocular manifestation of MS. It occurs as a result inflammation due to demyelination of the optic nerve and can potentially be blinding (Galetta et al., 2015). It presents with acute vision loss, which in 40–60% is associated with a degree of permanent visual loss, even after resolution of the acute inflammatory event (Wilhelm and Schabet, 2015). The irreversible changes in vision closely correlate with RNFL thinning, and this is attributed to permanent damage to RGC axons.

3.5.2. Apoptosis of RGC

It has been shown in experimental models of inflammatory demyelination that RGC apoptosis occurs in the early stages of disease – following demyelination and axonal injury (Shindler et al., 2008). RGC apoptosis has been identified in models of experimental autoimmune encephalomyelitis (Horstmann et al., 2013; Meyer et al., 2001).

3.5.3. Existing diagnostic tools

The McDonald criteria are used to determine the diagnosis of MS. It is currently diagnosed through MRI scans showing inflammation and atrophy in the form of demyelinating lesions disseminated in time and space in the brain and spinal cord and through examination of the CSF where the presence of oligoclonal bands are indicative of immune activity (Thompson et al., 2018).

OCT is increasingly advocated as a marker of disease severity in patients with MS after it was first used in 1999. It is a much faster and more cost-effective method of measuring the severity of MS when compared to repeated MRI scans, and has shown benefit in predicting levels of disability with MS and quality of life (Schinzel et al., 2014; Walter et al., 2012). Recent evidence has also shown that RNFL thickness correlates with MRI-estimated whole brain atrophy in MS patients (Dörr et al., 2011; Gordon-Lipkin et al., 2007).

Comparison of healthy and MS patients using OCT and post-mortem analysis have shown optic nerve damage in association with RGCs and microglia changes (Saidha et al., 2015; Sotirchos and Saidha, 2018),] with retinal thinning following microglia-mediated immune responses [(Pawlitzki et al., 2020; Saidha et al., 2015)]. OCT has been used to show that RNFL thinning occurs in the eyes of MS patients without prior history of optic neuritis (MS-NON) although to a lesser extent (Petzold et al., 2017).

3.5.4. Multiple sclerosis modelling

There is growing evidence that RCG apoptosis is responsible for the changes seen in the thinning RNFL of patients with optic neuritis (Garcia-Martin et al., 2014; Syc et al., 2012). This has been shown in models of experimental autoimmune encephalomyelitis (EAE) which is the most commonly used animal model of demyelinating disease where active immunisation is needed to induce optic neuritis and a MOG-specific TCR transgenic model (Guan et al., 2006; Shindler et al., 2008). They demonstrated that RGC apoptosis occurred after inflammatory cells infiltrated the optic nerve to induce demyelination, suggesting that an axonopathy resulted in RGC apoptosis (Guan et al., 2006; Shindler et al., 2008). They also investigated the timing of steroid treatment in EAE mice with two corticosteroids (dexamethasone and methylprednisolone) before (days 0–14) and after optic nerve inflammation (days 10–14) developed (Dutt et al., 2010). Their study found that early treatment with corticosteroids before the onset of inflammation suppressed development of optic neuritis and prevented RCG loss. Their results also suggested that chronic immunomodulation could prevent recurrent optic neuritis and RGC damage. However, all these results were histological, with no *in vivo* or longitudinal assessment of the same animals over time.

As DARC technology has been shown to be able to track retinal apoptosis and retinal layer changes over time, it can be feasibly applied with the same principles to an optic neuritis model to determine MS activity. There is no current way to identify patients who lose vision permanently. By identifying patients who are at high risk of permanent vision loss it may be possible to stratify patients and determine who can be targeted with immunotherapies to prevent this. As these immunotherapies are costly, using DARC technology to be able to identify those that will respond to the therapies and are at higher need of them, will aid significantly in resource allocation of these therapies.

4. Pre-clinical DARC

Annexin A5 has demonstrated impressive *in vivo* performance in the labelling of stressed and dying cells. Furthermore, fluorescent annexin has established that precise single-cell identification of stress is possible. However, achieving specific labelling of cell stress *in vivo* is a challenging feat in most animal tissues, particularly in the CNS, as flesh and bone obscure neuronal cells from non-invasive light-based imaging. The eye, on the other hand, having evolved to optimise the transmission of external light to the CNS, presents an unparalleled window through which to observe neuronal cells.

The unique power of being able to non-invasively observe the health (or lack thereof) of retinal neurons provides revolutionary new opportunities in the clinical treatment of glaucoma:

- An accelerated rate of RGC loss can implicate pathology before symptoms, irrespective of the type of glaucoma affecting a patient
- The level of apoptosis may predict the rate of RGC loss and be used as a surrogate of the endpoint of RGC and vision loss
- Thus the apoptosis level may be used instead of the rate of RGC loss to evaluate how well a patient is responding to a given treatment
- Novel treatments may be assessed based on changes to the apoptosis level and in turn to the rate of RGC loss

The studies that have used DARC to assess disease and treatments are discussed below, with a summary in Table 6 provided below.

It is also important to note that at least 4 groups have independently validated and published the use of *in vivo* administered Alexa Fluor 488 or FITC-conjugated annexin A5 in the retina as a marker of retinal cell apoptosis(Cheng et al., 2015; Ito et al., 2019; Kanamori et al., 2010; Reichstein et al., 2007). Furthermore, as far as we are aware there are 2 other publications which clearly show that annexin A5 can be used to detect *in vivo* retinal apoptotic changes(Ding et al., 2018; Head et al., 2017).

4.1. Establishing DARC principle

4.1.1. Early work and In vivo imaging

In 2004, a series of experiments were carried out to measure a fluorescent annexin signal *in vivo* in rat and non-human primate (macaques) models of RGC death as summarised in Table 7 (Cordeiro et al., 2004).

Recombinant human annexin A5, produced in BL21 E. Coli (Coxon et al., 2011), was conjugated with a 488 nm wavelength fluorophore (Alexa Fluor 488), and was then intravitreally injected. Utilising the 488 nm fluorophore meant that established fundus autofluorescence imaging equipment and protocols could be used as a starting point for DARC. The animal models used in this research were selected to demonstrate the utility of DARC most effectively, including a well-established rat OHT model of glaucoma, optic transection (which selectively results in RGC death), and a non-human primate model of widespread retinal neuronal death, forming a strong foundation for the applicability of

Table 6
Pre-clinical DARC studies. Note that * after the paper title denotes the use of 776 nm fluorescent annexin A5, all other papers used 488 nm fluorescent annexin A5.

Title	Summary	Reference
Real-time imaging of single nerve cell apoptosis in retinal neurodegeneration	Demonstrated *in vivo* cSLO imaging of retinal cells (in rats and primates) labelled with intravitreally-administered DARC. These cells were immunohistochemically identified as positive for anti-caspase-3, and positive for retrograde DiAsp labelling (applied at the superior colliculus) implicating the labelled cells as apoptosing RGCs. This demonstrated the utility of DARC as an *in vivo* marker of cell stress.	Cordeiro et al. (2004)
Retinal Ganglion Cell Apoptosis in Glaucoma Is Related to Intraocular Pressure and IOP-Induced Effects on Extracellular Matrix	DARC was intravitreally administered to a rat OHT model of glaucoma 2 h prior to death. Flat-mount retinas were fluorescently imaged using confocal laser scanning microscopy to show that apoptosis-linked enzyme MMP-9 colocalised with DARC labelling of cells. DARC-positive cells indicated a correlation between peak IOP and cell death in the retina. The count of DARC labelled cells in this model of glaucoma was contrasted to that of TUNEL, which labels fewer cells. This was attributed to the fact that PS externalisation occurs across a broad time span of cell stress, while TUNEL detects only a fraction of apoptosis at which DNA fragments.	Guo et al. (2005)
Assessment of Neuroprotective Effects of Glutamate Modulation on Glaucoma-Related Retinal Ganglion Cell Apoptosis *in vivo*	*In vivo* and histological DARC counts were used to assess the efficacy of NMDA receptor antagonism-based neuroprotective strategies in rat models of OHT and staurosporine-induced apoptosis. The treatment was observed to significantly reduce DARC count in a dose-dependent manner.	Guo et al. (2006)
Targeting amyloid-β in glaucoma treatment	Within a rat OHT model of glaucoma, it was investigated whether reduction of retinal Aβ (a pathological species suggested to play a role in glaucomatous optic neuropathy) using different intravitreally injected therapeutic agents would reduce RGC apoptosis. The use of intravitreally administered DARC allowed repeated *in vivo* measurements of RGC stress over the course of 4 months, demonstrating a reduction in DARC count in response to the administration of treatment.	Guo et al. (2007)
Assessment of Rat and Mouse RGC Apoptosis Imaging *in vivo* with Different Scanning Laser Ophthalmoscopes	Intravitreally injected staurosporine was used to induce RGC death in both rats and mice. DARC was subsequently administered intravitreally and imaged *in vivo*. DARC was observed to perform similarly in both species, with the apoptotic inducer resulting in the appearance of fluorescent points following DARC administration. The percentages of histologically measured apoptotic points that were observed *in vivo* were similar between rats and mice (60% and 54% respectively).	Annelie Maass et al. (2007)
Real-time *in vivo* imaging of retinal cell apoptosis after laser exposure	Using a laser to create retinal lesions in anaesthetised rats, apoptosis of retinal cells was assessed *in vivo* using DARC, imaging from baseline until 90 min post-insult. Fluorescent spots (indicative of apoptosis) were found to result from laser insult, predominantly located in the inner nuclear layer.	Schmitz-Valckenberg et al. (2008)
In vivo imaging of retinal cell apoptosis following acute light exposure	Retinal apoptosis resulting from 2 h of blue light damage in rats was demonstrated using DARC *in vivo*. No pathological retinal changes were detected immediately following light exposure, but DARC signal was observed 24 h later, which was histologically confirmed as photoreceptor apoptosis.	Schmitz-Valckenberg et al. (2010)
Imaging multiple phases of neurodegeneration: a novel approach to assessing cell death *in vivo*	Through DiI retrograde labelling of RGCs, PI labelling of necrotic cells, and DARC labelling apoptotic cells, the development of cell death in rat and mouse models of retinal pathology was imaged over the course of hours.	Cordeiro et al. (2010)
Imaging in DRY AMD	Histological imaging of intravitreally injected DARC was shown to label stressed cells in different layers of the retina within an ischaemic mouse model. The labelled layers were the inner nuclear layer, the outer nuclear layer, and the photoreceptor layer.	Normando et al. (2013a)
A semi-automated technique for labelling and counting of apoptosing retinal cells	A parametric-based image analysis technique was developed for the counting of DARC spots. This offered a faster and less labour-intensive alternative to manual counting.	Bizrah et al. (2014)
Unexpected low-dose toxicity of the universal solvent DMSO	By measuring DARC signal *in vivo*, it was discovered that surprisingly low doses of DMSO (as little 5 μL of 1% concentration) were sufficient to induce retinal cell stress and apoptosis.	Galvao et al. (2014)
Effect of the Ab Aggregation Modulator MRZ-99030 on Retinal Damage in an Animal Model of Glaucoma	Using the Aβ aggregation modulator MRZ-99030, intravitreally administered DARC counts (imaged *ex vivo*) in the IOP-based Morrison model of glaucoma in rats were observed to reduce in response to treatment. This effect was observed to occur without any reduction to IOP.	Salt et al. (2014)
Direct optic nerve sheath (DONS) application of Schwann cells prolongs retinal ganglion cell survival *in vivo*	Delivery of Schwann cells in a novel manner directly to the optic nerve (versus delivery via intravitreal injection) reduced RGC death in a partial optic nerve transection rat model. This effect was demonstrated by the *in vivo* measurement of DARC signal.	Guo et al. (2014)
Adenosine A3 receptor activation is neuroprotective against retinal neurodegeneration*	Activation of the adenosine A_3 receptor using 2-ClIB-MECA was demonstrated to be neuroprotective. This was demonstrated by treatment resulting in a significant DARC count reduction in a rat model of partial optic nerve transection.	Galvao et al. (2015)
The retina as an early biomarker of neurodegeneration in a rotenone-induced model of Parkinson's disease: evidence for a neuroprotective effect of rosiglitazone in the eye and brain*	DARC was imaged repeatedly over the course of 60 days to identify the presence of a rat rotenone-induced Parkinson's model. A significantly increased DARC signal in response to the administration of rotenone was observed to peak at 20 days into treatment.	Eduardo Maria Normando et al. (2016)
Non-amyloidogenic effects of α2 adrenergic agonists: implications for brimonidine-mediated neuroprotection	DARC was used to measure RGC apoptosis in a rat model of OHT at baseline, with and without treatment, 3 weeks, and 8 weeks post-surgery.	Nizari et al. (2016)

(*continued on next page*)

Table 6 (*continued*)

Title	Summary	Reference
	DARC counts in treatment groups could be statistically distinguished from non-treatment group, which was significantly different from the control group.	
Topical Coenzyme Q10 demonstrates mitochondrial-mediated neuroprotection in a rodent model of ocular hypertension*	A rat model of unilateral OHT received doses of the antioxidant and known neuroprotectant coenzyme Q10 twice daily for 3 weeks. DARC was administered after 3 weeks, prior to sacrifice. DARC spot count verified that the OHT model resulted in significantly increased cell stress than the control contralateral eye, and that CoQ10 treatment significantly reduced cell stress caused by OHT.	Davis et al. (2017)
Topical recombinant human Nerve growth factor (rh-NGF) is neuroprotective to retinal ganglion cells by targeting secondary degeneration	*In vivo* imaging of DARC in a rat model of partial optic nerve transection revealed that topical application of recombinant human nerve growth factor reduced RGC apoptosis.	Guo et al. (2020)

DARC to human glaucoma patients.

Animals had their pupils dilated while being held within a stereotaxic frame. A prototype Zeiss cLSO used a pair of mirrors to scan a focused spot produced by 488 nm argon laser across the retina of the animal. The fluorescence signal that resulted (which included light emitted by the Alexa Fluor 488 fluorophore) was optically focused onto a confocal aperture. A wide band-pass filter with a short-wavelength cut-off of 521 nm reduced irrelevant light wavelengths. Retinas were imaged prior to the administration of DARC to act as a baseline, and at various timepoints following administration. Manual counting was performed by condition-blinded observers to quantify DARC spots, and validated by histological counts of annexin A5 positivity.

4.1.2. *Verifying the DARC signal*

While annexin A5 labelling is a recognised marker for cell stress and death, the novel *in vivo* retinal application utilised in DARC technology required verification of the underlying principles. It was necessary to demonstrate that DARC-positivity was found in cells relevant to specific disease. However, as validation of cell type in the retina can only currently be performed histologically with staining to definitively identify different cells, the verification of the DARC signal has had to be performed in preclinical models.

4.1.2.1. Validation of DARC signal in glaucoma. In glaucoma, the key cell which is implicated is the RGC, and this was regarded as the target cell in which to perform an important assessment of annexin-specificity in experimental glaucoma models. These studies used retrograde labelling with DiASP applied to the superior colliculus to identify RGCs, as well as anti-caspase 3 antibody to confirm apoptosis. To accomplish this, following *in vivo* imaging, eyes were enucleated and fixed in 4% paraformaldehyde, with the retinas then dissected for histological analysis. Four radial cuts were made into retinas to flatten them, followed by either flat mounting on a microscope slide, or embedding in OCT and freezing to be sectioned at 7 μm thickness. Immunohistochemistry, summarised in Table 8, was used to label RGCs and cells undergoing caspase-dependent apoptosis. Fluorescent confocal laser scanning microscopy was used to image stained retinas, allowing precise control of the focal plane to restrict fluorescence measurements to the RGC layer.

Comparing baseline images and/or control eyes with those in receipt of damage, the application of DARC was able to distinguish between health and disease through a significant increase in fluorescent spot counts. DARC-positively labelled RGCs were identified histologically in these studies, with a higher level of labelling in disease versus controls. This effect was observed in all three experimental models used in the study. Furthermore, the rates of detection of RGC apoptosis were substantially higher with DARC, when compared to other methods of apoptosis detection, owing to the externalisation of PS occurring very early in the apoptotic process.

In the rat OHT model of glaucoma, the amount of DARC-detected apoptosis correlated strongly ($R^2 = 0.89$) with a function of IOP and days post-OHT induction. This provided further evidence to support the suggestion based on *in vitro* results that the magnitude of OHT, and exposure time, determine neuronal death in glaucoma.

The use of staurosporine as an apoptotic inducer resulted in a dose-dependent DARC signal. This finding provided a strong basis for the sensitivity of DARC in measuring conditions of cell stress, and was exemplary of its ability to not only detect the presence of disease, but also indicate severity on a granular scale.

By overlaying confocal images from histological tissue samples with images captured using cSLO *in vivo,* colocalisation of fluorescent signals demonstrated that apoptosing (DARC and anti-caspase 3 labelled) RGCs (DiAsp labelled) were recorded *in vivo* at a cellular resolution. In identifying both the cell type labelled, and the apoptotic status, a strong foundation was formed for the potential for DARC to diagnose glaucoma in humans.

4.1.2.2. Conclusions from early work in glaucoma. Cordeiro et al. (2004) measured apoptotic neurons *in vivo*, and set the groundwork for the future of DARC by demonstrating three key abilities of the technology: repeatable administration, precise quantification of cell stress, and sensitivity to a broad range of apoptotic stages. As summarised in Table 9, these qualities of DARC could facilitate its use in multiple situations both in the clinic and in research.

A rat model of glaucoma has been used to demonstrate that DARC can label apoptosing cells *in vivo*, an effect which was replicated with optic nerve transection and staurosporine administration. Indeed, the utility of DARC to investigate both retinal disease pathology and treatment efficacy *in vivo* would seem to be very promising, owing to the universal nature of measuring cell stress and apoptosis, integral aspects of disease. The applicability of DARC is limited only by the strength of disease models it is applied to. In order to broaden the horizons of DARC research, it would be essential to demonstrate DARC in the mouse, in order to take advantage of the many pathological mouse models available.

Following from the ability of DARC to label the presence and severity of retinal pathology, it stands to reason that if said retinal pathology were to be therapeutically ameliorated, the DARC signal would be reduced. Aided by the ability to image the same animal multiple times at different timepoints, DARC may be able to provide precise insights into the efficacy of treatments for retinal diseases. In future experiments, DARC should therefore be used to investigate the magnitude of therapeutic intervention on apoptosis in retinal pathology.

DARC images contain a large quantity of data, *in vivo* spot counts can number in the hundreds, and histological spot counts even more. While this high degree of fidelity in data allows for precise measurement of cell stress, it presents logistical issues in its quantification, which was achieved by manual counting in Cordeiro et al. (2004). The development of an automated counting method would be essential to enable timely assessment of data, not only in research, but also in potential clinical applications.

4.1.2.3. Verifying the DARC signal in AMD models. Animal models other

Table 7
Experimental conditions used in Cordeiro et al. (2004).

Animals	Number animals	Model	Model description	Dose of DARC	Imaging schedule
Adult Dark Agouti rats (150–200 g)	18	Ocular hypertension	Unilateral injection of saline into two episcleral veins (contralateral eye acted as control)	2.5 μg of DARC in 5 μL of PBS	2, 3, 4, 8, 12, and 16 weeks post-surgery
	12	Optic nerve transection	Unilaterally, the retrobulbar optic nerve was exposed, with nerve fibres transected 2–3 mm from the globe (contralateral eye acted as control)		8 h, 3, 7 and 12 days post-surgery
	15	Staurosporine-induced apoptosis	Intravitreal dose of 0, 0.125, 0.25, 0.5, or 1 μg of staurosporine in 5 μL of PBS		Immediately post-administration, for up to 6 h
Macaque monkeys	2		Under anaesthesia and paralysed, intravitreally injected with 2.5, 5, 7.5, 10 μg of staurosporine in 50 μL PBS	25 μg of DARC in 50 μL of PBS	Immediately post-administration, for at least 6 h

Table 8
Cell labelling methods used in experimental glaucoma models.

Fluorescence source	Labelled species	Application method
DARC	Stressed and dying cells	*In vivo* intravitreal injection
DiAsp ((4-(4-(didecylamino) styryl)-*N*-methylpyridinium iodide)	Retinal ganglion cells	*In vivo* superior colliculus injection
Anti-caspase-3	Cells undergoing caspase-dependent apoptosis	*Ex vivo* post-mortem immunohistochemistry
DAPI	Cell nucleus	*Ex vivo* post-mortem immunohistochemistry

Table 9
The translatable elements of DARC in early work.

Ability	Utility in disease assessment, diagnosis, and management	Utility in assessment of novel treatments
Repeat measurements of the same animal	Pathology can be tracked as it evolves, revealing insights such as changes in rate of progression. Response to treatment can also be measured	Facilitates more nuanced investigation of potential therapies, which for example may change in efficacy based on treatment duration or initial severity of pathology. Allows within-subjects statistical analysis
Granular 'dose' response	The severity of the pathology can be estimated with a high degree of precision, revealing details regarding treatment dose requirements and response to treatment	Small changes to pathological state can be detected, allowing more powerful statistical comparisons to be made in the assessment of treatment efficacy.
Sensitive to PS externalisation	By capturing early apoptotic stages, and continuing through to late apoptosis, a broad range of cell stress can be observed, potentially detecting pathological changes sooner	Capturing a broad range of apoptotic events allows more data regarding RGC stress to be captured in a single DARC image, making subtle treatment effects easier to detect

than glaucoma, have also been studied over the years, specifically those related to AMD. The target cells identified in these models are in the photoreceptor and inner nuclear layers, where DARC signal has been shown histologically to stain these cells. Firstly, a laser model (Nd:YAG laser at $\lambda = 532$ nm) was created to induce retinal damage in rats (Schmitz-Valckenberg et al., 2008). Annexin A5 positivity was demonstrated both *in vivo* and histologically in the inner nuclear layer following DARC. In another model of blue light phototoxicity, DARC was found to be able to detect apoptosis at 24 h after exposure to light, which was histologically confirmed as photoreceptor apoptosis (Schmitz-Valckenberg et al., 2010). In a mouse retinal ischaemic model, histological demonstration of annexin A5 positivity in inner nuclear, outer nuclear and photoreceptor layers has been demonstrated following intravitreal administration *in vivo* of Alexa Fluor 488-annexin (Normando et al., 2013a). More recent work has identified that DARC staining in a rabbit model of wet AMD localises to endothelial cells (Corazza et al., 2020).

4.2. Development of DARC technology

DARC has continued to be developed since its initial demonstration in Cordeiro et al. (2004), to improve the underlying technology and broaden its applications.

4.2.1. Comparison with TUNEL

In order to establish DARC as a tool for use in the assessment of retinal cell stress through the PS dependent labelling of apoptosing cells, it was necessary to compare it to similar existing tools. A common histological marker for apoptosis, TUNEL, stains DNA fragments which are formed at the final stages of apoptosis. When compared with DARC labelling in a rat model of OHT, it was found that DARC count was far greater than the TUNEL count previously described in the literature (Guo et al., 2005). This is to be expected, based on the mechanisms of PS exposure occurring very early in the apoptotic process, and continuing to the final stages of apoptosis. This finding highlights the sensitivity of DARC, and places it in a strong position as a tool to detect retinal disease in its early stages. Annexin labels PS exposure, which occurs in apoptotic cells that can later recover to normal function (Kenis et al., 2010), meaning that DARC may be able to detect pathology before widespread cell loss is occurring – an extremely valuable asset in the prevention of permanent sight impairment. Moreover, PS externalisation is also regarded as a sign of cell stress (Monastyrskaya et al., 2009).

4.2.2. Application in mice

In order to apply the technology to a broader range of animal models, it was necessary to extend DARC usage to the mouse, Maass et al. (2007) running a head-to-head analysis between mice and rats which were administered DARC in staurosporine-induced models of RGC death. The quantity of fluorescent points in both the rat and the mouse were sufficient to identify the presence of a toxic insult. Counting the DARC spots in both species also revealed similar results concerning the proportion of all apoptotic cells (identified histologically) that were labelled *in vivo*.

It was noted that the older Zeiss cSLO (used in Cordeiro et al., 2004) was unable to acquire *in vivo* images in the mouse. This older equipment was less sensitive than the Heidelberg cSLO that replaced it, and it is likely that the smaller eye of the mouse prohibited the collection of sufficient light to form an image. Utilising the more recent Heidelberg Retina Angiograph II resulted in high quality imaging in both rodent

species.

Critically, the successful expansion of DARC to mice not only opened the door to new research opportunities, but also served as an additional demonstration of the robustness of DARC technology to label retinal cell stress. This further strengthened the argument for DARC use in humans.

4.2.3. Automated counting methods

Counting fluorescent spots in the large volumes of data produced by DARC can be time-consuming to manually process, and subject to observer variability. Both of these shortcomings can be circumvented with the use of automated counting tools, making DARC faster and more reliable.

Bizrah et al. (2014) developed a semi-automated DARC counting program which identified objects within the cSLO image and judged their status as a DARC spot based on parameters such as size and shape of the object. While achieving a good correlation between automated counts and manual cell counts ($R^2 = 0.96$), this method was not ideal. A Bland-Altman plot revealed considerable variation between manual counts and automated counts, particularly when images contained few DARC spots (<100). It is cases where DARC spots are fewer in which accurate and reliable counting is most critical, as this can act as a cut off for diagnosis. Additionally, this counting method still required some user input to adjust for different lighting conditions at image acquisition, which thereby fails to exclude potential operator bias and the use of operator time.

In later years, a convolutional neural network (CNN) based on template matching was developed for the fully automated assessment of DARC images (Normando et al., 2020). In addition to offering full automation of counting, the accuracy of this CNN based approach allowed for precise discrimination between stable and progressive or high risk eyes (Corazza et al., 2020; Normando et al., 2020).

4.3. Using DARC to understand disease and treatment

In addition to diagnosing the presence of disease, the precise and granular data produced by DARC analyses make it possible to draw nuanced conclusions regarding how cells behave in pathology and in response to treatment. Table 6 summarises published experimental studies.

In vivo DARC assessment has provided real-time evidence of the efficacy of many neuroprotectant therapies. Guo et al. (2006) assessed the efficacy of modulating glutamate receptors (specifically NMDA receptors and group II mGluRs) in reducing neurodegeneration resulting from OHT or staurosporine-induced apoptosis in the rat. *In vivo* DARC counts demonstrated dose-dependent reductions in apoptosis resulting from treatment and identified greater therapeutic effect when combined treatments were applied.

By taking advantage of DARC's ability to be administered multiple times to the same animal, the effects of retinal damage resulting from harmful exposure to blue light were observed over the course of 24 h in rats(Schmitz-Valckenberg et al., 2010). By comparing images taken at baseline, immediately after exposure to harmful light, and one day later, the time course and severity of retinal apoptosis could be precisely quantified in each animal using within-subjects analysis. The use of such analysis allowed each animal to act as its own control, increasing the statistical power of the experiment.

The universal solvent, DMSO, widely used in many applications for the administration of therapeutic substances, was discovered to be toxic at surprisingly low concentrations (Galvao et al., 2014). The high sensitivity of DARC to conditions of cell stress revealed that intravitreal administration of DMSO resulted in a dose-dependent increase in DARC count, down to as little as 1% DMSO delivered in 5 μL intravitreally to the rat eye.

In assessing the efficacy of antioxidant coenzyme Q10 when applied to a rat model of OHT, the application of DARC was able to fulfil two functions. Firstly, it was able to demonstrate the severity of OHT-induced apoptosis resulting from the insult in the absence of treatment. Secondly, it was able to demonstrate that the application of coenzyme Q10 significantly reduced apoptosing cells in this model, providing further evidence for such a treatment to be applied in glaucoma.

5. Development pathway to clinical trials

The findings of successful *in vivo* applications of DARC provided strong evidence to support the use of such technology in humans. The main challenge here was to translate this technology for use in humans to determine its efficacy as a clinically useful tool.

The ANX776 molecule produced from one batch of GMP manufacturing run was used in both Phase 1 and 2 clinical trials (Corazza et al., 2020; Cordeiro et al., 2017; Normando et al., 2020). It was created by labelling a variant of the human annexin A5 molecule, rhAnnexin A5128 with the fluorophore Dy-776 (DY-776) (Cordeiro et al., 2017), illustrated in Fig. 6. ANX776 has a near infrared excitation wavelength, peaking at 771 nm, and an emission wavelength peaking at 793 nm. This is clinically significant as it is similar to the absorption and emission wavelengths of indocyanine green, a dye that is already well established for use in retinal angiography (Peiretti and Iovino, 2019). In addition to this, the use of wavelengths at the edge of the visible spectrum reduces patient discomfort as it is not perceived as visible light. These factors have enabled ANX776 to be easily translated to clinical trials.

Although annexin A5 had been used in over 30 clinical trials (Table 1), it was always labelled with a radionucleotide. As ANX776 was labelled with DY-776, and had never been used in patients before, it was regarded as an Investigational Medicinal Product requiring full regulatory assessment before a clinical trial could begin.

The development pathways required for clinical investigation of an IMP are particularly onerous in an academic environment, and the process was a real learning experience on the necessary precautions and red tape needed to enable a CTIMP (Clinical Trial of Investigational Medicinal Product).

5.1. GMP manufacture

The scale-up under GLP and GMP of ANX776 was the first challenge faced in the development of DARC. Technical transfer of our laboratory-based protocols were needed to ensure reproducible and consistent levels of protein and conjugation. To this end, specifications of the drug substance and drug product were compiled based on comprehensive analytics which were used to characterise the purity and effectiveness of

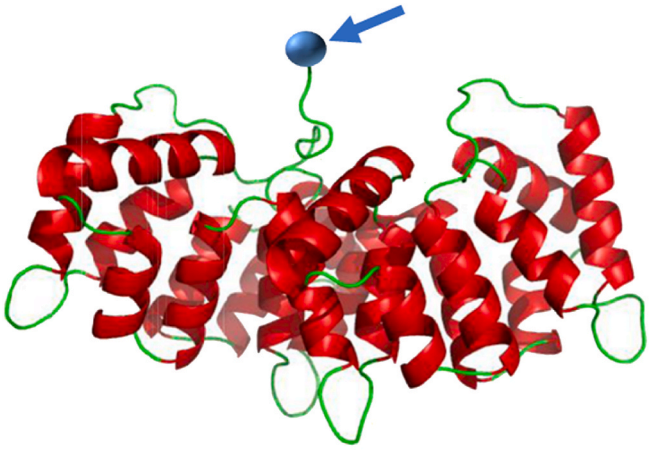

Fig. 6. Diagrammatic representation of a Dy-776-mal labelled Anx V128 molecule, with the annexin molecule in green and red and the Dy-776 represented by the blue (indicated by arrowhead).

the molecule. For example, the use of *in vitro* assays to prove binding of ANX776 to PS in preference to phosphatidylcholine lipids were used in addition to red blood cell displacement assays to test potency of annexin -binding as shown in Fig. 7.

An important aspect of this stage was establishing good Chemistry, Manufacturing and Controls (CMC) advice.

Finding the most appropriate manufacturer was a substantial task of vital importance, and unsuccessful in the beginning, causing significant delays in the project, but eventually, full GMP ANX776 manufacture was successfully completed in 2014, and an Investigational Medicinal Product Dossier (IMPD) finalised. The shelf-life of ANX776 was established as 3 years following a rigorous stability programme.

5.2. Safety and toxicology

As part of the regulatory package required by MHRA, a comprehensive non-clinical safety and toxicology programme was performed, including dose-ranging and repeated dose studies. These were of course completed under GLP study conditions.

Based on the toxicology studies conducted on the IMP (ANX776) as well as the components, Anx V128 and Dy-776, no indication of significant toxicological effects were observed in these studies. The No Observed Adverse Effect Level (NOAEL) was calculated to be 27-fold greater than the initial planned clinical dose of 0.1 mg. This formed part of the Investigators Brochure (IB) which was also completed.

Finally, following the submission of the IMPD, IB, and clinical trial protocol for the CTA (clinical trial authorisation), and the Ethics and R&D submissions the first DARC clinical trial was able to commence in 2015.

6. DARC clinical trials

6.1. Phase 1 clinical trial

6.1.1. Study design

The Phase 1 Clinical trial was a single-center, open label study conducted at The Western Eye Hospital, Imperial College Healthcare NHS Trust (ClinicalTrials.gov number NCT02394613) in 2015. Sixteen subjects were assessed: 8 healthy volunteers who were eligible according to strict criteria, and 8 glaucoma patients who were already under the care of the glaucoma team at The Western Eye Hospital. Glaucoma patients had to meet the inclusion criteria shown in Table 10 below to be eligible to participate in the study.

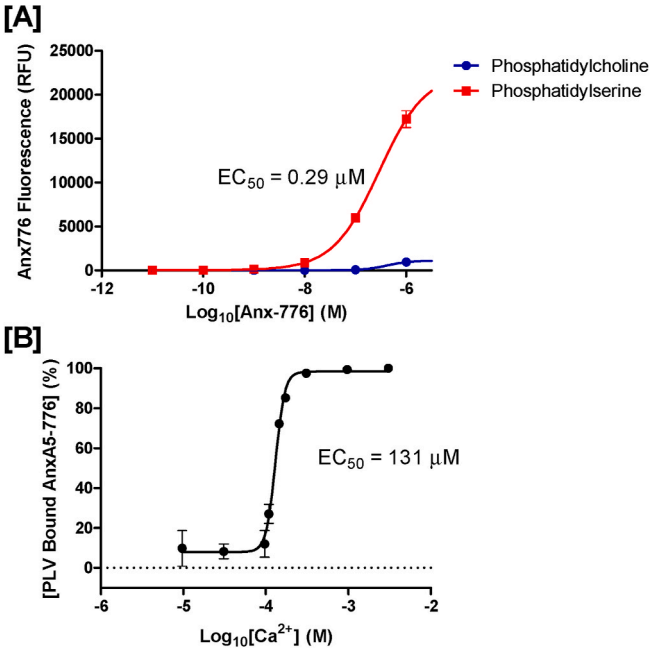

Fig. 7. Assay to test ANX776 affinity for phosphatidylserine (red) compared to phosphatidylcholine (blue) lipids in the presence of 2 mM calcium. (B) Binding of ANX776 to 400 µM PC85%¬PS15% liposomes is calcium dependent.

Progressive disease in the glaucoma subjects was defined by a significant negative slope in rate of progression in the retinal nerve fibre layer measurements at three diameters from the optic disc (3.5, 4.1 and 4.7 mm) and Bruch's membrane opening minimum rim width on an OCT.

Eight healthy controls were recruited through hospital advertisement and were included if they had no systemic or ocular disease, no evidence of glaucoma on OCT, RNFL or visual field testing and normal intraocular pressures (Cordeiro et al., 2017).

The subjects were sequentially enrolled and randomly divided into four different cohorts using a Storer study design to assess four different dosing regimens of ANX776 (single dose of 0.1 mg, 0.2 mg, 0.4 mg and 0.5 mg). Two patients with glaucoma and two healthy participants were randomly allocated to each cohort electronically with one further patient with glaucoma and healthy subject allocated in reserve in case of an adverse event.

The primary aim of the trial was to assess the safety, efficacy and tolerability of the DARC technique in humans. These assessments were carried out at regular intervals after the single injection of ANX776 was administered intravenously at short timepoints of 5, 15, 30, 60, 120, 240 and 300 min, with a longer follow up at 30 days.

6.1.2. Pharmacokinetics

Serum samples taken at the short timepoints showed ANX776 was rapidly absorbed and eliminated from the body at a dose-dependent rate with a half-life between 10 and 36 min with no accumulation. The 0.4 mg ANX776 dose had a half-life of 20.7 min.

The trial showed a good safety profile of ANX776 with no recorded serious adverse effects and no patients withdrawing from the study. Six separate mild, self-limiting adverse events occurred that were thought to be unrelated to ANX776 (discomfort during phlebotomy, haematoma at cannulation site, influenza, metatarsal inflammation, dizziness and headache).

6.1.3. Image capture and analysis

Images were acquired from all subjects after pupillary dilation using a confocal scanning laser ophthalmoscope at baseline, and then 15, 30, 60, 120, 240 and 360 min after ANX776 administration using the ICGA settings. The observed fluorescent puncta were identified as ANX776 positive-labelled cells and were visualised as hyperfluorescent spots on the retina of between 12 and 16 µm diameter. The approximate retinal area visualised was 78.73 mm^2 and the optimal dose of ANX776 to visualise these spots was found to be 0.4 mg. The retinal images produced were analysed with blinding to both the dose of ANX776 and the glaucoma status of the patient.

The near-infrared autofluorescent (NIRAF) image acquired at baseline was subtracted from each subsequent DARC image to remove non-specific autofluorescence and irrelevant features including the optic disc and blood vessels. The ANX776 positive-labelled spots were automatically counted for each image and the resulting DARC count was

Table 10
Inclusion criteria for Phase 1 Clinical Trial.

Inclusion criteria for glaucoma patients
No other ocular or systemic disease
Evidence of progressive disease in at least one eye
A minimum of three recent sequential assessments with
• optic disc tomography (OCT),
• retinal optical coherence tomography and
• standard automated perimetry.

identified as the first appearance of new and single ANX776-positive labelled spots.

The DARC count was found to be significantly higher in the glaucoma patients at all doses when compared to the healthy controls and even higher in those patients with more progressive glaucoma. This difference was most significant at 0.4 mg dose of ANX776. This suggests a high DARC count could predict an increased rate of glaucoma progression and be prognostic of neurodegenerative activity, even 18 months prior to changes on OCT and visual field testing.

A correlation between higher DARC count and increasing age was also found in the healthy subjects. This supports the association between apoptosis and ageing in addition to the progression of glaucoma and provides another avenue to study neurodegenerative diseases such as age-related macular degeneration (AMD), optic neuritis and Alzheimer-related disease.

These preliminary results were found to be promising, and suggested that DARC was translatable from experimental studies. However, the small numbers of patients per dose meant this was more like a proof-of-concept study. It was concluded that DARC would need more robust testing if it was to be successfully validated.

6.2. Phase 2 clinical trial

Following on from the promising results in Phase 1, it was recognised we needed to assess more patients with DARC. This was possible using the remaining ANX776 manufactured for the Phase 1 Clinical Trial, but the three-year shelf life meant we were limited in the number of patients and extent of the trial.

6.2.1. Study design

The Phase 2 clinical trial of DARC started in 2017, and was again conducted at the Western Eye Hospital, recruiting patients with glaucoma and healthy volunteers using the same criteria as described in the Phase 1 clinical trial, but in addition patients with AMD, optic neuritis and Down's syndrome were also included (ISRCTN10751859) (Corazza et al., 2020; Normando et al., 2020).

The aims of this study were to test the efficacy of DARC in more patients than Phase 1 (n = 120) but using a single dose of ANX776 (0.4 mg) and to further assess safety and tolerability.

To assess various conditions, patients were recruited into five different groups; healthy volunteers, patients with progressive glaucoma, age-related macular degeneration, optic neuritis (as a model for multiple sclerosis) and Down's syndrome where the pathology is thought to be similar to Alzheimer's disease (Cork, 1990).

The distribution of patients in Phase 2 is shown in Fig. 8 – in all, 113 patients received DARC. The specific inclusion and exclusion criteria used for the individual groups are detailed in Table 11.

All participants received a single intravenous dose of 0.4 mg of ANX776 (the optimum dose identified from the Phase 1 trial), with the image acquisition procedure of the Phase 1 trial being followed.

Initially, images were analysed by 5 blinded observers who manually identified the DARC spots from these images using the ImageJ (National Institutes of Mental Health USA) "multi-point" tool. In all, 906 anonymised images were assessed in this way, with images randomly displayed on the same monitor and under the same lighting conditions. There was poor agreement between observers (Krippendorff's alpha 0.51) with Kappa agreements ranging between 0.002 and 0.557 between pairs of observers. It was therefore decided to use a more robust and reproducible method to define DARC spots. Like Phase 1, the DARC count was defined as the number of ANX776-positive spots seen in each DARC retinal image after baseline spot subtraction to eliminate non-specific autofluorescence.

The analysis of all the patient cohorts is incomplete, with final analysis on the Down's Syndrome and Multiple Sclerosis patients still to be performed.

6.2.2. Establishment of automated CNN-aided algorithm for DARC count

The use of artificial intelligence (AI) and deep learning in the analysis of medical imaging has quickly become a leading interest worldwide (Pardue and Allen, 2018). Its use in retinal imaging has shown significant promise in analysing large datasets to classify conditions such as diabetic retinopathy and age-related macular degeneration to aid management (Hormel et al., 2021; Ting et al., 2019). Developing an innovative convolutional neural network (CNN), the use of deep learning was harnessed to create an automated method of DARC spot detection. (Normando et al., 2020).

Initially a template matching approach was used to find candidate spots in each processed image. From these candidate spots, a CNN was used to determine which spots could be classified as DARC spots. CNN training was performed at spot level, being trained using the manual counts from only the healthy control eyes where 2 or more manual observers had indicated the presence of a spot within 30 pixels of each other – that is, spots from different observers were classified as the same spot if they were within 30 pixels (150 μm) of each other, with only 50% of spots (58,730 spot candidates and 985 manual 2-agree spots) from control eyes used for training. Validation was then performed on the remaining 50% control eyes and showed accuracy of 97%, with 91.1% sensitivity and 97.1% specificity.

Fig. 9 below shows an overview of the process of analysing images to calculate the DARC count.

6.2.3. Analysis of glaucoma cohort

The CNN-aided algorithm was then tested on the glaucoma cohort of patients, using only the images at baseline and 120 min, and using the rate of progression (RoP) to classify glaucoma patients. (Normando et al., 2020). In this post-hoc analysis, glaucoma patients were followed up for 18 months after DARC and RoPs were calculated from serial Spectralis OCT global retinal nerve fibre layer (RNFL) measurements at 3.5 mm from the optic disc. Progression was defined by a significant negative slope RoP greater than 1 μm/year (to allow for age-related change) (Wu et al., 2017). Of the 29 eyes with follow-up data, 8 were found to be progressive. To test the predictive value of DARC, maximal sensitivity (90.0%) and specificity (85.71%) were calculated with an AUC of 0.89 produced by the CNN. This was found to perform superiorly in contrast to the manual observer count which reported maximal of sensitivity (85.0%) and specificity of (71.43%) with AUC of 0.79.

Using the CNN aided algorithm, the DARC count was found to be significantly ($p = 0.0044$) higher in patients progressing at 18 months (mean 26.13) compared to those who were stable (mean 9.71).

Interestingly, no eyes classified as 'stable' had a CNN DARC count above 30. This suggests a DARC count of 30 could be applied as a threshold that might be used to separate those at risk of glaucoma progression within 18 months, as illustrated in Fig. 10 below. This threshold may be useful in identifying those patients at greatest risk of progression in adaptive clinical PoC trials, where study population enrichment using biomarkers is often incorporated in the study design (Freidlin and Korn, 2014). The threshold of 30 is also important to define disease activity, such that patients with a DARC count above 30 clearly have active disease which results in significant progression 18 months later.

The CNN DARC count was amongst several parameters used in this study to look at prediction of progression at 18 months. These included baseline age, CCT, BP, visual field MD, VFI, average RNFL thickness and finally, topographically correspondent abnormal sectors on OCT RNFL and BMO-MRW imaging (Yang et al., 2020). Only the CNN DARC Count and the OCT RNFL and BMO-MRW sector parameter were found to be significantly predictive of progression. However, unlike the CNN DARC count, there was considerable overlap between the stable and progressing groups, with no clear threshold in the number of abnormal sectors that could be used to define those at greatest risk of progression. Nevertheless, the presence of predictive structural changes in the same eyes where the CNN DARC count was higher provides some degree of

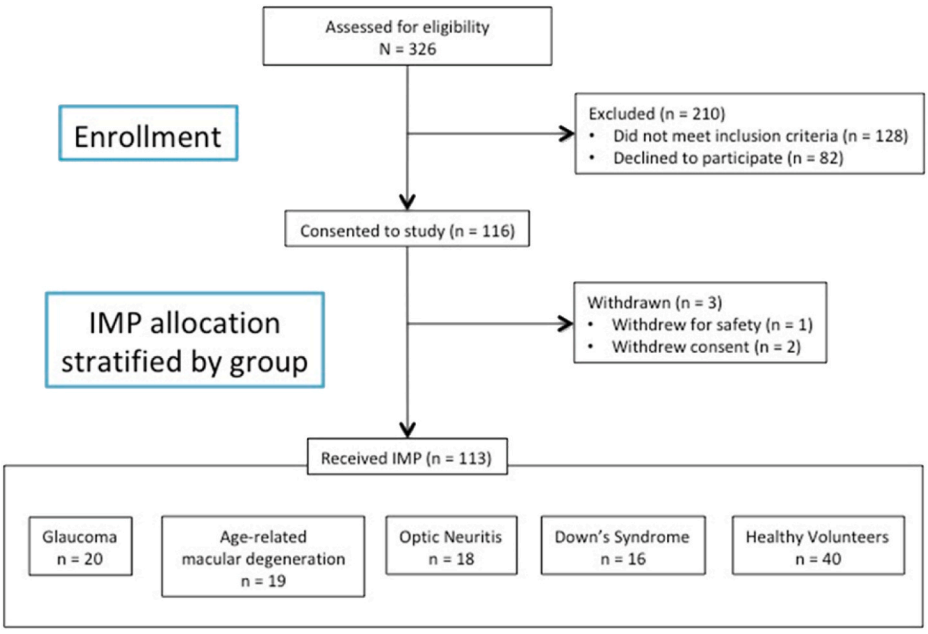

Fig. 8. Phase 2 clinical trial DARC patients.

Table 11
Inclusion and exclusion criteria for Phase 2 Clinical Trial.

	Inclusion Criteria	Exclusion Criteria
Glaucoma	Progression in at least one parameter as measured by visual fields or OCT in at least one eye with a diagnosis of glaucoma (abnormal optic disc and/or visual field defect or both) Glaucoma suspect or ocular hypertensive (elevated IOP) AND proven to be able to perform reliable visual field testing using the HFA 640, central 24-2 program (full threshold AND were able to have good fundoscopy with assessment of their optic disc	Uncontrolled I0P > 24 mmHg, Mean deviation in HVF testing worse than −12dB Diagnosed with angle closure/narrow angle glaucoma.
AMD	Either 'dry' or 'wet' AMD as defined by: early AMD mainly characterised by drusen, retinal pigment epithelium (RPE) pigment changes, Late AMD mainly characterised as geographic atrophy of the RPE (dry AMD) Neovascular (wet) AMD.	Presence of choroidal neovascularisation Current/previous use for more than 30 days of chloroquine, hydroxychloroquine, chlorpromazine, thioridazine, quinine sulfate, clofazimine, cisplatin, carmustine (BCNU), deferoxamine, amiodarone, isotretinoin, or gold.
Optic Neuritis	Clinical diagnosis of optic neuritis affecting one eye within two years, Visual acuity in affected eye ≤6/12 at worst point with corrected vision in unaffected eye ≥6/6, No history of optic neuritis or other ocular disease in either eye prior to the episode of optic neuritis AND have proven to be able to perform reliable visual field testing using the HFA 640, central 24-2 program, to yield full thresholds, AND to have had good fundoscopy with assessment of their optic disc.	No specific exclusion criteria
Down's syndrome	Confirmation of a Down's syndrome diagnosis as provided by parent or GP, Capacity to provide assent, Have previously participated in an invasive research trial with CIDDRG, Had no clinical diagnosis of dementia or other psychiatric illness, Had no evidence of serious cognitive decline or onset of dementia from historical records AND had no evidence of any eye disease.	Clinical diagnosis of dementia or other psychiatric illness, Evidence of serious cognitive decline or onset of dementia from historical records or Unable to give assent to the study, Unable to have a legal representative give full informed consent.
Healthy Volunteers	No ocular or systemic disease	Evidence of any historical retinal eye disease

confidence and validation of the DARC results.

6.2.4. Analysis of AMD cohort and development of new SRF

The same CNN DARC algorithm described above was used to investigate whether DARC technology could predict the development of new subretinal fluid (SRF) in patients with AMD (Corazza et al., 2020).

29 eyes were included using the inclusion criteria detailed in the table above as part of the Phase 2 clinical trial. All patients had OCT and DARC scans taken. The images were acquired with a cSLO as described above at 15, 120 and 240 min later. The baseline image was subtracted from the DARC image taken at 240 min to remove inherent auto fluorescent signals, and these anonymised images were used in the final analysis. Patients only had one DARC scan but multiple OCT scans as these were taken at every follow up visit, roughly every 6 months for a follow up period of 36 months. In all 427 OCT scans were performed, with a total of 20,629 slices available for analysis.

For the analysis of SRF on the OCT, a CNN was applied, due to the sheer number of OCT slices that needed annotation. This OCT SRF CNN was applied to the 20,629 OCT slices that were taken over the 36 month period from the 29 eyes. Patients who developed SRF that had not been present on the OCT in the earlier 6 month scan were identified as having new SRF.

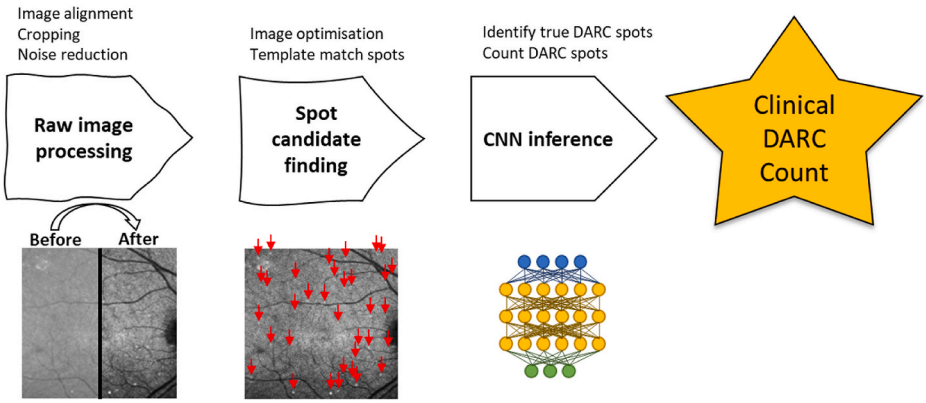

Fig. 9. Shows the steps involved in analysing an image with DARC technology using the CNN. The image is first optimised by aligning it to the baseline image and cropping any artefact. The light intensity is then standardised and any high-frequency noise removed. The candidate spots are then detected by applying a template made by combining 30 × 30 pixel images of the spots identified by manual observers. The thresholds were then set and filtered to be able to include all spots seen by manual observers. The CNN algorithm was then used to identify the DARC spots.

The DARC images from baseline are aligned with the corresponding series of OCT scans. Fig. 11 outlines the process of DARC and OCT image alignment, and Fig. 12 explains each step of this analysis. Briefly, the location of each DARC spot is defined by its coordinates, which after alignment with the OCT reflective baseline scan can then be easily located on corresponding OCT images at subsequent follow-up. Hence, if SRF was detected on subsequent OCT scans on follow-up, it was possible to see if a DARC spot at baseline was predictive of this.

Of the 29 eyes, 7 converted to new SRF or neovascular AMD over the 36 months. 3 of these were diagnosed as active CNV at baseline (of a total of 11, the other 8 had SRF on OCT at baseline) and converted at 6 months and 18 months. Two eyes converted from early AMD at baseline at 12 months and 30 months, one converted from late AMD at 6 months and 1 from the previous CNV group at 18 months.

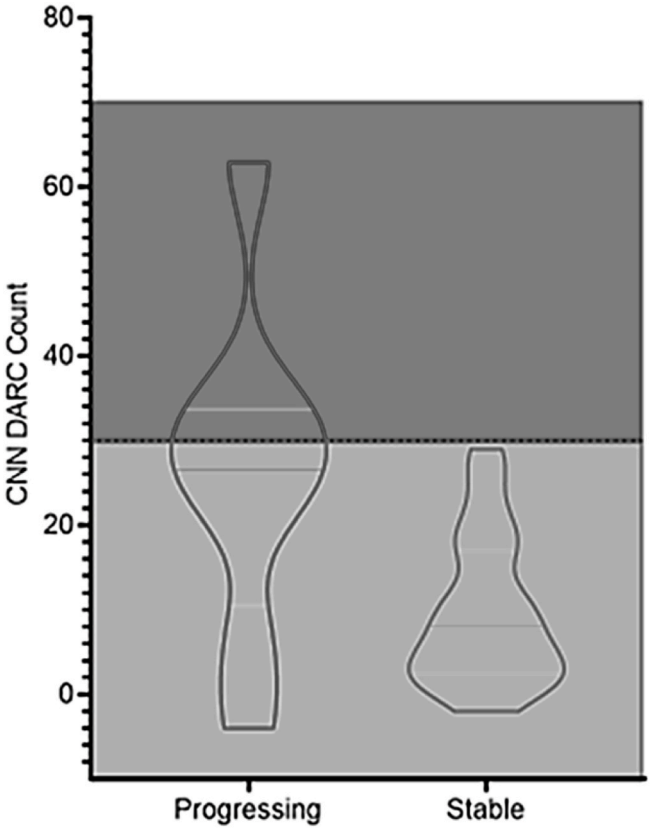

Fig. 10. Patients were classified according to a significant negative rate of progression slope greater than 1 μm/year on global retinal nerve fibre layer OCT measurements. A significantly higher ($p = 0.0044$) CNN DARC count was seen in the Progressing vs the Stable glaucoma group with all glaucoma patients having a DARC count >30 showing progression 18 months after DARC was performed.

The results showed that DARC was able to predict the development of new SRF. At 6 months, sensitivity of the DARC system was 83%, specificity was 90% with a PPV of 71% and NPV of 95%. The PPV reached a peak of 86% at 30 months and remained above 70% at all time points. The results demonstrated a CNN DARC count of >5 showed a statistically significant increased level of developing SRF when compared to those with a count of 5 or less. This was more apparent in the first 16 months of observation. The number of DARC spots appeared to correspond to disease activity, such that not only was a CNN DARC count >5 predictive of future SRF formation, but the higher the DARC count, the greater the volume of SRF accumulation from baseline up to 36 months follow-up.

This study is the first non-glaucoma clinical application of DARC. It is also linked to the mechanism of action previously elucidated in CNV, and discussed before, namely that the presence of DARC on endothelial cells is able to predict neovascular/vascular leakage activity.

Similar to the clinical trials in glaucoma, the DARC CNN allows the analysis of a large number of images, in this case 20,000 OCT images, substantially reducing the workload needed in manual analysis. While AI models are being developed to identify AMD from OCT models, DARC technology has the added benefit of being able to identify the progression to new neovascular AMD and SRF at a cellular level.

6.2.5. Analysis of expanding geographic atrophy in AMD cohort

Further analysis has also been performed in the AMD patients in the Phase 2 study with Geographic Atrophy (GA). 13 eyes were identified as having GA at baseline. All patients had only had one DARC assessment at the start of the study, but multiple OCT scans from follow-up to 36 months. All images were anonymised before any analysis was performed. The DARC image obtained by subtracting the baseline NIRAF from the 240-min DARC image captured at the level of the RNFL was used in this study, to eliminate intrinsic autofluorescence signal and identify true ANX776-positivity. An assessment of DARC technology in predicting the expansion of GA was performed using DARC baseline images and baseline and final follow-up OCT NIR reflectance images. The mean interval between baseline and final scans was 29.3 ± 5.0 months (SD).

The area of GA was annotated on the first and last OCT NIR reflectance image captured for each eye using VGG Image Annotator (VIA; Visual Geometry Group, Oxford University). The annotation was independently performed by senior medical retina specialist (PC), according to the method described by Abdelfattah et al. (2020), with the edge of the atrophic areas delineated with a mouse trackpad. Only eyes with a marked hyperreflective area and a pronounced demarcation edge of the atrophic area on the NIR image were included in the study. The process of analysis for GA is described in Fig. 13. Annotated GA areas on baseline NIR reflectance images were created for each eye providing an original

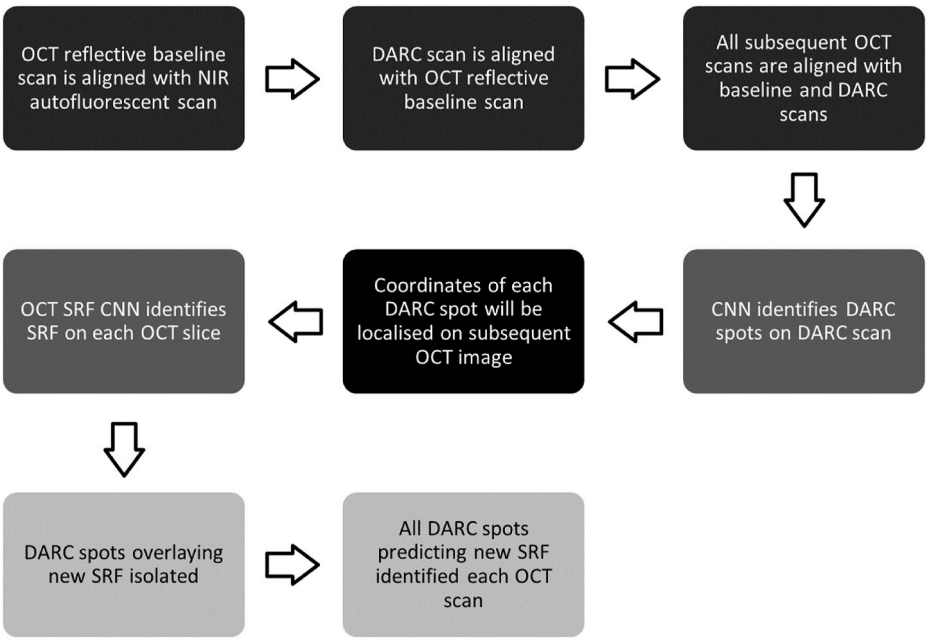

Fig. 11. Automatic process for the analysis of neovascular AMD in Phase 2 Clinical Trial DARC Patients.

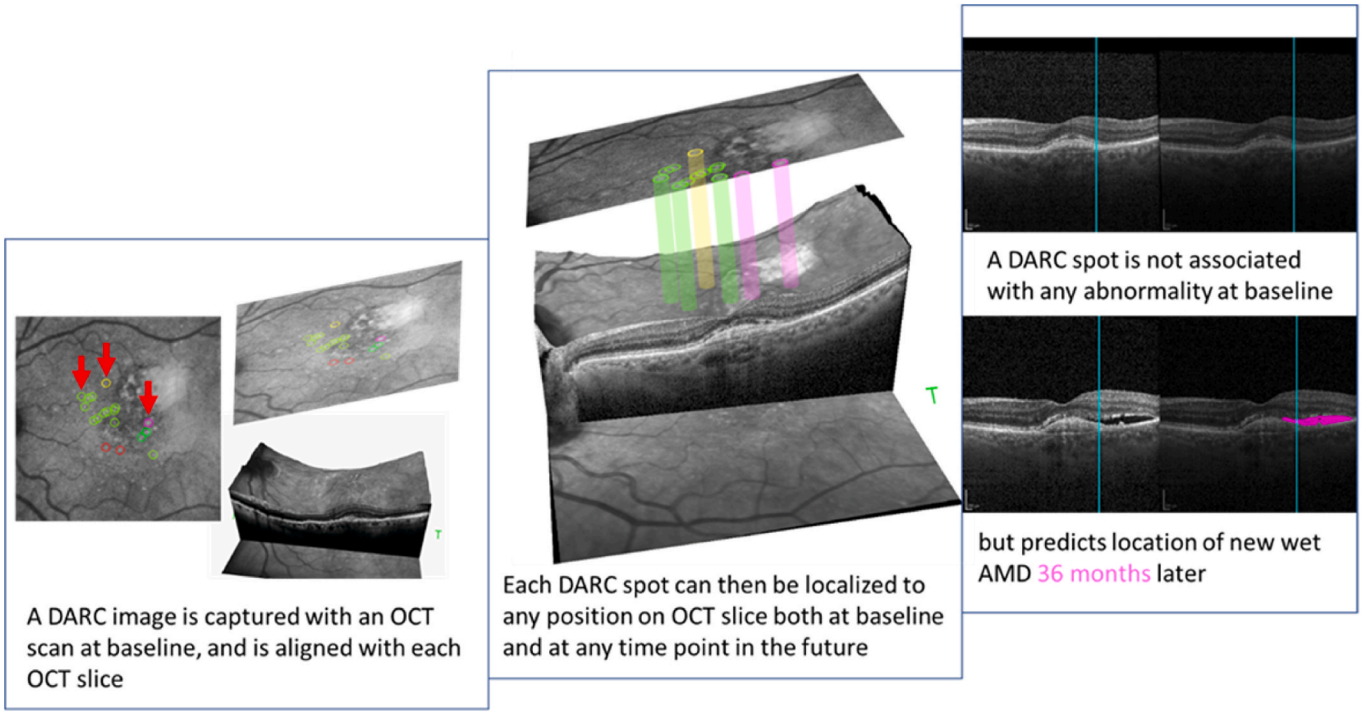

Fig. 12. Explanation of the steps involved in AMD analysis, examples of DARC spots are highlighted in the first panel with red arrows. These are then aligned to corresponding OCT scans, to enable identification of future SRF formation.

GA mask (Fig. 13A). Additionally, expanded baseline GA masks (Fig. 13B) were created by dilating the original GA mask using a disk kernel of size 50, and then subtracting the original mask from the dilated mask. Final GA masks were created to outline the area of atrophy in the final OCT NIR reflectance image (Fig. 13C), with a GA growth mask (Fig. 13D) obtained by subtracting the original baseline mask from the final GA mask.

Baseline autofluorescence and DARC images (240 min) were aligned automatically using an affine transformation followed by a non-rigid B-spline transformation, as described previously(Corazza et al., 2020). This was completed using multi-resolution alignment methods within SimpleITK (NumFOCUS, US) and a gradient descent optimiser. The reflectance image of the baseline and final Spectralis OCT scans of each GA eye were next aligned with the registered DARC image, by manual placement of fiducial markers on the cSLO autofluorescence and OCT reflectance images, then calculating and applying an affine transform. Once these images were aligned then a location on the 240-min DARC image could be selected with the same location being identified in corresponding OCT NIR reflectance and annotated images outlining atrophic areas including the original and expanded GA mask images.

Please refer to the Supplementary Information for individual eye data.

The CNN DARC algorithm described above was used to identify DARC spots on baseline images. The distance from the center of a DARC spot and the nearest area of expanding GA was calculated using a *Euclidian* distance transform where all non-feature pixels are represented by a distance to the nearest feature pixel (Borgefors, 1986). A heatmap of the DARC density was created using kernel density estimation (KDE) density map with radius 50 (Parzen, 1962; Rosenblatt, 1956), enabling a smooth heatmap to be created estimating the probability density function from the finite number of detected DARC spots using a gamma correction for normalisation (Fig. 13E). To enable visualisation of relationship between expanded GA and DARC spots, the expanded GA mask was overlaid on each DARC density heatmap (Fig. 13F and supplement).

The expanded baseline GA and GA growth areas were compared on a pixel-to-pixel basis using a balanced accuracy score per image(Pedregosa et al., 2011). The mean balanced accuracy score, where 1.0 is perfect agreement, was found to be 0.84 ± 0.13 (SD), showing a high correlation between expanded baseline GA and GA growth. (See Supplementary Information for more details).

Fig. 14 shows the main findings from the analysis of DARC in GA growth. Comparison between distances of DARC spots and non-DARC areas to the expanded baseline GA area was calculated using Euclidian distances. The mean distance between a DARC spot and the expanded baseline GA per eye was found to be significantly lower compared to that of other pixels (Fig. 14A, $p < 0.0001$, paired *t*-test). Moreover, the mean DARC distance to expanded atrophy was significantly associated with a large final GA area (>60,000 px), such that all eyes with a mean DARC distance less than 12 pixels developed large areas of final GA (Fig. 14B, $p = 0.014$, Mann-Whitney). The DARC density inside the expanded baseline GA area in each eye was significantly greater than outside (Fig. 14C, $p = 0.0046$, paired *t*-test). In a similar way, the number of DARC spots in the expanded GA area was significantly associated with a large area of final GA (>60,000 px), such that all eyes with a DARC count greater than 10 developed large areas of final atrophy. In other words, the level of DARC was predictive of GA activity, with a DARC count within this area >10 associated with increased large expansion of GA up to 36 months later. Fig. 14D shows the DARC count log transformed after adding 1 showing a significant increase in eyes with large final GA areas ($p = 0.0035$, Mann-Whitney, DARC count transformed).

The assessment of DARC metrics in the expanded baseline GA area enables its projection of disease as indicated by the final GA areas. These are the first results of DARC in GA, and suggests that DARC activity at baseline is predictive of final GA activity at a mean of 29.3 months later.

7. Future directions

Although the results reported so far for Phase 1 and 2 are encouraging, we recognise that it is only based on a small number of patients. This was primarily due to the limitations of only small amounts of ANX776 being available in the one batch GMP manufacturing run used to supply material for both Phase 1 and Phase 2 DARC trials. The opportunities afforded by the latest batch of new GMP ANX776 enables multisite and collaborations, with clinical trials already being planned around the world, and regulatory approval of DARC to be used in different countries, including Australia, where a trial is due to commence using DARC as an exploratory endpoint in May 2021. We hope to further validate our results with these larger prospective and longitudinal clinical trials, with strict protocols with respect to patient management. Although the clinical significance of DARC as a diagnostic is yet to be established, based on our results in glaucoma and AMD to date, it could be used as an exploratory endpoint and biomarker in clinical trials, as already approved by regulatory bodies discussed below.

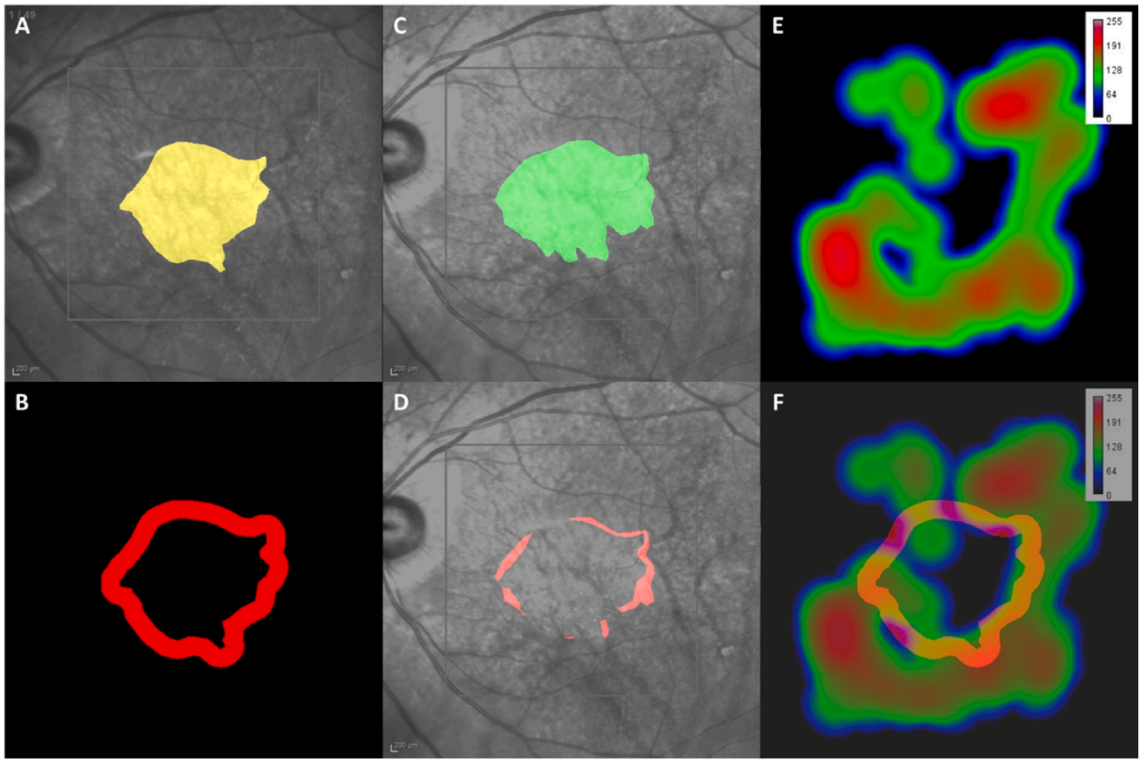

Fig. 13. Visualisation of expanding GA and DARC. Masks of original baseline GA (A), expanded baseline GA (B), final GA (C), and GA growth (D) were created from NIR reflectance images for each eye. The expanded baseline GA area (B) was found to be strongly correlated to GA growth (D) (balanced accuracy score = 0.84)). A DARC density heatmap (E) was constructed from the CNN-identified DARC spots for each DARC image. An overlay of the DARC heatmap on the expanded baseline GA (F) shows the relationship of increased DARC density with expanding GA activity, with the DARC density inside the area significantly greater than outside ($p = 0.0046$).

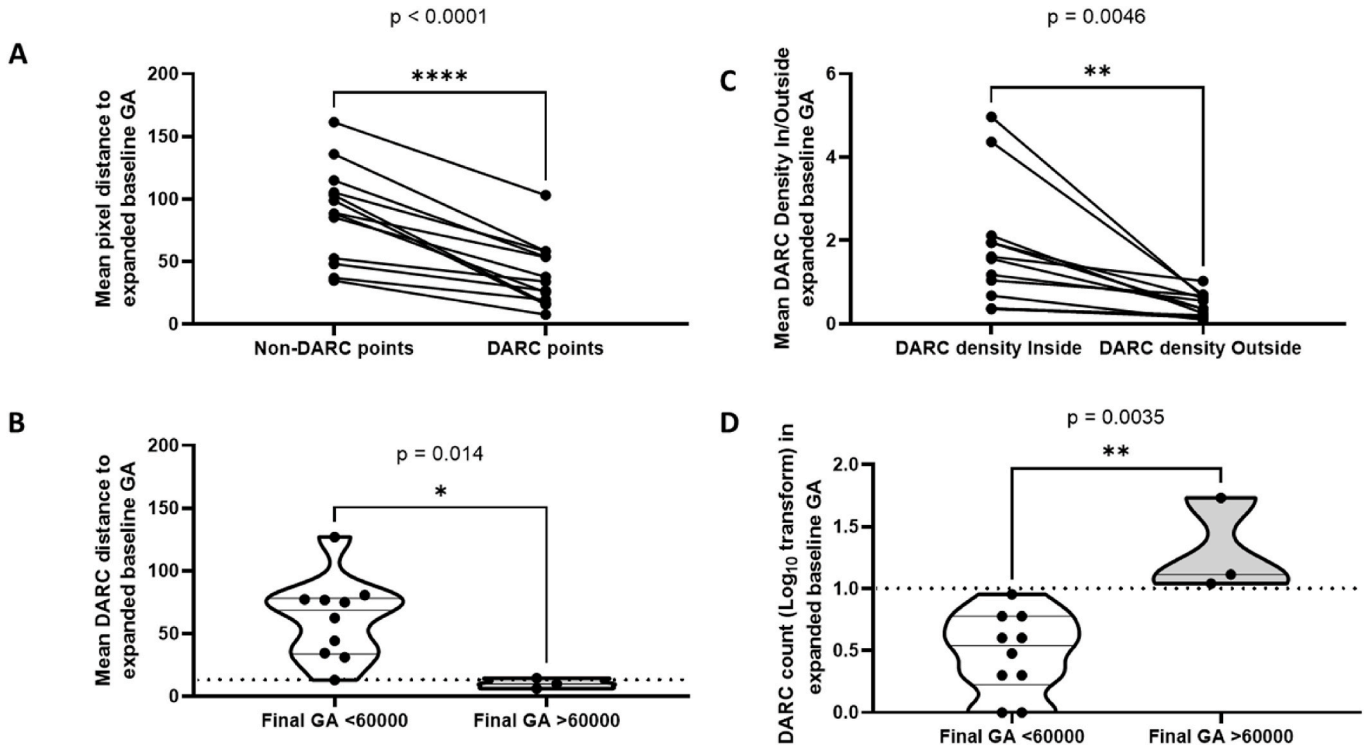

Fig. 14. DARC as a biomarker of GA activity. The proximity of DARC spots to the area of expanded GA was assessed using Euclidian distances. The mean distance between a DARC spot and the expanded baseline GA per eye (A) was found to be significantly ($p < 0.0001$, paired *t*-test) lower compared to that of other pixels (Fig. 14A). The mean DARC distance to expanded baseline atrophy (B) was significantly ($p = 0.014$, Mann-Whitney) associated with a large final GA area (>60,000 px); all eyes with a mean DARC distance < 12 pixels (dashed line) developed large areas of final GA. The DARC density inside compared to outside the expanded baseline GA area per eye was found to be significantly greater (Fig. 14C, $p = 0.0046$, paired *t*-test). The DARC count in the expanded baseline GA area (D) was significantly ($p = 0.0035$, Mann-Whitney, log transformed) associated with a large area of final GA (>60,000 px): all eyes with a DARC count > 10 (dashed line) developed large areas of final GA.

7.1. DARC as a biomarker

Up to now, DARC has only been assessed at a single time point in patients, providing a snapshot of disease activity. However, a singular biomarker level is often used in medicine for diagnostic and/or prognostic purposes. Examples of this include LDL cholesterol levels in coronary artery disease (Field and Vasan, 2018), human Chorionic Gonatadotrophin in gestational trophoblastic disease, (Ning et al., 2019), and circular RNA CDR1as/ciRS-7 for solid tumours (Zou et al., 2020). The Phase 1 and 2 clinical trials were designed to evaluate DARC in a cross-sectional analysis. As patients were able to be followed-up with conventional methods after undergoing a single DARC assessment, these studies have allowed analysis of the predictive powers of DARC to be a biomarker – hence in glaucoma to identify those at highest risk of progressive disease, and in AMD to predict those that go on to develop subretinal fluid, or at high risk of large progressive macular atrophy.

The initial use of DARC as an exploratory endpoint (as MHRA, FDA and TGA have already approved for individual trials) will be important in proof-of-concept clinical trials assessing new therapies. In these cases, DARC can be used not only to assess drug efficacy by a reduction in the DARC count compared to baseline, but also to enrich patient populations (Kompella et al., 2020), as described below.

DARC could be useful to stratify patients in clinical trials. It enables the identification of patients with rapid disease progression and therefore at higher risk. By assessing the rate of disease progression, patients can be classified into cohorts that will enable further investigation of the disease process, response to drug treatments based on how quickly the disease was progressing and allow comparison to cohorts with slower disease progression.

Fig. 15 illustrates how DARC could be used to firstly enrich patient population and secondly evaluate drug efficacy in a hypothetical glaucoma drug trial. A similar process could be applied to neovascular AMD and GA.

Although preclinically we have shown good evidence that DARC can be used as a measure of treatment efficacy, we have still not performed these trials in patients. However, new Phase 2b clinical trials are planned in glaucoma and AMD at Western Eye Hospital and other sites in 2021.

7.2. DARC as a diagnostic

There is insufficient data at present to clinically validate DARC as a diagnostic in any disease. For glaucoma, we believe this would require a large, prospective Phase 3 trial with longitudinal follow-up and age-matched controls, repeated testing and a strict protocol regarding patient management. Currently, glaucoma clinical DARC results are based on small numbers of patients with a single DARC assessment and a narrow range of disease severity (in the Phase 2 trial, the MD was between −1.61–2.22 dB). Comparison of DARC to gold standard is imperative in this feat, although it may also be interesting to evaluate DARC with conventional risk factors such as IOP using a multivariable analysis.

Moving forwards, we hope to obtain even more data on glaucoma patients, as Phase 2 had a small sample size. Moreover, previously patients were limited to a single assessment with DARC and we recognise the need to establish repeatability and test–retest metrics. In the future, we would hope to assess a wider spectrum of disease severity – as both Phase 1 and 2 glaucoma patients had relatively early disease. Until we perform further trials, it is not possible to compare DARC to existing gold standards such as visual fields and OCT for detecting glaucoma in clinical practice.

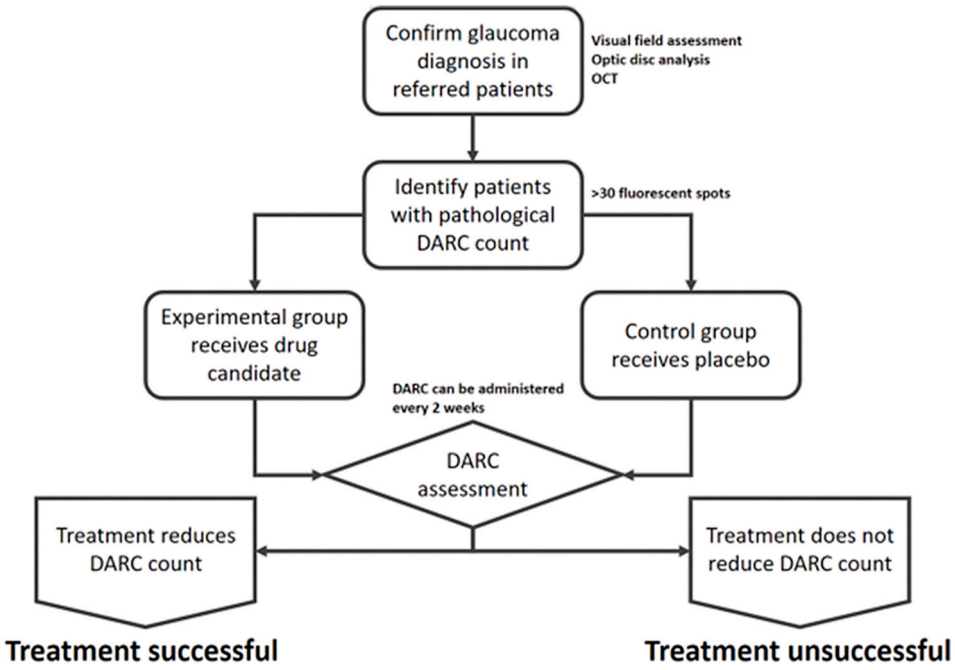

Fig. 15. Stratification of patients for glaucoma Proof-of-Concept (PoC) trial.

Larger numbers are also anticipated in the future AMD trials which will be performed prospectively to establish the natural history of both wet and dry AMD.

7.3. DARC AI

In glaucoma, GA and neovascular AMD we have shown the value of using a CNN algorithm to identify DARC spots. AI enables DARC to be scaled up for use in larger datasets with multiple applications and multiple sites. It also provides a rapid and objective measure of disease activity. This is increasingly important, not only because of the recognised poor agreement between clinicians using subjective tests, but also due the wider applicability of the technology in primary care settings.

It is also hoped that as more DARC data is acquired from different patients and diseases, AI will enable not only spatial analysis specific to patterns of disease, but also cell classification based on the morphological staining characteristics of ANX776. Spatial patterns of staining we believe to be potentially useful in glaucoma and AMD, although this still needs to be demonstrated in larger trials. We have hypothesised that in glaucoma, this would be predominantly at the papillomacular bundle following the anatomical arrangement of RGC axons, in keeping with characteristic arcuate patterns of visual field defects (Normando et al., 2013b). We have already used AI to spatially correlate DARC density and expanding GA (Fig. 13) clinically. Furthermore, we have applied automatic algorithms to analyse spatial distribution and cell morphology in preclinical models (Davis et al., 2020; Guo et al, 2014, 2020), which show translational potential to clinical studies.

Many high street optometrists have the capability to carry out retinal examinations with OCT, SLO and fundus imaging and it has been recognised by the NHS that these commercial suppliers of primary ophthalmic care perform a vital function in diagnosis and referral into NHS specialist care. However, interpretation of these scans needs direct clinical intervention – and there are not enough ophthalmologists available to do this. This has led to retinal imaging manufacturers providing "modules" with automatic algorithm to help non-specialists. The growth in AI in ophthalmology is very much to fulfil this need, although the accuracy of existing technologies is questionable for screening. As DARC identifies cellular levels of dysfunction, DARC AI would provide an objective measure of disease activity which is currently unavailable.

7.4. Intranasal DARC

At present, ANX776 is administered intravenously, which is an additional burden on clinical staff in hospitals. We already developed a nasal version which would make the technology relatively non-invasive, especially compared to intravenous administration. It would also enable the technology to have a wider application in outpatient and optometrist departments.

The ability to perform intranasal DARC in the future in optometry, community and well-man clinics, is important in enabling the technology to be used in primary care. The preclinical data suggests the pharmacokinetics of the intranasal are similar to intravenous routes, so it will take 2 h for optimal retinal visualisation. Potentially, the nasal formulation could be dispensed by a pharmacist and self-administered before the patient attends for retinal imaging screening.

7.5. Further indications

As the results from the Phase 2 clinical trial continue to be analysed, we hope to acquire more information about the application of DARC in early detection of dementia using results from the Down's syndrome cohort. Similarly, we hope to have the results from the multiple sclerosis/optic neuritis cohorts soon.

Following on from the results of preclinical studies, future work is also intended with clinical trials for DARC testing in Parkinson's disease, diabetes mellitus, retinal dystrophies, optic neuropathies (Yu-Wai-Man et al., 2011) and cancer.

The implications in early detection of these neurodegenerative conditions will not only allow early intervention but also the ability to test and develop neuroprotective agents to prevent progression and investigate the effect of current and future therapeutic agents on disease activity. These drugs could be tested in clinical settings, initially with glaucoma and AMD patients. Patients who are not responding to therapies could be detected earlier and a targeted treatment plan created. This will avoid patients continuing on ineffective medication that may not be required and reduce development of side effects while being more cost effective and patient centred.

7.6. Potential challenges and possible solutions

The clinical results so far have been very encouraging, despite the relatively small number of patients and the post hoc analysis in glaucoma and AMD. An important aspect in the next steps of this technology is the validation of these findings in prospective, multisite and larger clinical trials, where strict protocols will be devised to ensure standardisation of patient management and follow-up. This would be particularly useful in AMD patients where OCTA and FFA findings could help in classification of the CNV and dry AMD lesions.

Until now we have assumed the stressed and apoptotic cells identified by DARC reflect the specific cells that are known to be affected in different disease. This has been confirmed by our preclinical studies, outlined in Table 6, where histological validation is possible, as this is not achievable in clinical studies. However, as we move into more patients and diseases, our hope is to classify the morphological staining characteristics of ANX776 into cell type. We also believe that the use of adaptive optics will help in this assessment, and similar methods to overcome depth resolution.

Finally, the AI algorithms can be improved as the technology advances. The CNN can be affected by image intensity, and the use of intensity standardisation and augmenting the data by varying the intensity may be possible with a larger dataset. Moreover, the combination of spatial distribution on the retina and morphological staining patterns could enable more disease specific analysis in the future.

8. Conclusions

As discussed, the uses of DARC are far reaching and as the exciting results from the clinical trials continue to be analysed, its potential as a marker of disease activity grows. However, there is still much work to be done, especially in validating its use clinically.

DARC until earlier this year has received the majority of its funding from the Wellcome Trust. This has enabled DARC to get to Phase 2 in an academic setting. As DARC continues to develop, commercially-oriented funding through Novai Ltd has allowed DARC to continue on its journey, with the ultimate aim of helping patients to avoid functional disability through early identification and treatment.

Decalartion of competing interest

MFC/JM are named inventors on patents on DARC and the discussed algorithms, originally owned by UCL, and licenced to Novai Ltd in March 2020 of which MFC is a director and MFC/JM are shareholders. The authors have no other relevant affiliations or financial involvement with any organization or entity with a financial interest in or financial conflict with the subject matter or materials discussed in the manuscript apart from those disclosed.

Acknowledgements

The Wellcome Trust (WT099729; WT088029) provided funding for the DARC project from preclinical development to Phase 2 clinical trials.

Development of DARC technology would not have been possible without the contributions of the following individuals:

Li Guo, John Maddison, Vy Luong, Serge Miodragovic, Philip Bloom, Eduardo Normando, Zena Rodrigues, Paolo Bonetti, Seeham Jeylani, Anne Marie Downey, Jessica Bonetti, Faisal Ahmed, Laura Crawley, Daniel Hill, Tim Yap, Soyoung Choi, Aman Khan, Priyanka Bikkannavar, Claudia Sisa, Benjamin Davis, Ljuban Grigic, Nivedita Ravindram, Preeti Dev, Ehtesham Shamsher, Stephen Moss, Fred Fitzke, Seb Ourselin, Rachel Hemsley, Steve Dakin, Jorge Cardosa, Katie Coxon, James Duggan, Annelie Maass, Meng Liu, Mark Tilley, Shannon Shiobolath, Lisa Turner, George Heaton, Shereen Nizari, Joana Galvao, Giulia Malaguarnera, Jon Brenton, Clive Migdal, Mukhtar Bizrah, Valeria Bono, Abu Habib, Gibran Butt, Miles Parnell, Farzana Rahman, Shanika Gunasinghe, Gaia Pollorsa, Abeir Baltmr, Ma-Arej Ghaffer, James Brodie, Richard Nicholas, Madeleine Walpert, Tony Holland.

Appendix A. Supplementary data

Supplementary data to this article can be found online at https://doi.org/10.1016/j.preteyeres.2021.100976.

Author statement

Percentage of work contributed by each author in the production of the manuscript is as follows: Cordeiro 54%; Hill 16%; Patel 16%; Paolo Corazza 5%; John Maddison 7%; Saad Younis 2%

References

Abdelfattah, N.S., Sadda, J., Wang, Z., Hu, Z., Sadda, S., 2020. Near-infrared reflectance imaging for quantification of atrophy associated with age-related macular degeneration. Am. J. Ophthalmol. 212, 169–174. https://doi.org/10.1016/j.ajo.2020.01.005.

Ahmad, S.S., 2017. An introduction to DARC technology. Saudi J. Ophthalmol. https://doi.org/10.1016/j.sjopt.2016.08.001.

Ahn, J., Lee, J.Y., Kim, T.W., Yoon, E.J., Oh, S., Kim, Y.K., Kim, J.M., Woo, S.J., Kim, K. W., Jeon, B., 2018. Retinal thinning associates with nigral dopaminergic loss in de novo Parkinson disease. Neurology 91, e1003–e1012. https://doi.org/10.1212/WNL.0000000000006157.

Alasil, T., Wang, K., Yu, F., Field, M.G., Lee, H., Baniasadi, N., Boer, J.F.De, Coleman, A. L., Chen, C., 2015. Fields in Glaucoma: a broken stick model. Am. J. Ophthalmol. 157, 953–959. https://doi.org/10.1016/j.ajo.2014.01.014.Correlation.

Alber, J., Goldfarb, D., Thompson, L.I., Arthur, E., Hernandez, K., Cheng, D., DeBuc, D.C., Cordeiro, F., Provetti-Cunha, L., den Haan, J., Van Stavern, G.P., Salloway, S.P., Sinoff, S., Snyder, P.J., 2020. Developing retinal biomarkers for the earliest stages of Alzheimer's disease: what we know, what we don't, and how to move forward. Alzheimer's Dement. https://doi.org/10.1002/alz.12006.

Almasieh, M., Wilson, A.M., Morquette, B., Cueva Vargas, J.L., Di Polo, A., 2012. The molecular basis of retinal ganglion cell death in glaucoma. Prog. Retin. Eye Res. 31, 152–181. https://doi.org/10.1016/j.preteyeres.2011.11.002.

Ambati, J., Fowler, B.J., 2012. Mechanisms of age-related macular degeneration. Neuron. https://doi.org/10.1016/j.neuron.2012.06.018.

Anderson, D.R., 2003. Collaborative normal tension glaucoma study. Curr. Opin. Ophthalmol. https://doi.org/10.1097/00055735-200304000-00006.

Ansari, J., Kaur, G., Gavins, F.N.E., 2018. Therapeutic potential of annexin A1 in ischemia reperfusion injury. Int. J. Mol. Sci. https://doi.org/10.3390/ijms19041211.

Balasubramanian, K., Mirnikjoo, B., Schroit, A.J., 2007. Regulated externalization of phosphatidylserine at the cell surface: implications for apoptosis. J. Biol. Chem. 282, 18357–18364. https://doi.org/10.1074/jbc.M700202200.

Baudouin, C., Kolko, M., Melik-Parsadaniantz, S., Messmer, E.M., 2020. Inflammation in Glaucoma: from the back to the front of the eye, and beyond. In: Prog. Retin. Eye Res. https://doi.org/10.1016/j.preteyeres.2020.100916.

Belhocine, T., Steinmetz, N., Hustinx, R., Bartsch, P., Jerusalem, G., Seidel, L., Rigo, P., Green, A., 2002. Increased uptake of the apoptosis-imaging agent99mTc recombinant human annexin V in human tumors after one course of chemotherapy as a predictor of tumor response and patient prognosis. Clin. Canc. Res. 8, 2766–2774.

Belhocine, T.Z., Blankenberg, F.G., Kartachova, M.S., Stitt, L.W., Vanderheyden, J.L., Hoebers, F.J.P., Van de Wiele, C., 2015a. 99mTc-Annexin A5 quantification of apoptotic tumor response: a systematic review and meta-analysis of clinical imaging trials. Eur. J. Nucl. Med. Mol. https://doi.org/10.1007/s00259-015-3152-0.

Belhocine, T.Z., Blankenberg, F.G., Kartachova, M.S., Stitt, L.W., Vanderheyden, J.L., Hoebers, F.J.P., Van de Wiele, C., 2015b. 99mTc-Annexin A5 quantification of apoptotic tumor response: a systematic review and meta-analysis of clinical imaging trials. Eur. J. Nucl. Med. Mol. Imag. 42, 2083–2097. https://doi.org/10.1007/s00259-015-3152-0.

Beykin, G., Norcia, A.M., Srinivasan, V.J., Dubra, A., Goldberg, J.L., 2021. Discovery and clinical translation of novel glaucoma biomarkers. Prog. Retin. Eye Res. https://doi.org/10.1016/j.preteyeres.2020.100875.

Biehlmaier, O., Alam, M., Schmidt, W.J., 2007. A rat model of Parkinsonism shows depletion of dopamine in the retina. Neurochem. Bar Int. 50, 189–195. https://doi.org/10.1016/j.neuint.2006.08.001.

Bizrah, M., Dakin, S.C., Guo, L., Rahman, F., Parnell, M., Normando, E., Nizari, S., Davis, B., Younis, A., Cordeiro, M.F.F., 2014. A semi-automated technique for labeling and counting of apoptosing retinal cells. BMC Bioinf. 15 (169) https://doi.org/10.1186/1471-2105-15-169.

Blankenberg, F.G., 2009. Imaging the molecular signatures of apoptosis and injury with radiolabeled annexin V, in: proceedings of the American Thoracic Society. https://doi.org/10.1513/pats.200901-001AW.

Blankenberg, F.G., Kalinyak, J., Liu, L., Koike, M., Cheng, D., Goris, M.L., Green, A., Vanderheyden, J.L., Tong, D.C., Yenari, M.A., 2006. 99mTc-HYNIC-annexin V SPECT imaging of acute stroke and its response to neuroprotective therapy with anti-

Fas ligand antibody. Eur. J. Nucl. Med. Mol. Imag. 33, 566–574. https://doi.org/10.1007/s00259-005-0046-6.
Blankenberg, F.G., Katsikis, P.D., Tait, J.F., Davis, R.E., Naumovski, L., Ohtsuki, K., Kopiwopda, S., Abrams, M.J., Darkes, M., Robbins, R.C., Maecker, H.T., Strauss, H. W., 1998. In vivo detection and imaging of phosphatidylserine expression during programmed cell death. In: Proc. Natl. Acad. Sci. U. S. A, vol. 95, pp. 6349–6354. https://doi.org/10.1073/pnas.95.11.6349.
Bodis-Wollner, I., Kozlowski, P.B., Glazman, S., Miri, S., 2014. α-synuclein in the inner retina in Parkinson disease. Ann. Neurol. https://doi.org/10.1002/ana.24182.
Boersma, H.H., Liem, I.H., Kemerink, G.J., Thimister, P.W.L., Hofstra, L., Stolk, L.M.L., Van Heerde, W.L., Pakbiers, M.T.W., Janssen, D., Beysens, A.J., Reutelingsperger, C. P.M., Heidendal, G.A.K., 2003. Comparison between human pharmacokinetics and imaging properties of two conjugation methods for 99mTc-Annexin A5. Br. J. Radiol. 76, 553–560. https://doi.org/10.1259/bjr/30385847.
Borgefors, G., 1986. Distance transformations in digital images. Comput. Vision, Graph. Image Process. 34, 344–371. https://doi.org/10.1016/S0734-189X(86)80047-0.
Boyer, D.S., Schmidt-Erfurth, U., Van Lookeren Campagne, M., Henry, E.C., Brittain, C., 2017. The pathophysiology of geographic atrophy secondary to age-related macular degeneration and the complement pathway as a therapeutic target. Retina. https://doi.org/10.1097/IAE.0000000000001392.
Brandl, C., Brücklmayer, C., Günther, F., Zimmermann, M.E., Küchenhoff, H., Helbig, H., Weber, B.H.F., Heid, I.M., Stark, K.J., 2019. Retinal layer thicknesses in early age-related macular degeneration: results from the German AugUR study. Investig. Ophthalmol. Vis. Sci. https://doi.org/10.1167/iovs.18-25332.
Brookmeyer, R., Abdalla, N., Kawas, C.H., Corrada, M.M., 2018. Forecasting the prevalence of preclinical and clinical Alzheimer's disease in the United States. Alzheimer's Dementia. https://doi.org/10.1016/j.jalz.2017.10.009.
Brubaker, R.F., 2003. Targeting outflow facility in glaucoma management. Surv. Ophthalmol. 48 https://doi.org/10.1016/S0039-6257(03)00003-1.
Budson, A.E., Solomon, P.R., 2012. New criteria for alzheimer disease and mild cognitive impairment. Neurol. 18, 356–363. https://doi.org/10.1097/NRL.0b013e31826a998d.
Calianese, D.C., Birge, R.B., 2020. Biology of phosphatidylserine (PS): basic physiology and implications in immunology, infectious disease, and cancer. Cell Commun. Signal. https://doi.org/10.1186/s12964-020-00543-8.
Calkins, D.J., 2012. Critical pathogenic events underlying progression of neurodegeneration in glaucoma. Prog. Retin. Eye Res. https://doi.org/10.1016/j.preteyeres.2012.07.001.
Cao, L., Wang, H., Wang, F., Xu, D., Liu, F., Liu, C., 2013. Aβ-induced senescent retinal pigment epithelial cells create a proinflammatory microenvironment in AMD. Invest. Ophthalmol. Vis. Sci. https://doi.org/10.1167/iovs.13-11612.
Cascella, R., Strafella, C., Caputo, V., Errichiello, V., Zampatti, S., Milano, F., Potenza, S., Mauriello, S., Novelli, G., Ricci, F., Cusumano, A., Giardina, E., 2018. Towards the application of precision medicine in Age-Related Macular Degeneration. Prog. Retin. Eye Res. https://doi.org/10.1016/j.preteyeres.2017.11.004.
Chan, V.T.T., Sun, Z., Tang, S., Chen, L.J., Wong, A., Tham, C.C., Wong, T.Y., Chen, C., Ikram, M.K., Whitson, H.E., Lad, E.M., Mok, V.C.T., Cheung, C.Y., 2019. Spectral-Domain OCT measurements in Alzheimer's disease: a systematic review and meta-analysis. Ophthalmology. https://doi.org/10.1016/j.ophtha.2018.08.009.
Chang, E.E., Goldberg, J.L., 2012. Glaucoma 2.0: neuroprotection, neuroregeneration, neuroenhancement. Ophthalmology 119, 979–986. https://doi.org/10.1016/j.ophtha.2011.11.003.
Chaudhuri, K.R., Healy, D.G., Schapira, A.H.V., 2006. Non-motor symptoms of Parkinson's disease: diagnosis and management. Lancet Neurol. https://doi.org/10.1016/S1474-4422(06), 70373-70378.
Chen, H.H., Josephson, L., Sosnovik, D.E., 2011. Imaging of apoptosis in the heart with nanoparticle technology. Wiley Interdiscip. Rev. Nanomedicine Nanobiotechnology. https://doi.org/10.1002/wnan.115.
Cheng, Y., He, L., Prasad, V., Wang, S., Levy, R.J., 2015. Anesthesia-induced neuronal apoptosis in the developing retina: a window of opportunity. Anesth. Analg. https://doi.org/10.1213/ANE.0000000000000714.
Chew, E.Y., Clemons, T., Sangiovanni, J.P., Danis, R., Domalpally, A., McBee, W., Sperduto, R., Ferris, F.L., 2012. The age-related eye disease study 2 (AREDS2): study design and baseline characteristics (AREDS2 Report Number 1). Ophthalmology 119, 2282–2289. https://doi.org/10.1016/j.ophtha.2012.05.027.
Choi, S.H., Park, S.J., Kim, N.R., 2016. Macular ganglion cell -inner plexiform layer thickness is associated with clinical progression in mild cognitive impairment and alzheimers disease. PLoS One. https://doi.org/10.1371/journal.pone.0162202.
Choi, S.S., Zawadzki, R.J., Lim, M.C., Brandt, J.D., Keltner, J.L., Doble, N., Werner, J.S., 2011. Evidence of outer retinal changes in glaucoma patients as revealed by ultrahigh-resolution in vivo retinal imaging. Br. J. Ophthalmol. 95, 131–141. https://doi.org/10.1136/bjo.2010.183756.
Chopdar, A., Chakravarthy, U., Verma, D., 2003. Age related macular degeneration. Br. Med. J. https://doi.org/10.1136/bmj.326.7387.485.
Compston, A., Coles, A., 2008. Multiple sclerosis. Lancet 61620–61627. https://doi.org/10.1016/S0140-6736(08).
Corazza, P., Maddison, J., Bonetti, P., Guo, L., Luong, V., Garfinkel, A., Younis, S., Cordeiro, M.F., 2020. Predicting wet age-related macular degeneration (AMD) using DARC (detecting apoptosing retinal cells) AI (artificial intelligence) technology. Expert Rev. Mol. Diagn. https://doi.org/10.1080/14737159.2020.1865806.
Cordeiro, M.F., 2007. DARC: a new method for detecting progressive neuronal death. Eye 21, S15–S17. https://doi.org/10.1038/sj.eye.6702881.
Cordeiro, M.F., Guo, L., Coxon, K.M., Duggan, J., Nizari, S., Normando, E.M., Sensi, S.L., Sillito, A.M., Fitzke, F.W., Salt, T.E., Moss, S.E., 2010. Imaging multiple phases of neurodegeneration: a novel approach to assessing cell death in vivo. Cell Death Dis. 1 https://doi.org/10.1038/cddis.2009.3 e3–e3.
Cordeiro, M.F., Guo, L., Luong, V., Harding, G., Wang, W., Jones, H.E., Moss, S.E., Sillito, A.M., Fitzke, F.W., 2004. Real-time imaging of single nerve cell apoptosis in retinal neurodegeneration. In: Proc. Natl. Acad. Sci. U. S. A, vol. 101, pp. 13352–13356. https://doi.org/10.1073/pnas.0405479101.
Cordeiro, M.F., Normando, E.M., Cardoso, M.J., Miodragovic, S., Jeylani, S., Davis, B.M., Guo, L., Ourselin, S., A'Hern, R., Bloom, P.A., 2017. Real-time imaging of single neuronal cell apoptosis in patients with glaucoma. Brain 140, 1757–1767. https://doi.org/10.1093/brain/awx088.
Cordeiro, M.F.F., 2016. Eyeing the brain 132. https://doi.org/10.1007/s00401-016-1628-z.
Cork, L.C., 1990. Neuropathology of down syndrome and alzheimer disease. Am. J. Med. Genet. https://doi.org/10.1002/ajmg.1320370756.
Coxon, K.M., Duggan, J., Cordeiro, M.F., Moss, S.E., 2011. Purification of annexin V and its use in the detection of apoptotic cells. In: Methods Mol Biol, pp. 293–308. https://doi.org/10.1007/978-1-61779-080-5_24.
Creutz, C.E., Hira, J.K., Gee, V.E., Eaton, J.M., 2012. Protection of the membrane permeability barrier by annexins. Biochemistry. https://doi.org/10.1021/bi3013559.
Daleke, D.L., 2007. Phospholipid flippases. J. Biol. Chem. https://doi.org/10.1074/jbc.R600035200.
Datta, S., Cano, M., Ebrahimi, K., Wang, L., Handa, J.T., 2017. The impact of oxidative stress and inflammation on RPE degeneration in non-neovascular AMD. Prog. Retin. Eye Res. https://doi.org/10.1016/j.preteyeres.2017.03.002.
Davis, B.M., Crawley, L., Pahlitzsch, M., Javaid, F., Cordeiro, M.F., 2016. Glaucoma: the retina and beyond. Acta Neuropathol. 132 https://doi.org/10.1007/s00401-016-1609-2.
Davis, B.M., Guo, L., Ravindran, N., Shamsher, E., Baekelandt, V., Mitchell, H., Bharath, A.A., De Groef, L., Cordeiro, M.F., 2020. Dynamic changes in cell size and corresponding cell fate after optic nerve injury. Sci. Rep. 10 https://doi.org/10.1038/s41598-020-77760-1.
Davis, B.M., Tian, K., Pahlitzsch, M., Brenton, J., Ravindran, N., Butt, G., Malaguarnera, G., Normando, E.M., Guo, L., Cordeiro, M.F., 2017. Topical Coenzyme Q10 demonstrates mitochondrial-mediated neuroprotection in a rodent model of ocular hypertension. Mitochondrion 36, 114–123. https://doi.org/10.1016/j.mito.2017.05.010.
De Fauw, J., Ledsam, J.R., Romera-Paredes, B., Nikolov, S., Tomasev, N., Blackwell, S., Askham, H., Glorot, X., O'Donoghue, B., Visentin, D., van den Driessche, G., Lakshminarayanan, B., Meyer, C., Mackinder, F., Bouton, S., Ayoub, K., Chopra, R., King, D., Karthikesalingam, A., Hughes, C.O., Raine, R., Hughes, J., Sim, D.A., Egan, C., Tufail, A., Montgomery, H., Hassabis, D., Rees, G., Back, T., Khaw, P.T., Suleyman, M., Cornebise, J., Keane, P.A., Ronneberger, O., 2018. Clinically applicable deep learning for diagnosis and referral in retinal disease. Nat. Med. 24, 1342–1350. https://doi.org/10.1038/s41591-018-0107-6.
De Moraes, C.G., Liebmann, J.M., Levin, L.A., 2017. Detection and measurement of clinically meaningful visual field progression in clinical trials for glaucoma. Prog. Retin. Eye Res. https://doi.org/10.1016/j.preteyeres.2016.10.001.
DeMaagd, G., Philip, A., 2015. Parkinson's disease and its management part 1: disease entity, risk factors, pathophysiology, clinical presentation, and diagnosis. P T 40, 504–532.
Ding, J.-D., Johnson, L.V., Herrmann, R., Farsiu, S., Smith, S.G., Groelle, M., Mace, B.E., Sullivan, P., Jamison, J.A., Kelly, U., Harrabi, O., Bollini, S.S., Dilley, J., Kobayashi, D., Kuang, B., Li, W., Pons, J., Lin, J.C., Rickman, C.B., 2011. Anti-amyloid therapy protects against retinal pigmented epithelium damage and vision loss in a model of age-related macular degeneration. Proc. Natl. Acad. Sci. Unit. States Am. https://doi.org/10.1073/pnas.1100901108.
Ding, Y., Chow, S.H., Liu, G.S., Wang, B., Lin, T.W., Hsu, H.Y., Duff, A.P., Le Brun, A.P., Shen, H.H., 2018. Annexin V-containing cubosomes for targeted early detection of apoptosis in degenerative retinal tissue. J. Mater. Chem. B. https://doi.org/10.1039/c8tb02465k.
Dong, Z.M., Wollstein, G., Wang, B., Schuman, J.S., 2017. Adaptive optics optical coherence tomography in glaucoma. Prog. Retin. Eye Res. https://doi.org/10.1016/j.preteyeres.2016.11.001.
Dörr, J., Wernecke, K.D., Bock, M., Gaede, G., Wuerfel, J.T., Pfueller, C.F., Bellmann-Strobl, J., Freing, A., Brandt, A.U., Friedemann, P., 2011. Association of retinal and macular damage with brain atrophy in multiple sclerosis. PloS One. https://doi.org/10.1371/journal.pone.0018132.
Dunaief, J.L., Dentchev, T., Ying, G.S., Milam, A.H., 2002. The role of apoptosis in age-related macular degeneration. Arch. Ophthalmol. 120, 1435–1442. https://doi.org/10.1001/archopht.120.11.1435.
Dutt, M., Tabuena, P., Ventura, E., Rostami, A., Shindler, K.S., 2010. Timing of corticosteroid therapy is critical to prevent retinal ganglion cell loss in experimental optic neuritis. Investig. Ophthalmol. Vis. Sci. 51, 1439–1445. https://doi.org/10.1167/iovs.09-4009.
Duyckaerts, C., Sazdovitch, V., Seilhean, D., Delaere, P., Hauw, J.J., 1993. A brain bank in a neuropathology laboratory (with some emphasis on diagnostic criteria). In: Journal of Neural Transmission, Supplement, pp. 107–118.
Engbersen, R., Riksen, N.P., Mol, M.J., Bravenboer, B., Boerman, O.C., Meijer, P., Oyen, W.J.G., Tack, C., Rongen, G.A., Smits, P., 2012. Improved resistance to ischemia and reperfusion, but impaired protection by ischemic preconditioning in patients with type 1 diabetes mellitus: a pilot study. Cardiovasc. Diabetol. https://doi.org/10.1186/1475-2840-11-124.
Esteve-Rudd, J., Fernández-Sánchez, L., Lax, P., De Juan, E., Martín-Nieto, J., Cuenca, N., 2011. Rotenone induces degeneration of photoreceptors and impairs the dopaminergic system in the rat retina. Neurobiol. Dis. https://doi.org/10.1016/j.nbd.2011.06.009.

Fadok, V.A., Voelker, D.R., Campbell, P.A., Cohen, J.J., Bratton, D.L., Henson, P.M., 1992. Exposure of phosphatidylserine on the surface of apoptotic lymphocytes triggers specific recognition and removal by macrophages. J. Immunol. 148, 2207–2216.

Ferrari, L., Huang, S.C., Magnani, G., Ambrosi, A., Comi, G., Leocani, L., 2017. Optical coherence tomography reveals retinal neuroaxonal thinning in frontotemporal dementia as in Alzheimer's disease. J. Alzheim. Dis. https://doi.org/10.3233/JAD-160886.

Field, P.A., Vasan, R.S., 2018. LDL-cholesterol is not the only clinically relevant biomarker for coronary artery disease or acute coronary syndrome. Clin. Pharmacol. Ther. https://doi.org/10.1002/cpt.1126.

Fortea, J., Vilaplana, E., Carmona-Iragui, M., Benejam, B., Videla, L., Barroeta, I., Fernández, S., Altuna, M., Pegueroles, J., Montal, V., Valldeneu, S., Giménez, S., González-Ortiz, S., Muñoz, L., Estellés, T., Illán-Gala, I., Belbin, O., Camacho, V., Wilson, L.R., Annus, T., Osorio, R.S., Videla, S., Lehmann, S., Holland, A.J., Alcolea, D., Clarimón, J., Zaman, S.H., Blesa, R., Lleó, A., 2020. Clinical and biomarker changes of Alzheimer's disease in adults with Down syndrome: a cross-sectional study. Lancet. https://doi.org/10.1016/S0140-6736(20), 30689–9.

Freidlin, B., Korn, E.L., 2014. Biomarker enrichment strategies: matching trial design to biomarker credentials. Nat. Rev. Clin. Oncol. https://doi.org/10.1038/nrclinonc.2013.218.

Galetta, S.L., Villoslada, P., Levin, N., Shindler, K., Ishikawa, H., Parr, E., Cadavid, D., Balcer, L.J., 2015. Acute optic neuritis: unmet clinical needs and model for new therapies. Neurol. Neuroimmunol. NeuroInflammation. https://doi.org/10.1212/NXI.0000000000000135.

Galvao, J., Davis, B., Tilley, M., Normando, E., Duchen, M.R., Cordeiro, M.F.F., 2014. Unexpected low-dose toxicity of the universal solvent DMSO. Faseb. J. 28, 1317–1330. https://doi.org/10.1096/fj.13-235440.

Galvao, J., Elvas, F., Martins, T., Cordeiro, M.F., Ambrósio, A.F., Santiago, A.R., 2015. Adenosine A3 receptor activation is neuroprotective against retinal neurodegeneration. Exp. Eye Res. 140, 65–74. https://doi.org/10.1016/j.exer.2015.08.009.

Gao, L., Chen, X., Tang, Y., Zhao, J., Li, Q., Fan, X., Xu, H., Yin, Z.Q., 2015a. Neuroprotective effect of memantine on the retinal ganglion cells of APPswe/PS1δE9 mice and its immunomodulatory mechanisms. Exp. Eye Res. https://doi.org/10.1016/j.exer.2015.04.013.

Gao, L.Y., Liu, Y., Li, X.H., Bai, Q.H., Liu, P., 2015b. Abnormal retinal nerve fiber layer thickness and macula lutea in patients with mild cognitive impairment and Alzheimer's disease. Arch. Gerontol. Geriatr. https://doi.org/10.1016/j.archger.2014.10.011.

Garcia-Martin, E., Rodriguez-Mena, D., Satue, M., Almarcegui, C., Dolz, I., Alarcia, R., Seral, M., Polo, V., Larrosa, J.M., Pablo, L.E., 2014. Electrophysiology and optical coherence tomography to evaluate Parkinson disease severity. Investig. Ophthalmol. Vis. Sci. https://doi.org/10.1167/iovs.13-13062.

García-Santos, G., Antolín, I., Herrera, F., Martín, V., Rodriguez-Blanco, J., Carrera, M.D. P., Rodriguez, C., 2006. Melatonin induces apoptosis in human neuroblastoma cancer cells. J. Pineal Res. 41, 130–135. https://doi.org/10.1111/j.1600-079X.2006.00342.x.

Garcia-Valenzuela, E., Shareef, S., Walsh, J., Sharma, S.C., 1995. Programmed cell death of retinal ganglion cells during experimental glaucoma. Exp. Eye Res. 61, 33–44. https://doi.org/10.1016/S0014-4835(95)80056-5.

Gelles, J.D., Edward Chipuk, J., 2016. Robust high-throughput kinetic analysis of apoptosis with real-time high-content live-cell imaging. Cell Death Dis. https://doi.org/10.1038/cddis.2016.332.

Gerke, V., Moss, S.E., 2002. Annexins: from structure to function. Physiol. Rev. https://doi.org/10.1152/physrev.00030.2001.

Ghislat, G., Aguado, C., Knecht, E., 2012. Annexin A5 stimulates autophagy and inhibits endocytosis. J. Cell Sci. 125, 92–107. https://doi.org/10.1242/jcs.086728.

Gong, Y.N., Crawford, J.C., Heckmann, B.L., Green, D.R., 2019. To the edge of cell death and back. FEBS J. https://doi.org/10.1111/febs.14714.

Gordon-Lipkin, E., Chodkowski, B., Reich, D.S., Smith, S.A., Pulicken, M., Balcer, L.J., Frohman, E.M., Cutter, G., Calabresi, P.A., 2007. Retinal nerve fiber layer is associated with brain atrophy in multiple sclerosis. Neurology. https://doi.org/10.1212/01.wnl.0000295995.46586.ae.

Grimaldi, A., Brighi, C., Peruzzi, G., Ragozzino, D., Bonanni, V., Limatola, C., Ruocco, G., Di Angelantonio, S., 2018. Inflammation, neurodegeneration and protein aggregation in the retina as ocular biomarkers for Alzheimer's disease in the 3xTg-AD mouse model. Cell Death Dis. 9 https://doi.org/10.1038/s41419-018-0740-5.

Gualino, V., Tadayoni, R., Cohen, S.Y., Erginay, A., Fajnkuchen, F., Haouchine, B., Krivosic, V., Quentel, G., Vicaut, E., Gaudric, A., 2019. Optical coherence tomography, fluorescein angiography, and diagnosis of choroidal neovascularization in age-related macular degeneration. Retina. https://doi.org/10.1097/IAE.0000000000002220.

Guan, Y., Shindler, K.S., Tabuena, P., Rostami, A.M., 2006. Retinal ganglion cell damage induced by spontaneous autoimmune optic neuritis in MOG-specific TCR transgenic mice. J. Neuroimmunol. https://doi.org/10.1016/j.jneuroim.2006.05.019.

Guo, L., Davis, B., Nizari, S., Normando, E.M.M., Shi, H., Galvao, J., Turner, L., Shi, J., Clements, M., Parrinello, S., Cordeiro, M.F.F., 2014. Direct Optic Nerve Sheath (DONS) Application of Schwann Cells Prolongs Retinal Ganglion Cell Survival in Vivo, vol. 5, p. e1460. https://doi.org/10.1038/cddis.2014.399.

Guo, L., Davis, B.M., Ravindran, N., Galvao, J., Kapoor, N., Haamedi, N., Shamsher, E., Luong, V., Fico, E., Cordeiro, M.F., 2020. Topical recombinant human Nerve growth factor (rh-NGF) is neuroprotective to retinal ganglion cells by targeting secondary degeneration. Sci. Rep. 10 (3375) https://doi.org/10.1038/s41598-020-60427-2.

Guo, L., Moss, S.E., Alexander, R.A., Ali, R.R., Fitzke, F.W., Cordeiro, M.F., 2005. Retinal ganglion cell apoptosis in glaucoma is related to intraocular pressure and IOP-induced effects on extracellular matrix. Investig. Ophthalmol. Vis. Sci. 46, 175–182. https://doi.org/10.1167/iovs.04-0832.

Guo, L., Normando, E.M., Shah, P.A., De Groef, L., Cordeiro, M.F., 2018. Oculo-visual abnormalities in Parkinson's disease: possible value as biomarkers. Mov. Disord. 33, 1390–1406. https://doi.org/10.1002/mds.27454.

Guo, L., Salt, T.E., Luong, V., Wood, N., Cheung, W., Maass, A., Ferrari, G., Russo-Marie, F., Sillito, A.M., Cheetham, M.E., Moss, S.E., Fitzke, F.W., Cordeiro, M.F., 2007. Targeting amyloid-β in glaucoma treatment. Proc. Natl. Acad. Sci. U. S. A 104, 13444–13449. https://doi.org/10.1073/pnas.0703707104.

Guo, L., Salt, T.E., Maass, A., Luong, V., Moss, S.E., Fitzke, F.W., Cordeiro, M.F., 2006. Assessment of neuroprotective effects of glutamate modulation on glaucoma-related retinal ganglion cell apoptosis in vivo. Investig. Ophthalmol. Vis. Sci. 47, 626–633. https://doi.org/10.1167/iovs.05-0754.

Gupta, D., Chen, P.P., 2016. Glaucoma. Am. Fam. Physician 93, 668–674. https://doi.org/10.5937/halo1803189j.

Gupta, V.B., Chitranshi, N., Haan, J., den Mirzaei, M., You, Y., Lim, J.K., Basavarajappa, D., Godinez, A., Di Angelantonio, S., Sachdev, P., Salekdeh, G.H., Bouwman, F., Graham, S., Gupta, V., 2020. Retinal changes in Alzheimer's disease—integrated prospects of imaging, functional and molecular advances. Prog. Retin. Eye Res. https://doi.org/10.1016/j.preteyeres.2020.100899.

Haas, R.L.M., De Jong, D., Valdés Olmos, R.A., Hoefnagel, C.A., Van Den Heuvel, I., Zerp, S.F., Bartelink, H., Verheij, M., 2004. In vivo imaging of radiation-induced apoptosis in follicular lymphoma patients. Int. J. Radiat. Oncol. Biol. Phys. 59, 782–787. https://doi.org/10.1016/j.ijrobp.2003.11.017.

Hankins, H.M., Baldridge, R.D., Xu, P., Graham, T.R., 2015. Role of flippases, scramblases and transfer proteins in phosphatidylserine subcellular distribution. Traffic 16, 35–47. https://doi.org/10.1111/tra.12233.

Harnois, C., Di Paolo, T., 1990. Decreased dopamine in the retinas of patients with Parkinson's disease. Investig. Ophthalmol. Vis. Sci. 31, 2473–2475.

Hassenstein, A., Meyer, C.H., 2009. Clinical use and research applications of Heidelberg retinal angiography and spectral-domain optical coherence tomography - a review. Clin. Exp. Ophthalmol. https://doi.org/10.1111/j.1442-9071.2009.02017.x.

Hayes, M.J., Moss, S.E., 2004. Annexins and disease. Biochem. Biophys. Res. Commun. 322, 1166–1170. https://doi.org/10.1016/j.bbrc.2004.07.124.

Head, T., Dau, P., Duffort, S., Daftarian, P., Joshi, P.M., Vazquez-Padron, R., Deo, S.K., Daunert, S., 2017. An enhanced bioluminescence-based Annexin V probe for apoptosis detection in vitro and in vivo. Cell Death Dis. https://doi.org/10.1038/cddis.2017.141.

Heesterbeek, T.J., Lorés-Motta, L., Hoyng, C.B., Lechanteur, Y.T.E., den Hollander, A.I., 2020. Risk factors for progression of age-related macular degeneration. Ophthalmic Physiol. Opt. https://doi.org/10.1111/opo.12675.

Ho, C.Y., Troncoso, J.C., Knox, D., Stark, W., Eberhart, C.G., 2014. Beta-amyloid, phospho-tau and alpha-synuclein deposits similar to those in the brain are not identified in the eyes of Alzheimer's and Parkinson's disease patients. Brain Pathol. https://doi.org/10.1111/bpa.12070.

Hoebers, F.J.P., Kartachova, M., De Bois, J., Van Den Brekel, M.W.M., Van Tinteren, H., Van Herk, M., Rasch, C.R.N., Valdés Olmos, R.A., Verheij, M., 2008. 99mTc Hynic-rh-Annexin V scintigraphy for in vivo imaging of apoptosis in patients with head and neck cancer treated with chemoradiotherapy. Eur. J. Nucl. Med. Mol. Imag. 35, 509–518. https://doi.org/10.1007/s00259-007-0624-x.

Hofstra, L., Liem, I.H., Dumont, E.A., Boersma, H.H., Van Heerde, W.L., Doevendans, P. A., Demuinck, E., Wellens, H.J.J., Kemerink, G.J., Reutelingsperger, C.P.M., Heidendal, G.A., 2000. Visualisation of cell death in vivo in patients with acute myocardial infarction. Lancet 356, 209–212. https://doi.org/10.1016/S0140-6736(00)02482-X.

Holz, F.G., Sadda, S.V.R., Staurenghi, G., Lindner, M., Bird, A.C., Blodi, B.A., Bottoni, F., Chakravarthy, U., Chew, E.Y., Csaky, K., Curcio, C.A., Danis, R., Fleckenstein, M., Freund, K.B., Grunwald, J., Guymer, R., Hoyng, C.B., Jaffe, G.J., Liakopoulos, S., Monés, J.M., Oishi, A., Pauleikhoff, D., Rosenfeld, P.J., Sarraf, D., Spaide, R.F., Tadayoni, R., Tufail, A., Wolf, S., Schmitz-Valckenberg, S., 2017. Imaging protocols in clinical studies in advanced age-related macular degeneration: recommendations from classification of atrophy consensus Meetings. In: Ophthalmology. https://doi.org/10.1016/j.ophtha.2016.12.002.

Hormel, T.T., Hwang, T.S., Bailey, S.T., Wilson, D.J., Huang, D., Jia, Y., 2021. Artificial intelligence in OCT angiography. Prog. Retin. Eye Res. https://doi.org/10.1016/j.preteyeres.2021.100965.

Horstmann, L., Schmid, H., Heinen, A.P., Kurschus, F.C., Dick, H.B., Joachim, S.C., 2013. Inflammatory demyelination induces glia alterations and ganglion cell loss in the retina of an experimental autoimmune encephalomyelitis model. J. Neuroinflammation. https://doi.org/10.1186/1742-2094-10-120.

Huang, D., Swanson, E.A., Lin, C.P., Schuman, J.S., Stinson, W.G., Chang, W., Hee, M.R., Flotte, T., Gregory, K., Puliafito, C.A., Fujimoto, J.G., 1991. Optical coherence tomography. Science 254, 1178–1181. https://doi.org/10.1126/science.1957169 (80-.).

Iseri, P.K., Altinaş, Ö., Tokay, T., Yüksel, N., 2006. Relationship between cognitive impairment and retinal morphological and visual functional abnormalities in Alzheimer disease. J. Neuro Ophthalmol. https://doi.org/10.1097/01.wno.0000204645.56873.26.

Ito, A., Tsuda, S., Kunikata, H., Toshifumi, A., Sato, K., Nakazawa, T., 2019. Assessing retinal ganglion cell death and neuroprotective agents using real time imaging. Brain Res. https://doi.org/10.1016/j.brainres.2019.02.008.

Jonas, J.B., Aung, T., Bourne, R.R., Bron, A.M., Ritch, R., Panda-Jonas, S., 2017. Glaucoma. Lancet. https://doi.org/10.1016/S0140-6736(17), 31469–1.

Kaarniranta, K., Uusitalo, H., Blasiak, J., Felszeghy, S., Kannan, R., Kauppinen, A., Salminen, A., Sinha, D., Ferrington, D., 2020. Mechanisms of mitochondrial

dysfunction and their impact on age-related macular degeneration. Prog. Retin. Eye Res. 79 https://doi.org/10.1016/j.preteyeres.2020.100858, 100858.
Kanagasingam, Y., Bhuiyan, A., Abràmoff, M.D., Smith, R.T., Goldschmidt, L., Wong, T. Y., 2014. Progress on retinal image analysis for age related macular degeneration. Prog. Retin. Eye Res. https://doi.org/10.1016/j.preteyeres.2013.10.002.
Kanamori, A., Catrinescu, M.M., Kanamori, N., Mears, K.A., Beaubien, R., Levin, L.A., 2010. Superoxide is an associated signal for apoptosis in axonal injury. Brain. https://doi.org/10.1093/brain/awq105.
Kapetanakis, V.V., Chan, M.P.Y., Foster, P.J., Cook, D.G., Owen, C.G., Rudnicka, A.R., 2016. Global variations and time trends in the prevalence of primary open angle glaucoma (POAG): a systematic review and meta-analysis. Br. J. Ophthalmol. https://doi.org/10.1136/bjophthalmol-2015-307223.
Kartachova, M., Haas, R.L.M., Valdés Olmos, R.A., Hoebers, F.J.P., Van Zandwijk, N., Verheij, M., 2004. In vivo imaging of apoptosis by 99mTc-Annexin V scintigraphy: visual analysis in relation to treatment response. In: Radiotherapy and Oncology, pp. 333–339. https://doi.org/10.1016/j.radonc.2004.07.008.
Kartachova, M., van Zandwijk, N., Burgers, S., Van Tinteren, H., Verheij, M., Olmos, R.A. V., Valdes Olmos, R.A., 2007. Prognostic significance of 99mTc Hynic-rh-annexin V scintigraphy during platinum-based chemotherapy in advanced lung cancer. J. Clin. Oncol. 25, 2534–2539. https://doi.org/10.1200/JCO.2006.10.1337.
Kartachova, M.S., Valdés Olmos, R.A., Haas, R.L.M., Hoebers, F.J.P., Herk, van, M., Verheij, M., 2008. 99mTc-HYNIC-rh-annexin-V scintigraphy: visual and quantitative evaluation of early treatment-induced apoptosis to predict treatment outcome. Nucl. Med. Commun. 29, 39–44. https://doi.org/10.1097/MNM.0b013e3282f1bc22.
Kartachova, M.S., Valdés Olmos, R.A., Haas, R.L.M., Hoebers, F.J.P., Van Den Brekel, M. W., Van Zandwijk, N., Herk, M Van, Verheij, M., 2006. Mapping of treatment-induced apoptosis in normal structures: 99mTc-Hynic-rh-annexin V SPECT and CT image fusion. Eur. J. Nucl. Med. Mol. Imag. 33, 893–899. https://doi.org/10.1007/s00259-006-0070-1.
Kassoff, A., Kassoff, J., Buehler, J., Eglow, M., Kaufman, F., Mehu, M., Kieval, S., Mairs, M., Graig, B., Quattrocchi, A., Jones, D., Locatelli, J., Ruby, A., Capon, A.J., Garretson, B., Hassan, T., Trese, M.T., Williams, G.A., Regan, V., Manatrey, P., Streasick, P., Szydlowski, L., McIver, F., Bridges, C., Stanley, C., Cumming, K., Lewis, B., Zajechowski, M., Margherio, R.R., Cox, M.S., Werner, J.C., Falk, R., Siedlak, P., Neubert, C., Klein, M.L., Stout, J.T., O'Malley, A., Lauer, A.K., Robertson, J.E., Wilson, D.J., Beardsley, C., Anderson, H., Wallace, P., Smith, G., Howard, S., Dreyer, R.F., Ma, C., Chenoweth, R.G., Zilis, J.D., Johnson, M., Rice, P., Daniel, H., Crider, H., Parker, S., Sherman, K., Martin, D.F., Aaberg, S., Sternberg, P. J., Curtis, L.T., Ju, B., Gilman, J., Myles, B., Strittman, S., Gentry, C., Yi, H., Capone, A.J., Lambert, M., Meredith, T., Aaberg, J., Saperstein, D., Lim, J.I., Stribling, B., Armiger, D., Swords, R., Orth, D.H., Flood, T.P., Civantos, J., Debustros, S., Packo, K.H., Merrill, P.T., Cohen, J.A., Figliulo, C., Morrison, C., Bryant, D.A., Doherty, D., McVicker, M., Drefcinski, T., Seddon, J.M., Pinnolis, M.K., Davis, N., Burton, I., Taitsel, T., Walsh, D., Dubois-Moran, J., Callahan, C., Evans, C., Snow, K.K., Jones-Devonish, D.A., Crouse, V.D., 2001. A randomised, placebo-controlled, clinical trial of high-dose supplementation with vitamins C and E, beta carotene, and zinc for age-related macular degeneration and vision loss: AREDS report no. 8. Arch. Ophthalmol. 119, 1417–1436. https://doi.org/10.1001/archopht.119.10.1417.
Keane, P.A., Sadda, S.R., 2010. Imaging chorioretinal vascular disease. In: Eye, pp. 422–427. https://doi.org/10.1038/eye.2009.309.
Keenan, T.D., Clemons, T.E., Domalpally, A., Elman, M.J., Havilio, M., Agrón, E., Benyamini, G., Chew, E.Y., 2020. Retinal specialist versus artificial intelligence detection of retinal fluid from optical coherence tomography: AREDS2 10-year Follow-On. Ophthalmology. https://doi.org/10.1016/j.ophtha.2020.06.038.
Kemerink, G.J., Liu, X., Kieffer, D., Ceyssens, S., Mortelmans, L., Verbruggen, A.M., Steinmetz, N.D., Vanderheyden, J.L., Green, A.M., Verbeke, K., 2003. Safety, biodistribution, and dosimetry of 99mTc-HYNIC-Annexin V, a novel human recombinant annexin V for human application. J. Nucl. Med. 44, 947–952.
Kenis, H., Zandbergen, H.R., Hofstra, L., Petrov, A.D., Dumont, E.A., Blankenberg, F.D., Haider, N., Bitsch, N., Gijbels, M., Verjans, J.W.H., Narula, N., Naru, J., Reutelingsperger, C.P.M., 2010. Annexin A5 uptake in ischemic myocardium: demonstration of reversible phosphatidylserine externalization and feasibility of radionuclide imaging. J. Nucl. Med. 51, 259–267. https://doi.org/10.2967/jnumed.109.068429.
Kerrigan, L.A., Zack, D.J., Quigley, H.A., Smith, S.D., Pease, M.E., 1997. TUNEL-positive ganglion cells in human primary open-angle glaucoma. Arch. Ophthalmol. 115, 1031–1035. https://doi.org/10.1001/archopht.1997.01100160201010.
Kesler, A., Vakhapova, V., Korczyn, A.D., Naftaliev, E., Neudorfer, M., 2011. Retinal thickness in patients with mild cognitive impairment and Alzheimer's disease. Clin. Neurol. Neurosurg. https://doi.org/10.1016/j.clineuro.2011.02.014.
Khaw, P.T., Elkington, A.R., 2004. Glaucoma—1: diagnosis. BMJ 328 (97). https://doi.org/10.1136/bmj.328.7431.97.
Kietselaer, B.L., Reutelingsperger, C.P., Heidendal, G.A., Daemen, M.J., Mess, W.H., Hofstra, L., Narula, J., 2004. Noninvasive detection of plaque instability with use of radiolabeled annexin A5 in patients with carotid-artery atherosclerosis. N. Engl. J. Med. 350, 1472–1473.
Kietselaer, B.L.J.H., Reutelingsperger, C.P.M., Boersma, H.H., Heidendal, G.A.K., Ing, H. L., Crijns, H.J.G.M., Narula, J., Hofstra, L., 2007. Noninvasive detection of programmed cell loss with 99mTc-labeled annexin A5 in heart failure. J. Nucl. Med. 48, 562–567. https://doi.org/10.2967/jnumed.106.039453.
Kompella, U.B., Hartman, R.R., Patil, M.A., 2020. Extraocular, periocular, and intraocular routes for sustained drug delivery for glaucoma. Prog. Retin. Eye Res. https://doi.org/10.1016/j.preteyeres.2020.100901.
Koronyo-Hamaoui, M., Koronyo, Y., Ljubimov, A.V., Miller, C.A., Ko, M.H.K., Black, K.L., Schwartz, M., Farkas, D.L., 2011. Identification of amyloid plaques in retinas from Alzheimer's patients and noninvasive in vivo optical imaging of retinal plaques in a mouse model. Neuroimage 54, S204–S217. https://doi.org/10.1016/j.neuroimage.2010.06.020.
Koronyo, Y., Biggs, D., Barron, E., Boyer, D.S., Pearlman, J.A., Au, W.J., Kile, S.J., Blanco, A., Fuchs, D.T., Ashfaq, A., Frautschy, S., Cole, G.M., Miller, C.A., Hinton, D. R., Verdooner, S.R., Black, K.L., Koronyo-Hamaoui, M., 2017. Retinal amyloid pathology and proof-of-concept imaging trial in Alzheimer's disease. JCI insight 2. https://doi.org/10.1172/jci.insight.93621.
Koronyo, Y., Salumbides, B.C., Black, K.L., Koronyo-Hamaoui, M., 2012. Alzheimer's disease in the retina: imaging retinal Aβ plaques for early diagnosis and therapy assessment. Neurodegener. Dis. 10, 285–293. https://doi.org/10.1159/000335154.
Kouli, A., Torsney, K.M., Kuan, W.-L., 2018. Parkinson's disease: etiology, neuropathology, and pathogenesis. In: Parkinson's Disease: Pathogenesis and Clinical Aspects. https://doi.org/10.15586/codonpublications.parkinsonsdisease.2018.ch1.
Krieger, S.C., Cook, K., de Nino, S., Fletcher, M., 2016. The topographical model of multiple sclerosis: a dynamic visualization of disease course. Neurol. Neuroimmunol. https://doi.org/10.1212/NXI.0000000000000279. NeuroInflammation.
Kurihara, H., Yang, D.J., Cristofanilli, M., Erwin, W.D., Yu, D.F., Kohanim, S., Mendez, R., Kim, E.E., 2008. Imaging and dosimetry of 99mTc EC annexin V: preliminary clinical study targeting apoptosis in breast tumors. Appl. Radiat. Isot. 66, 1175–1182. https://doi.org/10.1016/j.apradiso.2008.01.012.
Lahorte, C.M.M., Van de wiele, C., Bacher, K., Van den bossche, B., Thierens, H., Van belle, S., Slegers, G., Dierckx, R.A., 2003. Biodistribution and dosimetry study of i-rh-annexin v in mice and humans. Nucl. Med. Commun. 24, 871–880. https://doi.org/10.1097/01.mnm.0000084585.29433.58.
Lambert, N.G., ElShelmani, H., Singh, M.K., Mansergh, F.C., Wride, M.A., Padilla, M., Keegan, D., Hogg, R.E., Ambati, B.K., 2016. Risk factors and biomarkers of age-related macular degeneration. Prog. Retin. Eye Res. https://doi.org/10.1016/j.preteyeres.2016.04.003.
Lampl, Y., Lorberboym, M., Blankenberg, F.G., Sadeh, M., Gilad, R., 2006. Annexin V SPECT imaging of phosphatidylserine expression in patients with dementia. Neurology 66, 1253–1254. https://doi.org/10.1212/01.wnl.0000208436.75615.8c.
Leske, M.C., Heijl, A., Hussein, M., Bengtsson, B., Hyman, L., Komaroff, E., Lee, P., 2003. Factors for glaucoma progression and the effect of treatment. Evid. Base Eye Care 4, 196–197. https://doi.org/10.1097/00132578-200310000-00007.
Li, T., Aredo, B., Zhang, K., Zhong, X., Pulido, J.S., Wang, S., He, Y., Huang, X., Brekken, R.A., Ufret-vincenty, R.L., 2015. Phosphatidylserine (PS) is exposed in choroidal neovascular Endothelium : PS-targeting antibodies inhibit choroidal angiogenesis in vivo and ex vivo. Invest. Ophthalmol. Vis. Sci. 56, 7137–7145. https://doi.org/10.1167/iovs.15-17302.
Li, X., Wang, C., Tan, H., Cheng, L., Liu, G., Yang, Y., Zhao, Y., Zhang, Y., Li, Y., Zhang, C., Xiu, Y., Cheng, D., Shi, H., 2016. Gold nanoparticles-based SPECT/CT imaging probe targeting for vulnerable atherosclerosis plaques. Biomaterials 108, 71–80. https://doi.org/10.1016/j.biomaterials.2016.08.048.
Liang, J., Williams, D.R., Miller, D.T., 1997. Supernormal vision and high-resolution retinal imaging through adaptive optics. J. Opt. Soc. Am. A 14 (2884). https://doi.org/10.1364/josaa.14.002884.
Lim, J.H., Wickremasinghe, S.S., Xie, J., Chauhan, D.S., Baird, P.N., Robman, L.D., Hageman, G., Guymer, R.H., 2012a. Delay to treatment and visual outcomes in patients treated with anti-vascular endothelial growth factor for age-related macular degeneration. Am. J. Ophthalmol. 153 https://doi.org/10.1016/j.ajo.2011.09.013.
Lim, L.S., Mitchell, P., Seddon, J.M., Holz, F.G., Wong, T.Y., 2012b. Age-related macular degeneration. Lancet 60282–60287. https://doi.org/10.1016/S0140-6736(12).
Liu, Z., Kurokawa, K., Zhang, F., Lee, J.J., Miller, D.T., 2017. Imaging and quantifying ganglion cells and other transparent neurons in the living human retina. Proc. Natl. Acad. Sci. U. S. A. https://doi.org/10.1073/pnas.1711734114.
Lorberboym, M., Blankenberg, F.G., Sadeh, M., Lampl, Y., 2006. In vivo imaging of apoptosis in patients with acute stroke: correlation with blood-brain barrier permeability. Brain Res. 1103, 13–19.
Maass, A., Von Leithner, P.L., Luong, V., Guo, L., Salt, T.E., Fitzke, F.W., Cordeiro, M.F., 2007a. Assessment of rat and mouse RGC apoptosis imaging in vivo with different scanning laser ophthalmoscopes. Curr. Eye Res. 32 https://doi.org/10.1080/02713680701585872.
Maass, Annelie, Von Leithner, P.L., Luong, V., Guo, L., Salt, T.E., Fitzke, F.W., Cordeiro, M.F.F., 2007b. Assessment of rat and mouse RGC apoptosis imaging in vivo with different scanning laser ophthalmoscopes. Curr. Eye Res. 32, 851–861. https://doi.org/10.1080/02713680701585872.
Mailankody, P., Battu, R., Khanna, A., Lenka, A., Yadav, R., Pal, P.K., 2015. Optical coherence tomography as a tool to evaluate retinal changes in Parkinson's disease. Park. Relat. Disord. https://doi.org/10.1016/j.parkreldis.2015.08.002.
Malerbi, F.K., Hatanaka, M., Vessani, R.M., Susanna, R., 2005. Intraocular pressure variability in patients who reached target intraocular pressure. Br. J. Ophthalmol. 89, 540–542. https://doi.org/10.1136/bjo.2004.058230.
Marcus, C., Mena, E., Subramaniam, R.M., 2014. Brain PET in the diagnosis of Alzheimer's disease. Clin. Nucl. Med. https://doi.org/10.1097/RLU.0000000000000547.
Martin, M., Leffler, J., Blom, A.M., 2012. Annexin A2 and A5 serve as new ligands for C1q on apoptotic cells. J. Biol. Chem. https://doi.org/10.1074/jbc.M112.341339.
Massalha, S., Ferro, P., Ascah, K., Carey, C., Marvin, B., Dwivedi, G., Wells, R.G., Ravasi, L., Ruddy, T., 2018. Detection of Apoptosis with 99mTc rh Annexin-V 128 Imaging in asymptomatic patients with carotid atherosclerotic plaque. In: J. Nucl. Med. Conf. Soc. Nucl. Med. Mol. Imaging Annu. Meet. SNMMI.
Meers, P., Mealy, T., 1993. Calcium-dependent annexin V binding to phospholipids: stoichiometry, specificity, and the role of negative charge. Biochemistry. https://doi.org/10.1021/bi00094a030.

Meijer, P., Oyen, W.J.G., Dekker, D., Van Den Broek, P.H.H., Wouters, C.W., Boerman, O. C., Scheffer, G.J., Smits, P., Rongen, G.A., 2009. Rosuvastatin increases extracellular adenosine formation in humans in vivo: a new 11 perspective on cardiovascular protection. Arterioscler. Thromb. Vasc. Biol. https://doi.org/10.1161/ATVBAHA.108.179622.

Meijer, P., Wouters, C.W., Oyen, W.J., Boerman, O.C., Scheffer, G.J., Smits, P., Rongen, G.A., 2011. Angiotensin II type 1 receptor blockade does not enhance apoptotic cell death during ischemia and reperfusion in humans in vivo. J. Cardiovasc. Pharmacol. 57, 702–706. https://doi.org/10.1097/FJC.0b013e318218ef21.

Meloni, B.P., Meade, A.J., Kitikomolsuk, D., Knuckey, N.W., 2011. Characterisation of neuronal cell death in acute and delayed in vitro ischemia (oxygen-glucose deprivation) models. J. Neurosci. Methods. https://doi.org/10.1016/j.jneumeth.2010.11.023.

Mettu, P.S., Allingham, M.J., Cousins, S.W., 2020. Incomplete response to Anti-VEGF therapy in neovascular AMD: exploring disease mechanisms and therapeutic opportunities. Prog. Retin. Eye Res. https://doi.org/10.1016/j.preteyeres.2020.100906.

Meyer, R., Weissert, R., Diem, R., Storch, M.K., De Graaf, K.L., Kramer, B., Bähr, M., 2001. Acute neuronal apoptosis in a rat model of multiple sclerosis. J. Neurosci. https://doi.org/10.1523/jneurosci.21-16-06214.2001.

Mogi, M., Togari, A., Kondo, T., Mizuno, Y., Komure, O., Kuno, S., Ichinose, H., Nagatsu, T., 2000. Caspase activities and tumor necrosis factor receptor R1 (p55) level are elevated in the substantia nigra from Parkinsonian brain. J. Neural. Transm. https://doi.org/10.1007/s007020050028.

Monastyrskaya, K., Babiychuk, E.B., Draeger, A., 2009. The annexins: spatial and temporal coordination of signaling events during cellular stress. Cell. Mol. Life Sci. https://doi.org/10.1007/s00018-009-0027-1.

More, S.S., Vince, R., 2015. Hyperspectral imaging signatures detect amyloidopathy in alzheimers mouse retina well before onset of cognitive decline. ACS Chem. Neurosci. https://doi.org/10.1021/cn500242z.

Murakami, Y., Takamatsu, H., Taki, J., Tatsumi, M., Noda, A., Ichise, R., Tait, J.F., Nishimura, S., 2004. 18F-labelled annexin V: a PET tracer for apoptosis imaging. Eur. J. Nucl. Med. Mol. Imag. 31, 469–474. https://doi.org/10.1007/s00259-003-1378-8.

Nagata, S., Suzuki, J., Segawa, K., Fujii, T., 2016. Exposure of phosphatidylserine on the cell surface. Cell Death Differ. https://doi.org/10.1038/cdd.2016.7.

Narula, J., Acio, E.R., Narula, N., Samuels, L.E., Fyfe, B., Wood, D., Fitzpatrick, J.M., Raghunath, P.N., Tomaszewski, J.E., Kelly, C., Steinmetz, N., Green, A., Tait, J.F., Leppo, J., Blankenberg, F.G., Jain, D., Strauss, H.W., 2001. Annexin-V imaging for noninvasive detection of cardiac allograft rejection. Nat. Med. 7, 1347–1352. https://doi.org/10.1038/nm1201-1347.

Ning, F., Hou, H., Morse, A.N., Lash, G.E., 2019. Understanding and management of gestational trophoblastic disease. F1000Research. https://doi.org/10.12688/f1000research.14953.1.

Nizari, S., Guo, L., Davis, B.M., Normando, E.M., Galvao, J., Turner, L.A., Bizrah, M., Dehabadi, M., Tian, K., Cordeiro, M.F., 2016. Non-amyloidogenic effects of α2 adrenergic agonists: implications for brimonidine-mediated neuroprotection. Cell Death Dis. 7 https://doi.org/10.1038/cddis.2016.397.

Normando, E.M., Davis, B.M., De Groef, L., Nizari, S., Turner, L.A., Ravindran, N., Pahlitzsch, M., Brenton, J., Malaguarnera, G., Guo, L., Somavarapu, S., Cordeiro, M. F., 2016a. The retina as an early biomarker of neurodegeneration in a rotenone-induced model of Parkinson's disease: evidence for a neuroprotective effect of rosiglitazone in the eye and brain. Acta Neuropathol. Commun 4. https://doi.org/10.1186/s40478-016-0346-z.

Normando, Eduardo Maria, Davis, B.M., De Groef, L., Nizari, S., Turner, L.A., Ravindran, N., Pahlitzsch, M., Brenton, J., Malaguarnera, G., Guo, L., Somavarapu, S., Cordeiro, M.F., 2016b. The retina as an early biomarker of neurodegeneration in a rotenone-induced model of Parkinson's disease: evidence for a neuroprotective effect of rosiglitazone in the eye and brain. Acta Neuropathol. Commun 4. https://doi.org/10.1186/s40478-016-0346-z.

Normando, E.M., Tilley, M., Guo, L., Cordeiro, M.F., 2013a. Imaging in DRY AMD. Drug discov. Today Ther. Strateg. https://doi.org/10.1016/j.ddstr.2013.02.001.

Normando, E.M., Turner, L.A., Cordeiro, M.F., 2013b. The potential of annexin-labelling for the diagnosis and follow-up of glaucoma. Cell Tissue Res. 353, 279–285. https://doi.org/10.1007/s00441-013-1554-5.

Normando, E.M., Yap, T.E., Maddison, J., Miodragovic, S., Bonetti, P., Almonte, M., Mohammad, N.G., Ameen, S., Crawley, L., Ahmed, F., Bloom, P.A., Cordeiro, M.F., 2020. A CNN-aided method to predict glaucoma progression using DARC (Detection of Apoptosing Retinal Cells). Expert Rev. Mol. Diagn. https://doi.org/10.1080/14737159.2020.1758067.

Ohtsuki, K., Akashi, K., Aoka, Y., Blankenberg, F.G., Kopiwoda, S., Tait, J.F., Strauss, H. W., 1999. Technetium-99m HYNIC-annexin V: a potential radiopharmaceutical for the in-vivo detection of apoptosis. Eur. J. Nucl. Med. 26, 1251–1258. https://doi.org/10.1007/s002590050580.

Pagano, G., Niccolini, F., Politis, M., 2016. Imaging in Parkinson's disease. Clin. Med. J. R. Coll. Physicians London. https://doi.org/10.7861/clinmedicine.16-4-371.

Paradis, E., Douillard, H., Koutroumanis, M., Goodyer, C., LeBlanc, A., 1996. Amyloid β peptide of Alzheimer's disease downregulates bcl-2 and upregulates bax expression in human neurons. J. Neurosci. https://doi.org/10.1523/jneurosci.16-23-07533.1996.

Pardue, M.T., Allen, R.S., 2018. Neuroprotective strategies for retinal disease. Prog. Retin. Eye Res. 65, 50–76. https://doi.org/10.1016/j.preteyeres.2018.02.002.

Parisi, V., Ziccardi, L., Costanzo, E., Tedeschi, M., Barbano, L., Manca, D., Di Renzo, A., Giorno, P., Varano, M., Parravano, M., 2020. Macular functional and morphological changes in intermediate age-related maculopathy. Investig. Ophthalmol. Vis. Sci. https://doi.org/10.1167/IOVS.61.5.11.

Park, H.Y.L., Jeon, S.H., Park, C.K., 2012. Enhanced depth imaging detects lamina cribrosa thickness differences in normal tension glaucoma and primary open-angle glaucoma. Ophthalmology 119, 10–20. https://doi.org/10.1016/j.ophtha.2011.07.033.

Park, J.H., Jang, J.H., Choi, E.J., Kim, Y.S., Lee, E.J., Jung, I.D., Han, H.D., Wu, T.C., Hung, C.F., Kang, T.H., Park, Y.M., 2016. Annexin A5 increases survival in murine sepsis model by inhibiting HMGB1-mediated proinflammation and coagulation. Mol. Med. https://doi.org/10.2119/molmed.2016.00026.

Parviz, M., Esfandiari, H., Behnaz, N., Fatemeh, J., Sima, A., Javadi, Mohammad Ali, Kalantarion, M., 2017. Toward the art of robotic assisted vitreoretinal surgery. J. Ophthalmic Vis. Res. 12, 270–274. https://doi.org/10.4103/jovr.jovr.

Parzen, E., 1962. On estimation of a probability density function and mode. Ann. Math. Stat. 33, 1065–1076. https://doi.org/10.1214/aoms/1177704472.

Pawlitzki, M., Horbrügger, M., Loewe, K., Kaufmann, J., Opfer, R., Wagner, M., Al-Nosairy, K.O., Meuth, S.G., Hoffmann, M.B., Schippling, S., 2020. MS optic neuritis-induced long-term structural changes within the visual pathway. Neurol. Neuroimmunol. neuroinflammation. https://doi.org/10.1212/NXI.0000000000000665.

Pedregosa, F., Varoquaux, G., Gramfort, A., Michel, V., Thirion, B., Grisel, O., Blondel, M., Prettenhofer, P., Weiss, R., Dubourg, V., Vanderplas, J., Passos, A., Cournapeau, D., Brucher, M., Perrot, M., Duchesnay, E., 2011. Scikit-learn: machine learning in Python. J. Mach. Learn. Res. 12, 2825–2830.

Peiretti, E., Iovino, C., 2019. Indocyanine green angiography. In: Central Serous Chorioretinopathy. https://doi.org/10.1016/B978-0-12-816800-4.00009-7.

Petzold, A., Balcer, L., Calabresi, P.A., Costello, F., Frohman, T., Frohman, E., Martinez-Lapiscina, E.H., Green, A., Kardon, R., Outteryck, O., Paul, F., Schippling, S., Vermersch, P., Villoslada, P., Balk, L., Aktas, O., Albrecht, P., Ashworth, J., Asgari, N., Black, G., Boehringer, D., Behbehani, R., Benson, L., Bermel, R., Bernard, J., Brandt, A., Burton, J., Calabresi, P., Calkwood, J., Cordano, C., Courtney, A., Cruz-Herranz, A., Diem, R., Daly, A., Dollfus, H., Fasser, C., Finke, C., Frederiksen, J., Garcia-Martin, E., Suárez, I.G., Pihl-Jensen, G., Graves, J., Havla, J., Hemmer, B., Huang, S.C., Imitola, J., Jiang, H., Keegan, D., Kildebeck, E., Klistorner, A., Knier, B., Kolbe, S., Korn, T., LeRoy, B., Leocani, L., Leroux, D., Levin, N., Liskova, P., Lorenz, B., Preiningerova, J.L., Martínez-Lapiscina, E.H., Mikolajczak, J., Montalban, X., Morrow, M., Nolan, R., Oberwahrenbrock, T., Oertel, F.C., Oreja-Guevara, C., Osborne, B., Papadopoulou, A., Ringelstein, M., Saidha, S., Sanchez-Dalmau, B., Sastre-Garriga, J., Shin, R., Shuey, N., Soelberg, K., Toosy, A., Torres, R., Vidal-Jordana, A., Waldman, A., White, O., Yeh, A., Wong, S., Zimmermann, H., 2017. Retinal layer segmentation in multiple sclerosis: a systematic review and meta-analysis. Lancet Neurol. https://doi.org/10.1016/S1474-4422(17), 30278–8.

Quigley, H.A., Broman, A.T., 2006. The number of people with glaucoma worldwide in 2010 and 2020. Br. J. Ophthalmol. 90, 262–267.

Raftery, J., Clegg, A., Jones, J., Seng, C.T., Lotery, A., 2007. Ranibizumab (lucentis) versus bevacizumab (avastin): modelling cost effectiveness. Br. J. Ophthalmol. https://doi.org/10.1136/bjo.2007.116616.

Reichstein, D., Ren, L., Filippopoulos, T., Mittag, T., Danias, J., 2007. Apoptotic retinal ganglion cell death in the DBA/2 mouse model of glaucoma. Exp. Eye Res. 84, 13–21. https://doi.org/10.1016/j.exer.2006.08.009.

Rescher, U., Gerke, V., 2004. Annexins - unique membrane binding proteins with diverse functions. J. Cell Sci. https://doi.org/10.1242/jcs.01245.

Rongen, G.A., Oyen, W.J.G., Ramakers, B.P., Riksen, N.P., Boerman, O.C., Steinmetz, N., Smits, P., 2005. Annexin A5 scintigraphy of forearm as a novel in vivo model of skeletal muscle preconditioning in humans. Circulation 111, 173–178. https://doi.org/10.1161/01.CIR.0000151612.02223.F2.

Rosenblatt, M., 1956. Remarks on some nonparametric estimates of a density function. Ann. Math. Stat. 27, 832–837. https://doi.org/10.1214/aoms/1177728190.

Rosenfeld, P.J., 2016. Optical coherence tomography and the development of antiangiogenic therapies in neovascular age-related macular degeneration. Invest. Ophthalmol. Vis. Sci. https://doi.org/10.1167/iovs.16-19969, 57, OCT14-OCT26.

Rossi, E.A., Granger, C.E., Sharma, R., Yang, Q., Saito, K., Schwarz, C., Walters, S., Nozato, K., Zhang, J., Kawakami, T., Fischer, W., Latchney, L.R., Hunter, J.J., Chung, M.M., Williams, D.R., 2017. Imaging individual neurons in the retinal ganglion cell layer of the living eye. In: Proc. Natl. Acad. Sci. U. S. A, vol. 114, pp. 586–591. https://doi.org/10.1073/pnas.1613445114.

Sadda, S.R., Guymer, R., Holz, F.G., Schmitz-Valckenberg, S., Curcio, C.A., Bird, A.C., Blodi, B.A., Bottoni, F., Chakravarthy, U., Chew, E.Y., Csaky, K., Danis, R.P., Fleckenstein, M., Freund, K.B., Grunwald, J., Hoyng, C.B., Jaffe, G.J., Liakopoulos, S., Monés, J.M., Pauleikhoff, D., Rosenfeld, P.J., Sarraf, D., Spaide, R.F., Tadayoni, R., Tufail, A., Wolf, S., Staurenghi, G., 2018. Consensus definition for atrophy associated with age-related macular degeneration on OCT: classification of atrophy report 3. Ophthalmology. https://doi.org/10.1016/j.ophtha.2017.09.028.

Saidha, S., Al-Louzi, O., Ratchford, J.N., Bhargava, P., Oh, J., Newsome, S.D., Prince, J. L., Pham, D., Roy, S., Van Zijl, P., Balcer, L.J., Frohman, E.M., Reich, D.S., Crainiceanu, C., Calabresi, P.A., 2015. Optical coherence tomography reflects brain atrophy in multiple sclerosis: a four-year study. Ann. Neurol. https://doi.org/10.1002/ana.24487.

Salt, T.E., Nizari, S., Cordeiro, M.F., Russ, H., Danysz, W., 2014. Effect of the aβ aggregation modulator MRZ-99030 on retinal damage in an animal model of glaucoma. Neurotox. Res. 26, 440–446. https://doi.org/10.1007/s12640-014-9488-6.

Satue, M., Rodrigo, M.J., Obis, J., Vilades, E., Gracia, H., Otin, S., Fuertes, M.I., Alarcia, R., Crespo, J.A., Polo, V., Larrosa, J.M., Pablo, L.E., Garcia-Martin, E., 2017. Evaluation of progressive visual dysfunction and retinal degeneration in patients

with Parkinson's disease. Investig. Ophthalmol. Vis. Sci. https://doi.org/10.1167/iovs.16-20460.
Schinzel, J., Zimmermann, H., Paul, F., Ruprecht, K., Hahn, K., Brandt, A.U., Dörr, J., 2014. Relations of low contrast visual acuity, quality of life and multiple sclerosis functional composite: a cross-sectional analysis. BMC Neurol. https://doi.org/10.1186/1471-2377-14-31.
Schmitz-Valckenberg, S., Guo, L., Cheung, W., Moss, S.E., Fitzke, F.W., Cordeiro, M.F., 2010. [In vivo imaging of retinal cell apoptosis following acute light exposure]. Ophthalmologe 107, 22–29. https://doi.org/10.1007/s00347-009-1952-y.
Schmitz-Valckenberg, S., Guo, L., Maass, A., Cheung, W., Vugler, A., Moss, S.E., Munro, P.M.G., Fitzke, F.W., Cordeiro, M.F., 2008. Real-time in vivo imaging of retinal cell apoptosis after laser exposure. Investig. Ophthalmol. Vis. Sci. 49, 2773–2780. https://doi.org/10.1167/iovs.07-1335.
Seddon, J.M., 2017. Macular degeneration epidemiology: nature-nurture, lifestyle factors, genetic risk, and gene-environment interactions – the weisenfeld award lecture. Invest. Ophthalmol. Vis. Sci. 58, 6513–6528. https://doi.org/10.1167/iovs.17-23544.
Shamsher, E., Guo, L., Davis, B.M., Luong, V., Ravindran, N., Somavarapu, S., Cordeiro, M.F., 2019. Curcumin nanoparticles are neuroprotective in a mouse model of Alzheimer's disease. Investig. Ophthalmol. Vis. Sci. 60.
Shen, S.Y., Wong, T.Y., Foster, P.J., Loo, J.L., Rosman, M., Loon, S.C., Wong, W.L., Saw, S.M., Aung, T., 2008. The prevalence and types of glaucoma in Malay people: the Singapore Malay eye study. Investig. Ophthalmol. Vis. Sci. 49, 3846–3851. https://doi.org/10.1167/iovs.08-1759.
Shen, Y., Shi, Z., Jia, R., Zhu, Y., Cheng, Y., Feng, W., Li, C., 2013. The attenuation of retinal nerve fiber layer thickness and cognitive deterioration. Front. Cell. Neurosci. https://doi.org/10.3389/fncel.2013.00142.
Shindler, K.S., Ventura, E., Dutt, M., Rostami, A., 2008. Inflammatory demyelination induces axonal injury and retinal ganglion cell apoptosis in experimental optic neuritis. Exp. Eye Res. 87, 208–213. https://doi.org/10.1016/j.exer.2008.05.017.
Sit, A.J., 2014. Intraocular pressure variations: causes and clinical significance. Can. J. Ophthalmol. 49, 484–488. https://doi.org/10.1016/j.jcjo.2014.07.008.
Smith, C.A., Chauhan, B.C., 2018. In vivo imaging of adeno-associated viral vector labelled retinal ganglion cells. Sci. Rep. https://doi.org/10.1038/s41598-018-19969-9.
Sotirchos, E.S., Saidha, S., 2018. OCT is an alternative to MRI for monitoring MS – YES. Mult. Scler. J. https://doi.org/10.1177/1352458517753722.
Sun, X., Dai, Y., Chen, Y., Yu, D.Y., Cringle, S.J., Chen, J., Kong, X., Wang, X., Jiang, C., 2017. Primary angle closure glaucoma: what we know and what we don't know. Prog. Retin. Eye Res. 57, 26–45. https://doi.org/10.1016/j.preteyeres.2016.12.003.
Syc, S.B., Saidha, S., Newsome, S.D., Ratchford, J.N., Levy, M., Ford, E., Crainiceanu, C. M., Durbin, M.K., Oakley, J.D., Meyer, S.A., Frohman, E.M., Calabresi, P.A., 2012. Optical coherence tomography segmentation reveals ganglion cell layer pathology after optic neuritis. Brain. https://doi.org/10.1093/brain/awr264.
Tait, J.F., Gibson, D.F., Smith, C., 2004. Measurement of the affinity and cooperativity of annexin V-membrane binding under conditions of low membrane occupancy. Anal. Biochem. 329, 112–119. https://doi.org/10.1016/j.ab.2004.02.043.
Takayama, K., Ooto, S., Hangai, M., Ueda-Arakawa, N., Yoshida, S., Akagi, T., Ikeda, H. O., Nonaka, A., Hanebuchi, M., Inoue, T., Yoshimura, N., 2013. High-resolution imaging of retinal nerve fiber bundles in glaucoma using adaptive optics scanning laser ophthalmoscopy. Am. J. Ophthalmol. 155, 870–881. https://doi.org/10.1016/j.ajo.2012.11.016.
Tatham, A.J., Medeiros, F.A., 2017. Detecting structural progression in glaucoma with optical coherence tomography. Ophthalmology 124, S57–S65. https://doi.org/10.1016/j.ophtha.2017.07.015.
Telegina, D.V., Kozhevnikova, O.S., Kolosova, N.G., 2017. Molecular mechanisms of cell death in retina during development of age-related macular degeneration. Adv. Gerontol. https://doi.org/10.1134/S2079057017010155.
Thimister, P.W.L., Hofstra, L., Ing, H.L., Boersma, H.H., Kemerink, G., Reutelingsperger, C.P.M., Heidendal, G.A.K., 2003. In vivo detection of cell death in the area at risk in acute myocardial infarction. J. Nucl. Med. 44, 391–396.
Thompson, A.J., Banwell, B.L., Barkhof, F., Carroll, W.M., Coetzee, T., Comi, G., Correale, J., Fazekas, F., Filippi, M., Freedman, M.S., Fujihara, K., Galetta, S.L., Hartung, H.P., Kappos, L., Lublin, F.D., Marrie, R.A., Miller, A.E., Miller, D.H., Montalban, X., Mowry, E.M., Sorensen, P.S., Tintoré, M., Traboulsee, A.L., Trojano, M., Uitdehaag, B.M.J., Vukusic, S., Waubant, E., Weinshenker, B.G., Reingold, S.C., Cohen, J.A., 2018. Diagnosis of multiple sclerosis: 2017 revisions of the McDonald criteria. Lancet Neurol. https://doi.org/10.1016/S1474-4422(17), 30470-30472.
Tielsch, J.M., Katz, J., Singh, K., Quigley, H.A., Gottsch, J.D., Javitt, J., Sommer, A., 1991. A population-based evaluation of glaucoma screening: the baltimore eye survey. Am. J. Epidemiol. 134, 1102–1110. https://doi.org/10.1093/oxfordjournals.aje.a116013.
Ting, D.S.W., Pasquale, L.R., Peng, L., Campbell, J.P., Lee, A.Y., Raman, R., Tan, G.S.W., Schmetterer, L., Keane, P.A., Wong, T.Y., 2019. Artificial intelligence and deep learning in ophthalmology. Br. J. Ophthalmol. https://doi.org/10.1136/bjophthalmol-2018-313173.
Tojo, N., Abe, S., Miyakoshi, M., Hayashi, A., 2016. Correlation between short-term and long-term intraocular pressure fluctuation in glaucoma patients. Clin. Ophthalmol. 10, 1713–1717. https://doi.org/10.2147/OPTH.S116859.
Van de Wiele, C., Lahorte, C., Vermeersch, H., Loose, D., Mervillie, K., Steinmetz, N.D., Vanderheyden, J.L., Cuvelier, C.A., Slegers, G., Dierck, R.A., 2003. Quantitative tumor apoptosis imaging using Technetium-99m-HYNIC annexin V single photon emission computed tomography. J. Clin. Oncol. 21, 3483–3487. https://doi.org/10.1200/JCO.2003.12.096.
Van Den Brande, Koehler, J.M.H., Zelinkova, T.C., Bennink, Z., Te, R.J., Velde, A.A., Ten Cate, F.J.W., Van Deventer, S.J.H., Peppelenbosch, M.P., Hommes, D.W., 2007. Prediction of antitumour necrosis factor clinical efficacy by real-time visualisation of apoptosis in patients with Crohn's disease. Gut 56, 509–517. https://doi.org/10.1136/gut.2006.105379.
Vermeersch, H., Ham, H., Rottey, S., Lahorte, C., Corsetti, F., Dierckx, R., Steinmetz, N., Van De Wiele, C., 2004a. Intraobserver, interobserver, and day-to-day reproducibility of quantitative 99mTc-HYNIC annexin-V imaging in head and neck carcinoma. In: Cancer Biotherapy and Radiopharmaceuticals, pp. 205–210. https://doi.org/10.1089/108497804323071986.
Vermeersch, H., Loose, D., Lahorte, C., Mervillie, K., Dierckx, R., Steinmetz, N., Vanderheyden, J.L., Cuvelier, C., Slegers, G., Van de Wiele, C., 2004b. 99mtc-hynic annexin-v imaging of primary head and neck carcinoma. Nucl. Med. Commun. 25, 259–263. https://doi.org/10.1097/00006231-200403000-00008.
Vermeersch, H., Mervillie, K., Lahorte, C., Loose, D., Dierck, R.A., Steinmetz, N., Cuvelier, C., Slegers, G., Van De Wiele, C., 2004c. Relationship of 99mTc-HYNIC annexin V uptake to microvessel density, FasL and MMP-9 expression, and the number of tumour-infiltrating lymphocytes in head and neck carcinoma. Eur. J. Nucl. Med. Mol. Imag. 31, 1016–1021. https://doi.org/10.1007/s00259-004-1499-8.
Vermes, I., Haanen, C., Steffens-Nakken, H., Reutellingsperger, C., 1995. A novel assay for apoptosis Flow cytometric detection of phosphatidylserine expression on early apoptotic cells using fluorescein labelled Annexin V. J. Immunol. Methods 184, 39–51. https://doi.org/10.1016/0022-1759(95)00072-I.
Wallberg, F., Tenev, T., Meier, P., 2016. Time-lapse imaging of cell death. Cold Spring Harb. Protoc. https://doi.org/10.1101/pdb.prot087395.
Walter, S.D., Ishikawa, H., Galetta, K.M., Sakai, R.E., Feller, D.J., Henderson, S.B., Wilson, J.A., Maguire, M.G., Galetta, S.L., Frohman, E., Calabresi, P.A., Schuman, J. S., Balcer, L.J., 2012. Ganglion cell loss in relation to visual disability in multiple sclerosis. Ophthalmology. https://doi.org/10.1016/j.ophtha.2011.11.032.
Wang, N., Xie, X., Yang, D., Xian, J., Li, Y., Ren, R., Peng, X., Jonas, J.B., Weinreb, R.N., 2012. Orbital cerebrospinal fluid space in glaucoma: the Beijing intracranial and intraocular pressure (iCOP) study. Ophthalmology 119, 2065–2074. https://doi.org/10.1016/j.ophtha.2012.03.054.
Wang, P., Yang, H., Liu, C., Qiu, M., Ma, X., Mao, Z., Sun, Y., Liu, Z., 2020a. Recent advances in the development of activatable multifunctional probes for in vivo imaging of caspase-3. Chin. Chem. Lett. 32, 168–178. https://doi.org/10.1016/j.cclet.2020.11.056.
Wang, Y.X., Panda-Jonas, S., Jonas, J.B., 2020b. Optic nerve head anatomy in myopia and glaucoma, including parapapillary zones alpha, beta, gamma and delta: histology and clinical features. Prog. Retin. Eye Res. https://doi.org/10.1016/j.preteyeres.2020.100933.
Webb, R.H., Hughes, G.W., 1981. Scanning laser ophthalmoscope. IEEE Trans. Biomed. Eng. https://doi.org/10.1109/TBME.1981.324734.
Weinreb, R.N., Aung, T., Medeiros, F.A., 2014. The pathophysiology and treatment of glaucoma: a review. JAMA - J. Am. Med. Assoc. 311, 1901–1911. https://doi.org/10.1001/jama.2014.3192.
Weinreb, R.N., Friedman, D.S., Fechtner, R.D., Cioffi, G.A., Coleman, A.L., Girkin, C.A., Liebmann, J.M., Singh, K., Wilson, M.R., Wilson, R., Kannel, W.B., 2004. Risk assessment in the management of patients with ocular hypertension. Am. J. Ophthalmol. 138, 458–467. https://doi.org/10.1016/j.ajo.2004.04.054.
Weinreb, R.N., Leung, C.K.S., Crowston, J.G., Medeiros, F.A., Friedman, D.S., Wiggs, J.L., Martin, K.R., 2016. Primary open-angle glaucoma. Nat. Rev. Dis. Prim 2. https://doi.org/10.1038/nrdp.2016.67.
Weller, J., Budson, A., 2018. Current understanding of Alzheimer's disease diagnosis and treatment. F1000Research. https://doi.org/10.12688/f1000research.14506.1.
Wilding, C., Bell, K., Beck, S., Funke, S., Pfeiffer, N., Grus, F.H., 2014. γ-synuclein antibodies have neuroprotective potential on neuroretinal cells via proteins of the mitochondrial apoptosis pathway. PloS One. https://doi.org/10.1371/journal.pone.0090737.
Wilhelm, H., Schabet, M., 2015. The diagnosis and treatment of optic neuritis. Dtsch. Aerzteblatt. https://doi.org/10.3238/arztebl.2015.0616.
Wong, K.Y., Roy, J., Fung, M.L., Heng, B.C., Zhang, C., Lim, L.W., 2020. Relationships between mitochondrial dysfunction and neurotransmission failure in Alzheimer's disease. Aging Dis. https://doi.org/10.14336/AD.2019.1125.
Wu, H., De Boer, J.F., Chen, T.C., 2011. Reproducibility of retinal nerve fiber layer thickness measurements using spectral domain optical coherence tomography. J. Glaucoma 20, 470–476. https://doi.org/10.1097/IJG.0b013e3181f3eb64.
Wu, Z., Saunders, L.J., Zangwill, L.M., Daga, F.B., Crowston, J.G., Medeiros, F.A., 2017. Impact of normal aging and progression definitions on the specificity of detecting retinal nerve fiber layer thinning. Am. J. Ophthalmol. 181, 106–113. https://doi.org/10.1016/j.ajo.2017.06.017.
Wynne, N., Carroll, J., Duncan, J.L., 2021. Promises and pitfalls of evaluating photoreceptor-based retinal disease with adaptive optics scanning light ophthalmoscopy (AOSLO). Prog. Retin. Eye Res. https://doi.org/10.1016/j.preteyeres.2020.100920.
Xie, X., Chen, W., Li, Z., Thomas, R., Li, Y., Xian, J., Yang, D., Wang, H., Zhang, S., Kang, Z., Wang, N., 2018. Noninvasive evaluation of cerebrospinal fluid pressure in ocular hypertension: a preliminary study. Acta Ophthalmol. 96, e570–e576. https://doi.org/10.1111/aos.13724.
Yang, H., Luo, H., Hardin, C., Wang, Y., Jeoung, J.W., Albert, C., Vianna, J.R., Sharpe, G. P., Reynaud, J., Demirel, S., Mansberger, S.L., Fortune, B., Nicolela, M., Gardiner, S. K., Chauhan, B.C., Burgoyne, C.F., 2020. Optical coherence tomography structural abnormality detection in glaucoma using topographically correspondent rim and retinal nerve fiber layer criteria. Am. J. Ophthalmol. 213, 203–216. https://doi.org/10.1016/j.ajo.2019.12.020.

Yao, F., Zhang, E., Gao, Z., Ji, H., Marmouri, M., Xia, X., 2018. Did you choose appropriate tracer for retrograde tracing of retinal ganglion cells? The differences between cholera toxin subunit B and Fluorogold. PloS One 13, e0205133. https://doi.org/10.1371/journal.pone.0205133.

Yap, T.E., Balendra, S.I., Almonte, M.T., Cordeiro, M.F., 2019. Retinal correlates of neurological disorders. Ther. Adv. Chronic Dis. https://doi.org/10.1177/2040622319882205.

Yap, T.E., Davis, B.M., Guo, L., Normando, E.M., Cordeiro, M.F., 2018. Annexins in glaucoma. Int. J. Mol. Sci. https://doi.org/10.3390/ijms19041218.

Yu-Wai-Man, P., Griffiths, P.G., Chinnery, P.F., 2011. Mitochondrial optic neuropathies - disease mechanisms and therapeutic strategies. Prog. Retin. Eye Res. https://doi.org/10.1016/j.preteyeres.2010.11.002.

Yu, M., Lin, C., Weinreb, R.N., Lai, G., Chiu, V., Leung, C.K.S., 2016. Risk of visual field progression in glaucoma patients with progressive retinal nerve fiber layer thinning A 5-year prospective study. Ophthalmology. https://doi.org/10.1016/j.ophtha.2016.02.017.

Zhang, N., Wang, J., Chen, B., Li, Y., Jiang, B., 2021. Prevalence of primary angle closure glaucoma in the last 20 Years: a meta-analysis and systematic review. Front. Med. https://doi.org/10.3389/fmed.2020.624179.

Zille, M., Harhausen, D., De Saint-Hubert, M., Michel, R., Reutelingsperger, C.P., Dirnagl, U., Wunder, A., 2014. A dual-labeled annexin A5 is not suited for SPECT imaging of brain cell death in experimental murine stroke. J. Cerebr. Blood Flow Metabol. 34, e1–e7. https://doi.org/10.1038/jcbfm.2014.115.

Zou, Y., Zheng, S., Deng, X., Yang, A., Kong, Y., Kohansal, M., Hu, X., Xie, X., 2020. Diagnostic and prognostic value of circular RNA CDR1as/ciRS-7 for solid tumours: a systematic review and meta-analysis. J. Cell Mol. Med. https://doi.org/10.1111/jcmm.15619.